AD-A181 198 STRAINS AND STRESSES NEAR EXPLOSIONS AND EARTHQUAKES 1/2
(U) WOODWARD-CLYDE CONSULTANTS PASADENA CA
L J BURDICK ET AL. 15 OCT 86 WCCP-R-86-02
UNCLASSIFIED AFGL-TR-87-0089 F19628-85-C-0036 F/G 19/9 NL

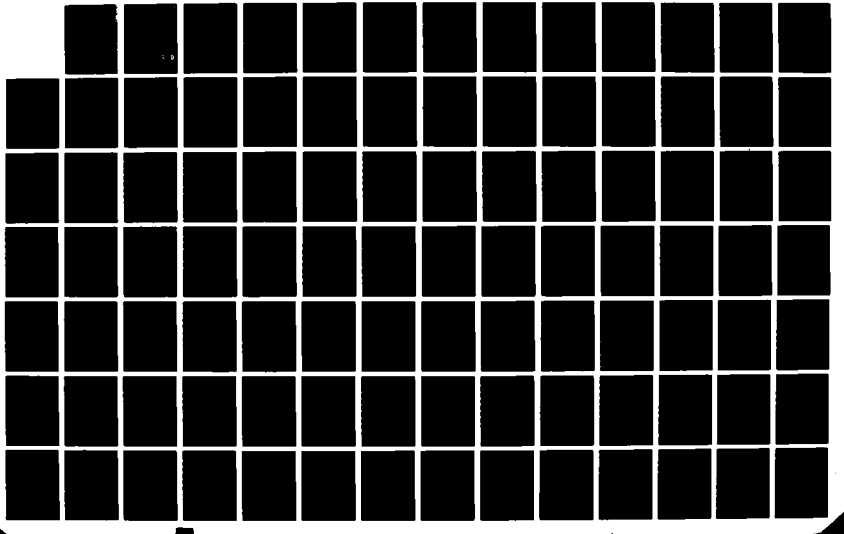

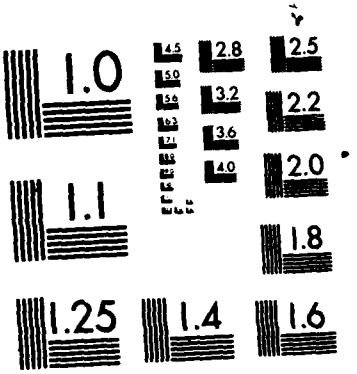

MICROCOPY RESOLUTION TEST CHART
NATIONAL BUREAU OF STANDARDS-1963-A

DTIC FILE COPY

(12)

AD-A181 198

AFGL-TR-87-0089

Strains and Stresses Near Explosions and Earthquakes

by L. J. Burdick and J. S. Barker

Woodward-Clyde Consultants
566 El Dorado Street
Pasadena, CA 91101

15 October 1986

Scientific Report No. 3

Approved for public release; distribution unlimited

DTIC
ELECTE
JUN 11 1987
S D
E

Air Force Geophysics Laboratory
Air Force Systems Command
United States Air Force
Hanscom Air Force Base, Massachusetts 01731

"This technical report has been reviewed and is approved for publication"

JAMES F. LEWKOWICZ
Contract Manager

HENRY A. OSSING
Branch Chief

FOR THE COMMANDER

DONALD H. ECKHARDT
Division Director

This report has been reviewed by the ESD Public Affairs Office (PA) and is releasable to the National Technical Information Service (NTIS).

Qualified requestors may obtain additional copies from the Defense Technical Information Center. All others should apply to the National Technical Information Service.

If your address has changed, or if you wish to be removed from the mailing list, or if the addressee is no longer employed by your organization, please notify AFGL/DAA, Hanscom AFB, MA 01731. This will assist us in maintaining a current mailing list.

Do not return copies of this report unless contractual obligations or notices on a specific document requires that it be returned.

Unclassified
SECURITY CLASSIFICATION OF THIS PAGE

AD-A181 198

REPORT DOCUMENTATION PAGE

1a. REPORT SECURITY CLASSIFICATION: Unclassified	1b. RESTRICTIVE MARKINGS
2a. SECURITY CLASSIFICATION AUTHORITY	3. DISTRIBUTION/AVAILABILITY OF REPORT: Approved for public release Distribution Unlimited
2b. DECLASSIFICATION/DOWNGRADING SCHEDULE	
4. PERFORMING ORGANIZATION REPORT NUMBER(S): WCCP-R-86-02	5. MONITORING ORGANIZATION REPORT NUMBER(S): AFGL-TR-87-0089
6a. NAME OF PERFORMING ORGANIZATION: Woodward Clyde Cons. / 6b. OFFICE SYMBOL (If applicable)	7a. NAME OF MONITORING ORGANIZATION: Air Force Geophysics Laboratory
6c. ADDRESS (City, State and ZIP Code): 566 El Dorado Street, Suite 100 Pasadena, CA 91101	7b. ADDRESS (City, State and ZIP Code): Hanscom Air Force Base Massachusetts 01731 - 5000
8a. NAME OF FUNDING/SPONSORING ORGANIZATION: DARPA / 8b. OFFICE SYMBOL (If applicable)	9. PROCUREMENT INSTRUMENT IDENTIFICATION NUMBER: F19628-85-C-0036
8c. ADDRESS (City, State and ZIP Code): 1400 Wilson Blvd. Arlington VA 22209	10. SOURCE OF FUNDING NOS.

PROGRAM ELEMENT NO	PROJECT NO	TASK NO	WORK UNIT NO
62714E	5A10	DA	Av

11. TITLE (Include Security Classification): Strains and Stresses Near Explosions and Earthquakes

12. PERSONAL AUTHOR(S): L. J. Burdick and J. S. Barker

13a. TYPE OF REPORT	13b. TIME COVERED	14. DATE OF REPORT (Yr, Mo, Day)	15. PAGE COUNT
Scientific Rpt 3	FROM 3/5/86 TO 9/5/86	86/10/15	120

16. SUPPLEMENTARY NOTATION

17. COSATI CODES			18. SUBJECT TERMS (Continue on reverse if necessary and identify by block number)
FIELD	GROUP	SUB GR	strain, stress, explosive source, earthquake source, nonlinear material response

19. ABSTRACT (Continue on reverse if necessary and identify by block number)

Laboratory evidence indicates that when strains exceed 10^{-6} in media under low confining pressure, certain nonlinear processes begin to occur. They are manifested by a reduction in apparent Q. Since direct measurements of near field strain are rare, it has been difficult to evaluate whether or not this phenomenon is significant near to realistic seismic sources. A high frequency theory for computing stresses and strains using generalized ray theory has been developed. It can be shown using this theory that near field body wave strain pulses are closely related to near field velocity pulses. Large data bases of near field velocity records and crustal structures for modeling them are available. Transfer functions for transforming velocity pulses into estimated strain pulses can be computed by deconvolving theoretical versions of the former from the latter. In most cases they are

20. DISTRIBUTION AVAILABILITY OF ABSTRACT	21. ABSTRACT SECURITY CLASSIFICATION
UNCLASSIFIED UNLIMITED ☐ SAME AS RPT ☒ DTIC USERS ☐	Unclassified

22a. NAME OF RESPONSIBLE INDIVIDUAL	22b. TELEPHONE NUMBER (Include Area Code)	22c. OFFICE SYMBOL
James Lewkowicz	(617) 377-3028	AFGL/LWH

DD FORM 1473, 83 APR — EDITION OF 1 JAN 73 IS OBSOLETE

Unclassified
SECURITY CLASSIFICATION OF THIS PAGE

delta-like functions. These transfer operators have been computed for a suite of velocity records from 5 Pahute Mesa Nuclear explosions ranging in yield from 155 to 1300 kt and for an Imperial Valley earthquake of M_0=.6*10^{24} dyne-cm. For the explosion data base the strains were as high as 10^{-3}; 3 orders of magnitude higher than the level at which the laboratory data suggests that nonlinear effects become important. The earthquake data base indicated strains levels between 10^{-6} and 10^{-5}. Because of the pressure dependence of the nonlinear phenomenon, it is probably only important in a thin layer near the surface of the earth.

Accession For	
NTIS GRA&I	☒
DTIC TAB	☐
Unannounced	☐
Justification	
By	
Distribution/	
Availability Codes	
Dist	Avail and/or Special
A-1	

DTIC COPY INSPECTED 1

INTRODUCTION

The exact solution for the dynamic stress and strain waves generated by a point explosive source in a whole space is a simple linear combination of the reduced displacement potential, the displacement pulse and the velocity pulse. The first decays as R^{-3}, the second as R^{-2}, and the third as R^{-1} (Haskell 1964). The far-field strain wave pulse can be generated from the velocity pulse by simply multiplying the latter by the slowness of the medium. This suggests that a similar close relationship between the dynamic strain and stress fields and the dynamic velocity field might exist in more general media. Large data bases of near-field velocity recordings have been collected and analyzed in the past whereas high frequency dynamic strain measurements have seldom if ever been made. The purpose of this study has been to attempt to use the data base of velocity records to infer the levels of dynamic strain and stress that typically occur near to explosions and earthquakes.

The reason that near-field dynamic strains are of current interest is that a variety of laboratory studies have shown that some typical geological materials begin to behave in a nonlinear fashion at shear strain levels between 10^{-5} and 10^{-6} (Mavko, 1979). This nonlinearity manifests itself as a lowering of effective Q. The phenomenon is frequency, amplitude and overburden pressure dependent. Day and Minster (1986) have discussed the potential significance of nonlinear behavior on interpretation of ground motion data from a series of small explosions in salt, but the events were so small that it is not straightforward to relate their results to nuclear explosions or earthquakes. Also, the recording geometry of their experiment was so simple that they could use whole space wave propagation results. Near-field wave propagation is usually much more complex near to general seismic sources (Burdick et. al., 1986, Heaton and Helmberger, 1978). It is important to establish the levels of dynamic strain that occur for these more typical sources in media where wave propagation is more complex.

We present here the results of an investigation of the relationship between the velocity and strain fields near to seismic sources in realistic crustal structures. First we develop the theory necessary for computing stresses and strains (rather than seismic motions) using the generalized ray methodology. Then we demonstrate that in a layered half space the far field strain wave is indeed very similar to the far field velocity wave. We develop a transfer operator which, when convolved with an observed velocity record, produces an estimate of a strain record. As noted above, in a whole space, this operator would be a delta function with the amplitude of the slowness of the medium. We show that in a layered half space it is a delta-like function with approximately the amplitude of the slowness at the receiver. (For some strain components, it is the amplitude of the vertical slowness and for others the horizontal slowness.) Next we apply these transfer functions to a suite of velocity records from nuclear explosions and from a small earthquake to establish the levels of dynamic stress and strain which they generated. The strain levels for the earthquake were found to be comparable to those for a modest nuclear explosion once the difference in source depths is accounted for. Presuming that the laboratory measurements of nonlinearity are relevant to the earth, the results of this study indicate that there is a thin region at the surface of the earth where effective Q can be expected to be very low.

STRESSES AND STRAINS IN A WHOLE SPACE

The strain tensor in a whole space for a point explosive source has only one nonzero, far field component in spherical coordinates. This, the radial component, is given by

$$E_{RR} = \partial U_R / \partial R = -2\psi / R^3 - 2\psi' / \alpha R^2 - \psi'' / \alpha^2 R \qquad (1)$$

The radial stress is given by

$$P_{RR} = -4\rho\beta^2 \left[\psi / R^3 + \psi' / \alpha R^2 \right] - \rho\psi'' / R \qquad (2)$$

Ψ is the reduced displacement potential, α, β and ρ are the compressional velocity, shear velocity and density of the medium and the primes denote differentiation. The last term on the right in Equation 1 is just the far field velocity pulse divided by the compressional velocity. Thus, the strain and stress fields are given exactly in terms of linear combinations of the RDP and its derivatives. Seismic motion parameters generally have a near-field term which decays as R^{-2} and a far-field term decaying as R^{-1}. Strains and stresses have additional near field terms that decay as R^{-3}.

Of course, these expressions become much more complicated for a general point source in a layered half space where, among other complications, cylindrical coordinates must be used. However, these half space expressions become much more tractable if near-field terms can be neglected. The simple whole space expressions can be used to estimate over what ranges the near-field terms are significant. Figure 1 shows the radial strains for two point explosions with yields of 100 and 1000 kt. The RDP's were computed using the formalism of Helmberger and Hadley (1981) with the yield scaling relations published by Burger et al. (1987). The medium parameters are given in Table 1. The far-field term is shown in the top row, the near-field terms in the second row and the sum at the bottom. At a range of 1 km, the near-field terms are important. By 3 km however, they have become relatively insignificant. This result appears to have little dependence on yield. In the next section, we will present a theory for computing body wave stresses and strains using only the far-field terms. Based on this calculation, it should be valid for ranges larger than 3 km.

The amplitudes of the strain pulses shown in Figure 1 should give a preliminary indication of how significant the nonlinear material behavior observed by Mavko (1979) is likely to be. Figure 2 has been redrafted from his paper and illustrates his basic result. The value of Q is observed to

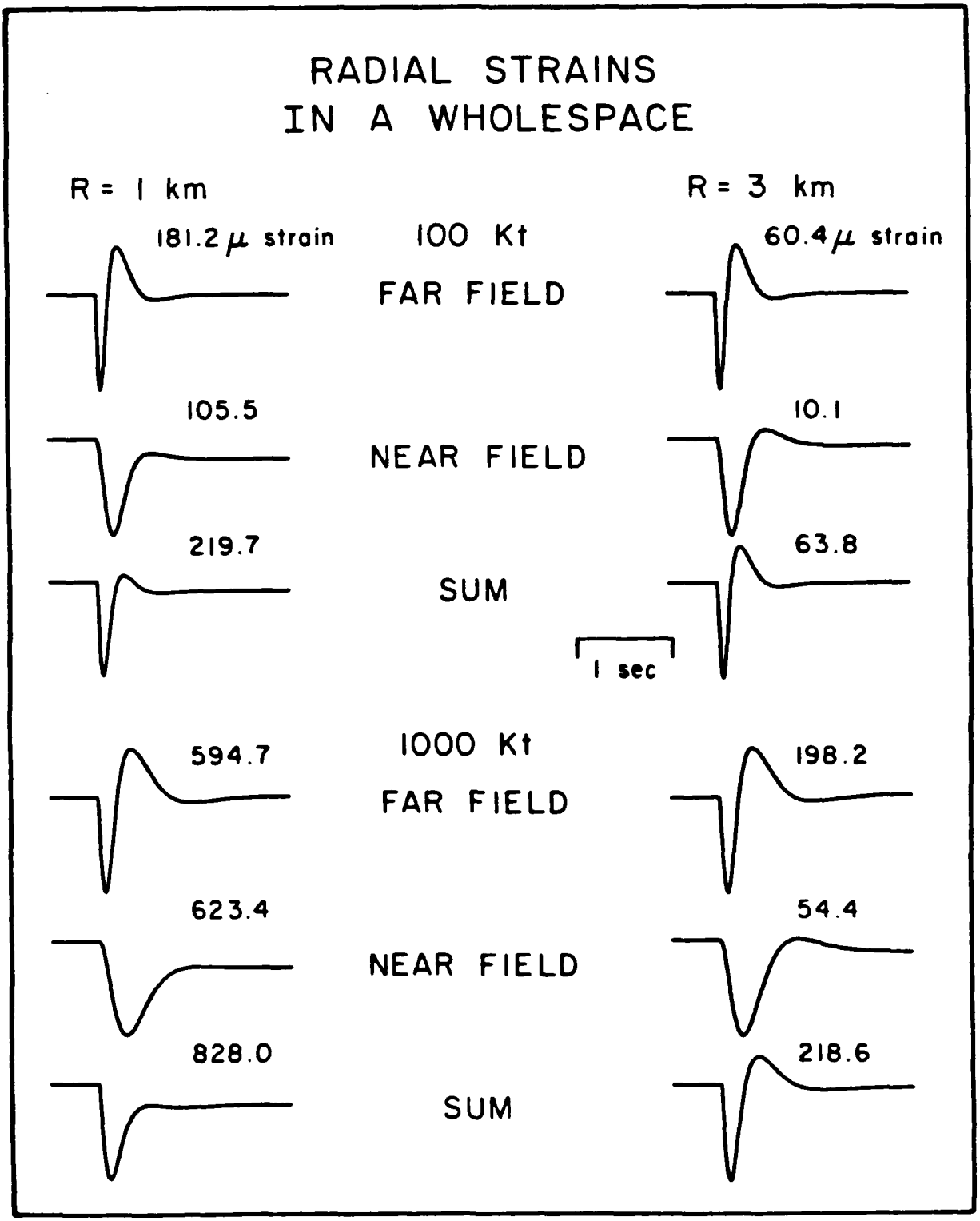

Figure 1. The analytic solution for the radial strain generated by a point explosion in a whole space. The left column is for a range of 1 km. and the right for a range of 3 km. An RDP for a 100 kt. explosion is shown at the top and for a 1000 kt. shot at the bottom. In each instance the near field terms are shown first by themselves, then the far field term and then the sum or complete solution. The near field terms become insignificant by 3 km.

Table 1: CRUSTAL MODELS

Whole Space and Half Space Calculations

P-Velocity (km./sec.)	S-Velocity (km./sec.)	Density (gm./cc.)	Thickness (km.)
5.00	3.00	2.00	

Pahute Mesa Calculations

2.30	1.35	1.90	0.360
2.80	1.50	2.00	0.800
3.30	1.52	2.25	0.300
4.00	1.90	2.30	0.700
4.60	2.00	2.40	0.750
5.30	2.50	2.50	0.800
5.50	2.95	2.70	2.250
6.10	3.50	3.00	10.00
7.00	4.00	3.01	10.00

Imperial Valley Calculations

1.69	0.35	1.52	0.210
1.72	0.50	1.56	0.210
1.93	0.70	1.74	0.210
2.10	0.90	1.89	0.210
2.25	1.15	2.03	0.339
2.50	1.50	2.26	0.480
2.67	1.64	2.36	0.320
2.85	1.74	2.39	0.320
3.45	2.08	2.48	0.800
3.69	2.21	2.51	0.160
4.20	2.50	2.60	0.160
4.55	2.71	2.63	0.395
4.75	2.75	2.65	0.395
4.92	2.84	2.65	0.501
5.09	2.94	2.65	0.501
5.37	3.10	2.65	1.130
5.65	3.26	2.65	1.137
5.68	3.28	2.66	1.144
5.72	3.30	2.68	0.588
5.75	3.32	2.70	0.563
5.79	3.34	2.72	1.158
5.83	3.36	2.74	0.750
5.85	3.38	2.76	0.970
7.20	4.17	3.07	1.440
7.27	4.20	3.10	1.454
7.34	4.24	3.12	1.469
7.42	4.28	3.14	0.746

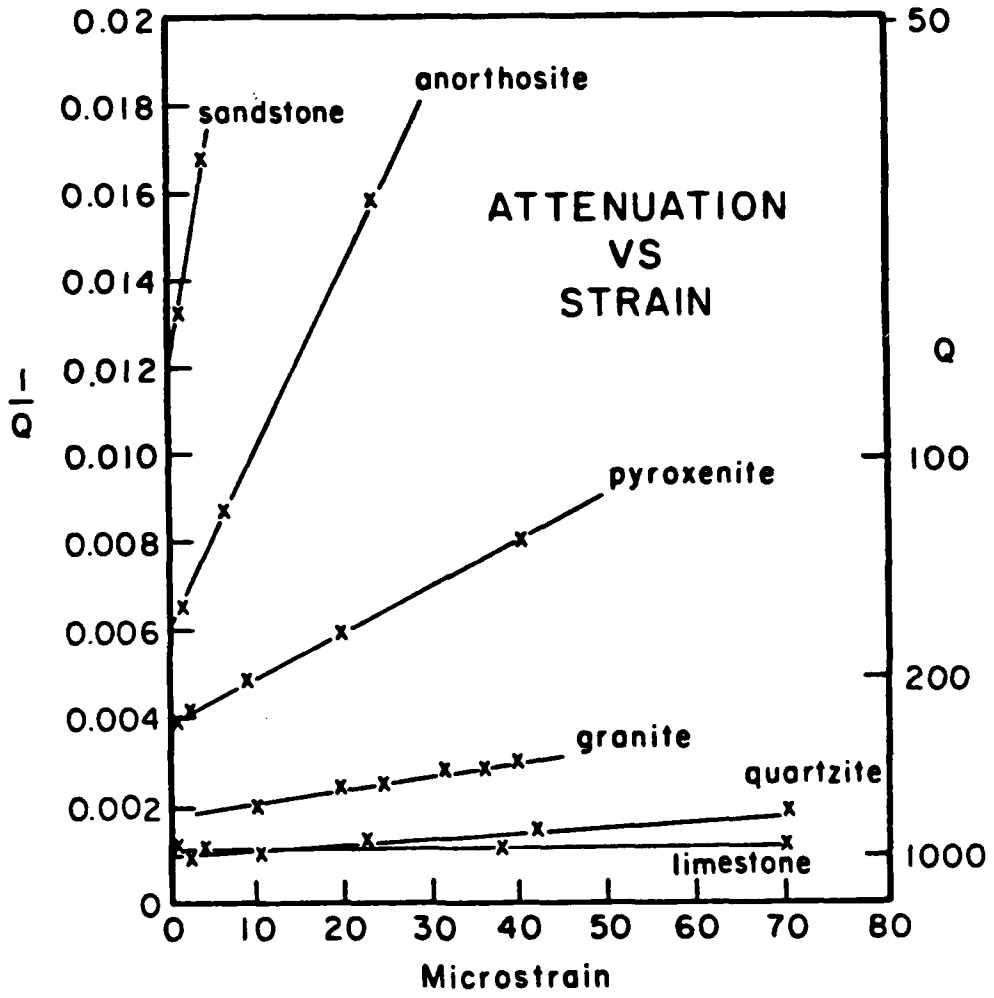

Figure 2. Linear plot of attenuation versus strain amplitude for six different dry rocks (redrawn from Mavko (1979)).

begin to increase at about 10^{-6} strain. By 10^{-5} strain the effect is very significant in most cases. The magnitude of the effect appears to also depend strongly on the geologic material involved. It is generally believed that the decrease in Q is caused by frictional sliding on cracks (Stewart et al., 1983). The observed effect should therefore also depend on the density of cracks in the material. As overburden pressure closes these cracks, it becomes increasingly difficult for sliding to occur. Thus the nonlinear zone probably does not extend to any great depth in the earth. Extending the 1 km result in Figure 1 out in range by dividing by R, we find that for a 1000 kt explosion, far-field strain drops to 10^{-5} at about 60 km and does not fall to 10^{-6} until almost 600 km The nonlinear zone would appear to occur over a very significant region.

STRESSES AND STRAINS IN A LAYERED HALF SPACE

Once a far-field approximation has been made in generalized ray theory, the differences in the expressions for seismic motions and seismic strains are actually quite small. Stress tensors can be generated from strain tensors through the usual definitions. The necessary modifications can be most easily demonstrated by beginning with the expressions presented by Langston and Helmberger (1975). Figure 3 shows the coordinate system in which their formalism is based. The small rectangle at the origin represents a fault with given dip (δ) and rake (λ). Here we will consider the possibility of explosive sources as well. The vertical, radial and tangential motions are given by W, Q and V respectively. The displacements are given in terms of the Laplace transformed seismic potentials ϕ, Ω and X by the Langston and Helmberger (1975) equation 5

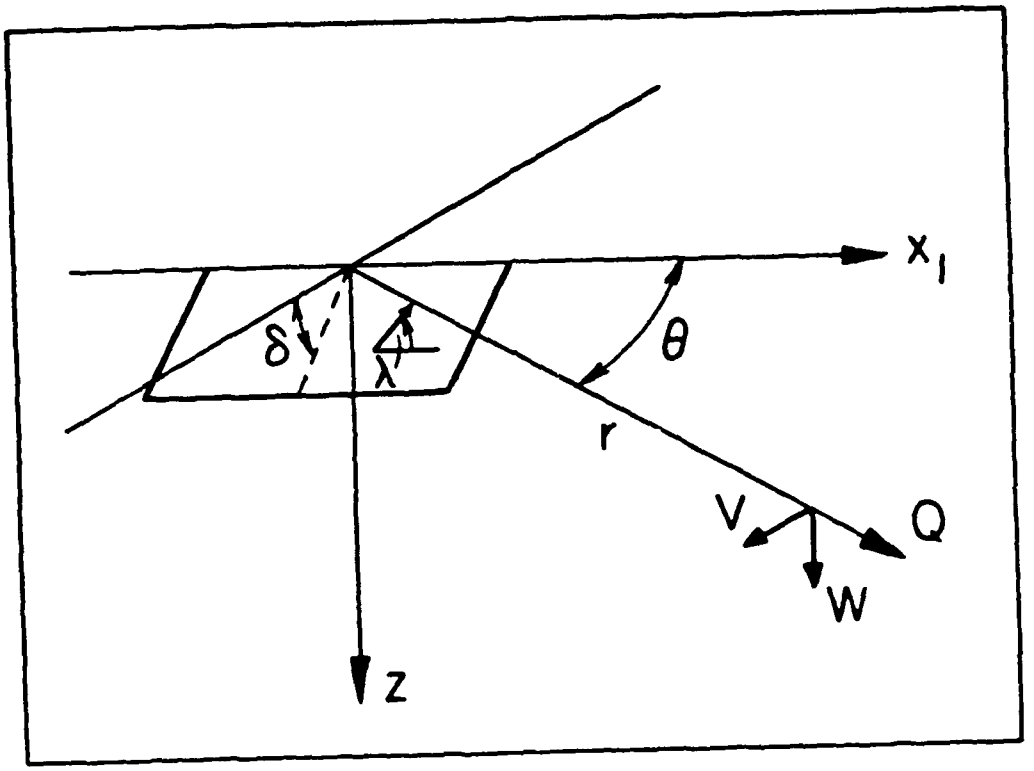

Figure 3. Coordinate system for the seismic wave equation solution. Note that z is positive downward.

$$\hat{W} = \frac{\partial \hat{\phi}}{\partial z} + sp\hat{\Omega}$$

$$\hat{V} = -\frac{\partial \hat{\chi}}{\partial r} \qquad (3)$$

$$\hat{Q} = \frac{\partial \hat{\phi}}{\partial r} - \frac{1}{sp}\frac{\partial^2 \hat{\Omega}}{\partial r \partial z}$$

where the near-field terms they give have been dropped. The Laplace transformed potentials for a generalized ray are given in their equation 6 by

$$\hat{\phi} = \frac{M_0}{4\pi\rho}\sum_{j=0}^{3} A_j(\theta,\lambda,\delta)\frac{2}{\pi} Im \int_0^{+i\infty} \prod C_j \frac{p}{\eta_\alpha}\sqrt{\left(\frac{\pi}{2spr}\right)} \times \exp(P)dp$$

$$\hat{\Omega} = \frac{M_0}{4\pi\rho}\sum_{j=1}^{3} A_j(\theta,\lambda,\delta)\frac{2}{\pi} Im \int_0^{+i\infty} \prod SV_j \frac{p}{\eta_\beta}\sqrt{\left(\frac{\pi}{2spr}\right)} \times \exp(P)dp \qquad (4)$$

$$\hat{\chi} = \frac{M_0}{4\pi\rho}\sum_{j=1}^{2} A_{(j+3)}(\theta,\lambda,\delta)\frac{2}{\pi} Im \int_0^{+i\infty} \prod SH_j \frac{p}{\eta_\beta}\sqrt{\left(\frac{\pi}{2spr}\right)} \times \exp(P)dp$$

M_0 is the seismic moment, ρ is the density at the source and p and η are the horizontal and vertical slownesses respectively. The phase of the ray, P, is

$$P = -s\left(pr + \sum_i th_i\eta_i\right) \qquad (5)$$

where the th_i's are the thicknesses of the layers encountered by a given ray. The A_j's are horizontal radiation pattern terms and the C_j's, SV_j's and SH_j's are vertical radiation pattern terms. The j indices, 0 through 3, denote an explosion, a vertical strike slip, a vertical dip-slip and a 45 ° dipping normal fault viewed at an azimuth of 45° respectively. Any other point source can be built from these fundamental sources through linear combination. These radiation terms are not of importance to this discussion, so they will not be explicitly written out here. They are given in Langston and Helmberger (1975), though we have added the index 0 for an explosion source which they did not. For an explosion, A_0 is 1 and C_0 is $1/\alpha^2$. The factor Π represents

the product of transmission and reflection coefficients along the raypath. The inverse transform is evaluated using the usual Cagniard de-Hoop method (Wiggins and Helmberger, 1974, Helmberger, 1974). It is important to follow in some detail how the displacements in Equation 3 are related to the potentials given in Equation 4. The spatial derivatives in Equation 3 can be evaluated prior to the inverse transforms. If near field terms are neglected, they simply produce some additional multiplicative factors in Equation 4. Helmberger (1974) discussed these factors in some detail, and we shall follow his notation and utilize many of his results here. We need to derive these factors for both the case in which the receiver is embedded in the half space and when it is on the free surface. We shall show that the only difference between seismic motion generalized rays and strain generalized rays is that they have slightly different multiplicative factors, hereafter called receiver functions.

To illustrate how these receiver functions are derived, let us consider the case shown in Figure 4. We have an incident P generalized ray and receiver points buried at depth h in the top layer of the stratified half space. The arriving P ray carries with it a ϕ potential with initial amplitude A_0. If we wish to compute the vertical component of motion, we substitute the expression for the ϕ from Equation 4 into the expression for W in Equation 3. For a single ray in the ray sum, the result is of the form

$$W = \int_0^{\infty} s R_{PZ} A_0 dp \qquad (6)$$

$$R_{PZ} = -\epsilon' \eta_\alpha$$

The factor of s generates a time derivative, and R_{PZ} is the receiver function. The first of the subscripts indicates that the initial potential was for a P wave. The second indicates that the vertical component of motion was computed. The converted wave shown at the top of Figure 4 would have produced a similar result except that the receiver function would be R_{SZ}. Also, the

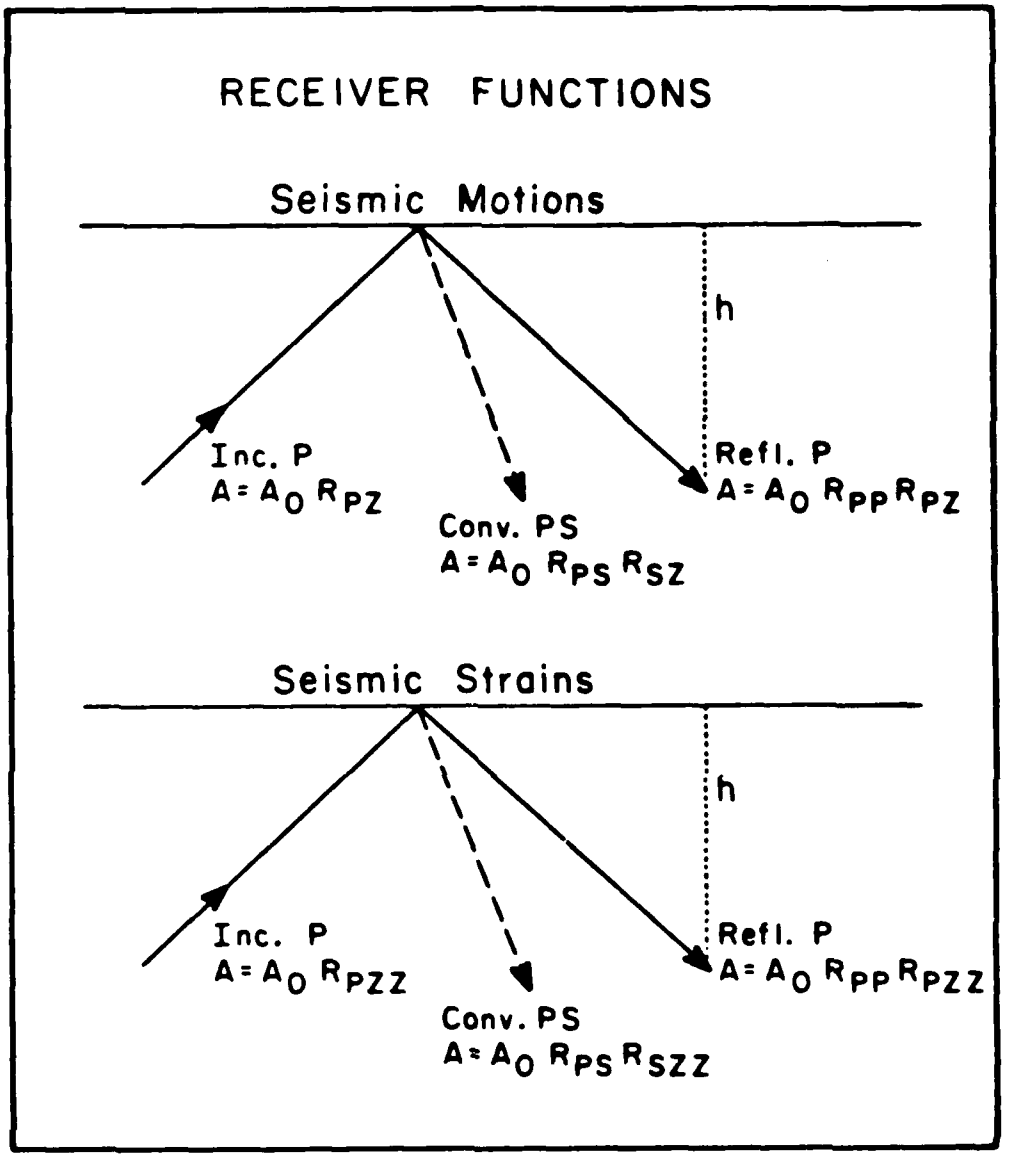

Figure 4. Schematic of the waves that must be considered in the computation of motion at depth h in the earth. Seismic motions and seismic strains vary only in their receiver coefficients. Motions and strains at the free surface are computed by taking the limit as h goes to zero.

product Π would include the free surface conversion coefficient R_{PS}. For the reflected P, the receiver function would again be R_{PZ}, but the value of the function would change sign due to the factor ϵ'. It is defined to be -1 if the last leg of the ray is upgoing (incident P) and +1 if the last leg of the ray is downgoing (reflected P). It arises because the phase of the ray is increasing with z in one case and decreasing in the other. It is primed to distinguish it from the similar term, ϵ defined by Langston and Helmberger (1975) which has similar properties depending on whether or not the ray is up or downgoing at the source rather than the receiver. As indicated at the top of Figure 4, the free surface reflection coefficient, R_{PP} would again be included. The complete set of receiver functions for receivers buried in a layer are given at the top left of Table 2. It shows that converting potentials to displacements involves no more than multiplying by plus or minus the vertical or horizontal slowness of a ray.

We next consider the computation of strains within the medium using generalized ray theory. To transform the three component displacement, D, into a strain we need to take spatial derivatives according to the form

$$E_{ij} = \frac{1}{2}\left(\partial D_i/\partial x_j + \partial D_j/\partial x_i\right) \qquad (7)$$

We can again take these derivatives of Equation 3 prior to the inverse Laplace transform. Again, they will result in additional multiplying factors of -sp or $-s\epsilon'\eta$. Just as in the whole space case, transforming from seismic motion to strain requires only multiplication by slowness. The additional factor of s causes a time derivative which transforms the displacement components to velocity. The strain and velocity time histories appear to be closely related just as in the whole space case. The additional slowness multipliers will cause phase shifts in the inverse Laplace transforms so the two pulses are no longer exactly proportional. We shall show, however, that in most cases the effect of the phase shifting is not large. The strain

TABLE 2

Receiver Functions

Seismic Motions

In the Medium	At the Free Surface
$R_{pz} = -\epsilon' \eta_\alpha$	$R_{pz} = 2\eta_\alpha(\eta_\beta^2 - p^2)/\beta^2 R(p)$ with $R(p) = (\eta_\beta^2 - p^2)^2 + 4p^2\eta_\alpha\eta_\beta$
$R_{pr} = -p$	$R_{pr} = -4\eta_\alpha\eta_\beta/\beta^2 R(p)$
$R_{sz} = p$	$R_{sz} = 4p\eta_\alpha\eta_\beta/\beta^2 R(p)$
$R_{sr} = -\epsilon' \eta_\beta$	$R_{sr} = 2\eta_\beta(\eta_\beta^2 - p^2)/\beta^2 R(p)$
$R_{s\theta} = p$	$R_{s\theta} = 2p$

Strains

$R_{pzz} = -\epsilon' \eta_\alpha R_{pz}$	$R_{pzz} = -cpR_{sz}$ with $c = (\alpha^2 - 2\beta^2)/\alpha^2$
$R_{pzr} = -pR_{pz}$	$R_{pzr} = -pR_{pz}$
$R_{prz} = -\epsilon' \eta_\alpha R_{pr}$	$R_{prz} = pR_{pz}$
$R_{prr} = -pR_{pr}$	$R_{prr} = -pR_{pr}$
$R_{szz} = -\epsilon' \eta_\beta R_{sz}$	$R_{szz} = cpR_{sr}$
$R_{szr} = -pR_{sz}$	$R_{szr} = -pR_{sz}$
$R_{srz} = -\epsilon' \eta_\beta R_{sr}$	$R_{srz} = pR_{sz}$
$R_{srr} = -pR_{sr}$	$R_{srr} = -pR_{sr}$
$R_{s\theta z} = -\epsilon' \eta_\beta R_{s\theta}$	$R_{s\theta z} = 0$
$R_{s\theta r} = -pR_{s\theta}$	$R_{s\theta r} = -pR_{s\theta}$

receiver functions for receiver points within the medium are given at the bottom left of Table 2. A natural extension of the notation of Helmberger (1974) has been used. The contribution to the zz component of the strain tensor due to an incident P wave is computed using the coefficient R_{PZZ} For an incident S wave, it would be R_{SZZ} and so on. There are 10 strain receiver coefficients and only 5 motion coefficients, but as shown in Table 2 they are very closely related and they appear in Equation 6 in an identical fashion

Most velocity records from explosions and earthquakes come from instruments located on the surface of the earth. It would thus be best if we could establish something about the levels of stress and strain in the near-field utilizing this information. Furthermore, if we can develop models that successfuly predict levels of strain and strain decay rates at the surface of the earth, we can then use these models with some confidence to predict strain levels and decay rates within the earth. To derive the seismic motion receiver functions, we determine the composite response of the three phases illustrated at the top of Figure 4 in the limit that h becomes small compared to the shortest wavelength of interest. These are essentially factors which are the sums of the amplitudes of the direct and reflected waves near the free surface. The geometry for the incident P wave case is illustrated in Figure 4. When the P, pP and pS arrive coincident in time the composite amplitude of the response is just $A_0(R_{PZ}+R_{PP}R_{PZ}+R_{PS}R_{SZ})$. The reflected waves for incident SV would be SS+SP and for SH just SS. This means there is some finite depth under a surface velocity receiver (defined by the shortest wavelength of interest criterion) where the strains estimated from that receiver can be thought of as existing. The highest frequency of interest here is about 5 hz and the slowest wave speed about 1 km/sec. Thus, the strains that we estimate probably exist in the earth down to depths of 200 m or more

The final step needed is to derive the receiver coefficients for strain at the free surface. It may appear that a reasonable way to accomplish this

would be to differentiate Equation 6 while inserting the appropriate displacement receiver coefficient and to make the usual far field approximation. However, this approach leads to nonzero vertical stresses on the free surface. To obtain the correct result, it is important to first take the required spatial derivatives of the displacements generated by the three phases shown at the bottom of Figure 4 and then to take the limit as h becomes small. The changes in sign caused by the factor ϵ' and the factors of η_β generated by vertical derivatives of the S wave potential instead of η_α generated by the P wave potential cause a very significant difference. The correct receiver functions for computation of free surface strains are shown at the bottom right of Table 2. They are factors of • slowness and • a dimensionless constant times different seismic motion receiver coefficients. Note, however, that for motions in the medium R_{PZZ} is generated from R_{PZ} whereas at the free surface it is generated from R_{SZ}. Several other similar changes exist. The cancellation of the terms R_{PZR} and R_{PRZ} along with R_{SZR} and R_{SRZ} guarentees that E_{ZR} will be zero. The $(\partial W/\partial\Theta)$ has no far field contribution, and $R_{S\Theta Z}$ is identically zero, so $E_{Z\Theta}$ will be zero. The diagonal term E_{ZZ} is a linear combination of the terms R_{PZZ}, R_{PRR}, R_{SZZ} and R_{SZR} which always remains zero though the algebraic details are somewhat more complicated. The free surface condition is satisfied by the strain receiver coefficients at the bottom right of Table 2.

The preceding has shown that the relationship between velocity and strain in a half space is very similar to their relationship in a whole space. Instead of multiplying velocity by the composite slowness of the medium to obtain strain, however, it is necessary to multiply by either the vertical or horizontal slowness. Figure 5 illustrates the degree to which this is true for a homogeneous half space. The source is the same 1000 kt explosion used in Figure 1, and the medium parameters are again given in Table 1. On the left are the velocity traces. Each generalized ray in the sum has been multiplied by a constant value of slowness equal to the value of p or η at

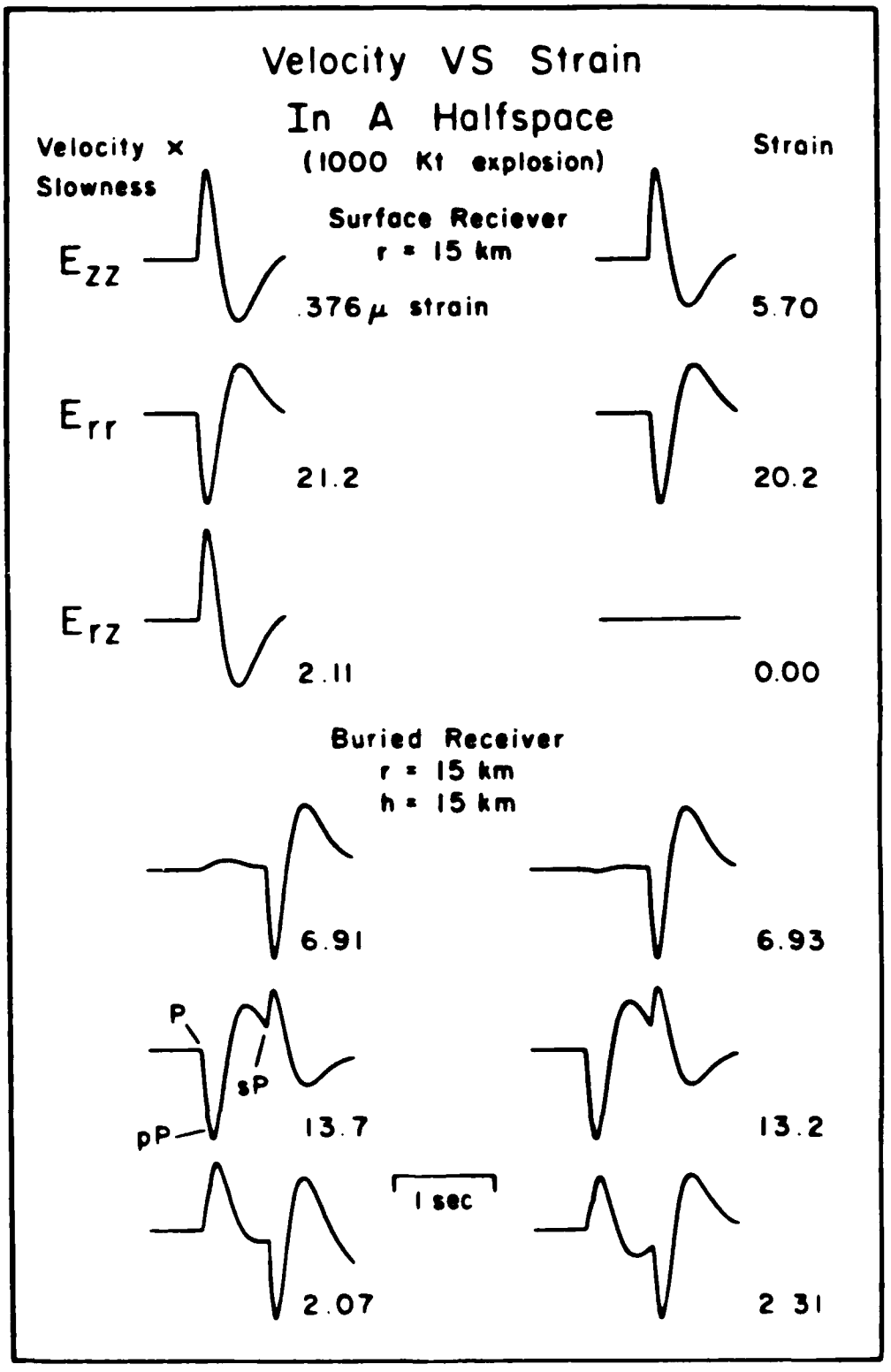

Figure 5. A comparison of velocity traces multiplied by constant values of slowness (left) with actual strain traces (right) The traces compare well when the receiver is buried. Differences occur when the receiver is on the free surface due to the free surface condition

which the Cagniard contour for that ray leaves the real axis. On the right are the exact strains. The case of a surface receiver is shown on the top and of a receiver buried at 15 km on the bottom. In each case, the range is 15 km. At the surface, the shape of the velocity times slowness pulse shape is virtually the same as the E_{ZZ} shape. The difference in amplitude is due to the fact that R_{PZZ} is not just $\eta_\alpha R_{PZ}$ but the more complicated form given in Table 2. If the velocity pulse is multiplied by the correct factor, again evaluated at the constant value of p, then the amplitudes of the pulses agree. The E_{RR} pulses agree in shape and amplitude. The true E_{RZ} strain is identically zero which is not predicted by the approximation. Within the medium, the approximation works very well. The reason it does not work exactly is because of the phase shifting that occurs as p evolves along the complex Cagniard contour.

Though the effect of the phase shifting in Figure 5 is small, a homogeneous half space is a very simplified medium. In more realistic crustal structures where unusual raypaths may be important, the phase shifts can have a large effect. It is necessary to find a way to account for this phase shifting no matter whether it is strong or weak. The most straightforward approach to devising such a velocity to strain transfer method is to utilize theoretical frequency dependent transfer operators. These operators are generated by computing a theoretical velocity and a theoretical strain response for a site and deconvolving the former from the latter. Estimates of strain records are generated from velocity records by convolving the velocity records with the transfer operators. We shall illustrate in the following that in most cases these transfer operators are very delta-like functions with amplitudes controlled by the velocity at the receiver site. The latter is a relatively well known quantity and we believe that as long as the frequency shift between the velocity and the strain records is small the transformed records should be good estimates of actual strain-time histories

STRESSES AND STRAINS NEAR TO NUCLEAR EXPLOSIONS

The first data base to be processed using the transfer operators is a suite of near field velocity recordings from five NTS nuclear explosions. The events, which were detonated at Pahute Mesa, are SCOTCH (155 kt), INLET (324 kt), MAST (406 kt), ALMENDRO (670 kt) and BOXCAR (1300 kt). (The yields are taken from Burger et. al. (1987).) The recording sites were at horizontal ranges between 3.3 and 22.5 km. The recording instruments were L7 velocity meters which have a response flat to velocity throughout the seismic band, so the signals recorded on them are essentially velocity versus time. The event locations, recording lines and receiver locations are shown on a map of Pahute Mesa in Figure 6. Not all of the available records were suitable for use here since some were too close and since some recording channels failed.

Each recording site used needed to have produced a three component data set. In order to compute the transfer functions, it is also necessary to have theoretical estimates of the velocity and strain pulses for each source-station pair. The methodology for computing such synthetics is discussed in Helmberger and Hadley (1981) and in Burdick et al. (1984). Computation of body waves which are the phases of interest here is accomplished through summation of generalized rays. Several possible plane layered models for the crustal structure at Pahute Mesa are available in the literature, but not all of them produce synthetic near field seismograms which closely match the observations. The one used in this study was provided by S. H. Hartzell (personal communication) and was specifically developed to produce accurate near field synthetics. It is shown in Figure 7 along with the alternate models of Helmberger and Hadley (1981), Hamilton and Healy (1969) and Carroll (1966). The three models are in basic agreement, differing only in the fine detail of the gradients. The parameters of the model are given in Table 1.

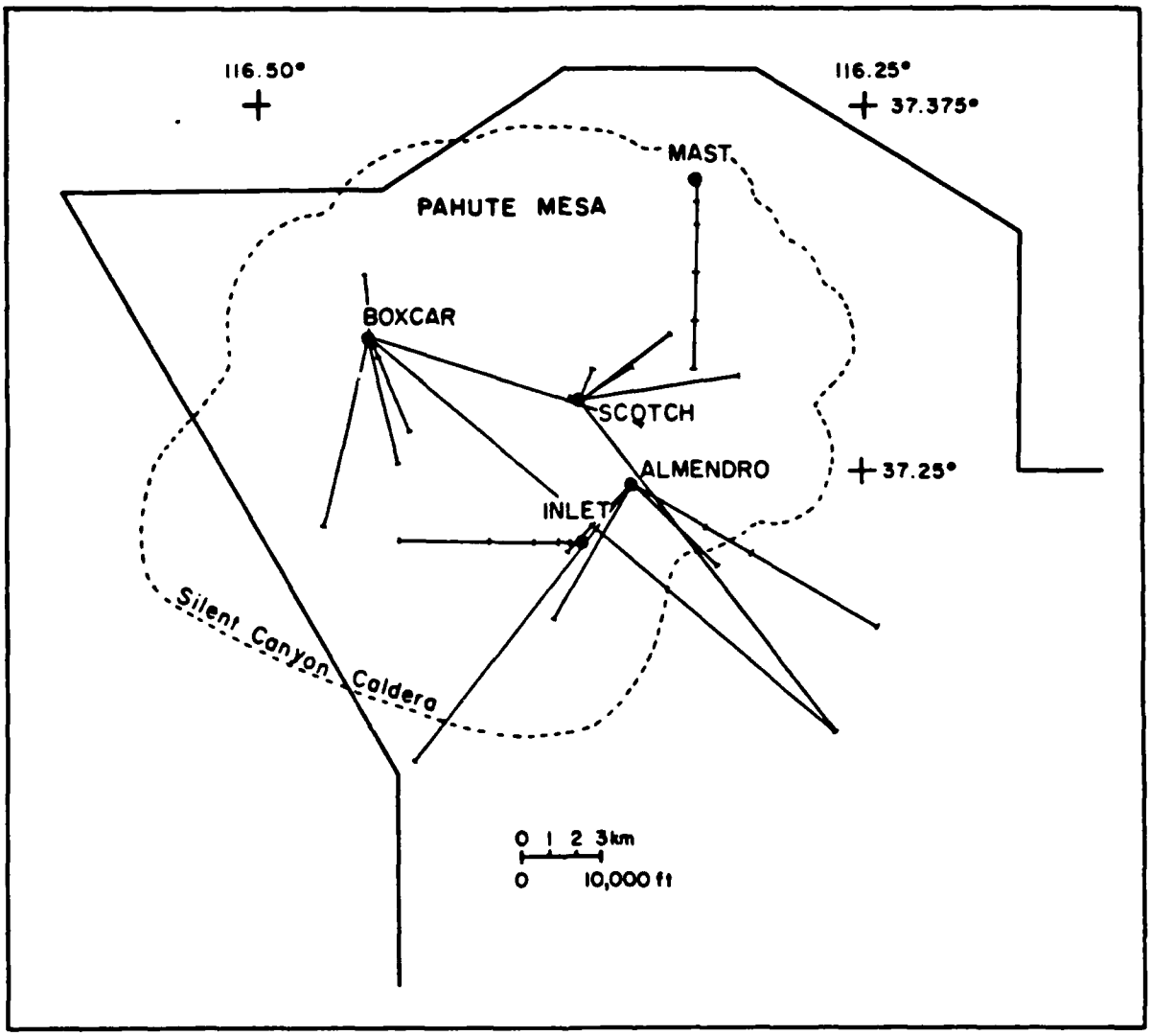

Figure 6. A map of the NTS events studied along with the station lines and locations.

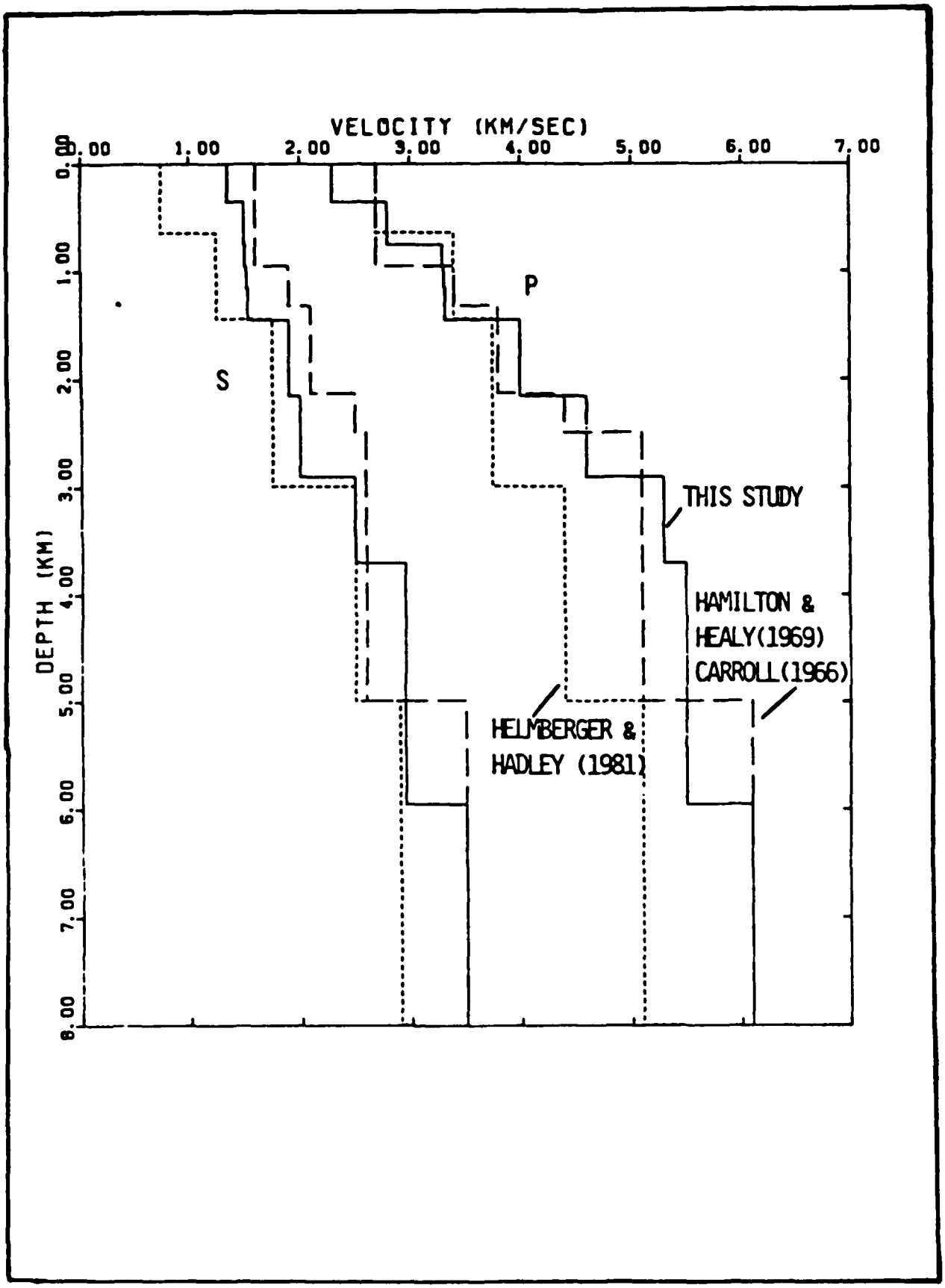

Figure 7. P and S-wave velocity structure for Pahute Mesa obtained in this study (solid curve) compared with two other proposed structures for the area (dashed and dotted curves).

An example of the computation of a transfer function for the Pahute Mesa crustal structure is given in Figure 8. The calculation is for the same theoretical 1000 kt event considered in Figure 1 and Figure 5. It was placed at a depth of 1 km in the crust. The synthetic vertical and radial velocity pulses are shown on the left, the four nonzero partial derivatives of velocity with respect to spatial coordinates in the center and the transfer functions are on the right. The generalized ray sum used in computing the medium response contained the primary rays of the P and pP type and near receiver conversions of the PS type. The amplitude of the P wave velocity pulse is about 10 cm/s, the strain amplitudes are a few tens of μstrain and the transfer functions a few hundreds of μstrain/cm. The top strain is E_{zz}, and the bottom is E_{RR}. The center two must be summed to form E_{ZR}. Note that they sum exactly to zero which guarantees the conservation of the free surface condition. The transfer functions are computed by transforming the velocity pulse and corresponding partial derivative pulse into the frequency domain using a fast fourier transform algorithm. The latter is divided by the former and the inverse transform taken. The resulting transfer operator strongly resembles a delta function with a signal to noise ratio of better than 5 to 1. To suppress the noise further a gaussian filter with a cutoff of 5 hz is applied before convolving the transfer function with actual data.

A typical example of what happens when the transfer operators are applied to observations is shown in Figure 9. The records are from the BOXCAR event at a range of 7.3 km. The vertical and radial velocity traces are shown on the left. They display a relatively impulsive and simple P wave arrival. The amplitude of the first peak is about 30 cm./sec. on either component. Transfer operators like those shown in Figure 8 were computed and convolved through to produce the four derivative traces on the right. In this example partial derivatives of the vertical velocity trace are generated from the vertical trace and derivatives of the radial from the radial. In principle, this need not be the case as we discuss in the following. The first peak of

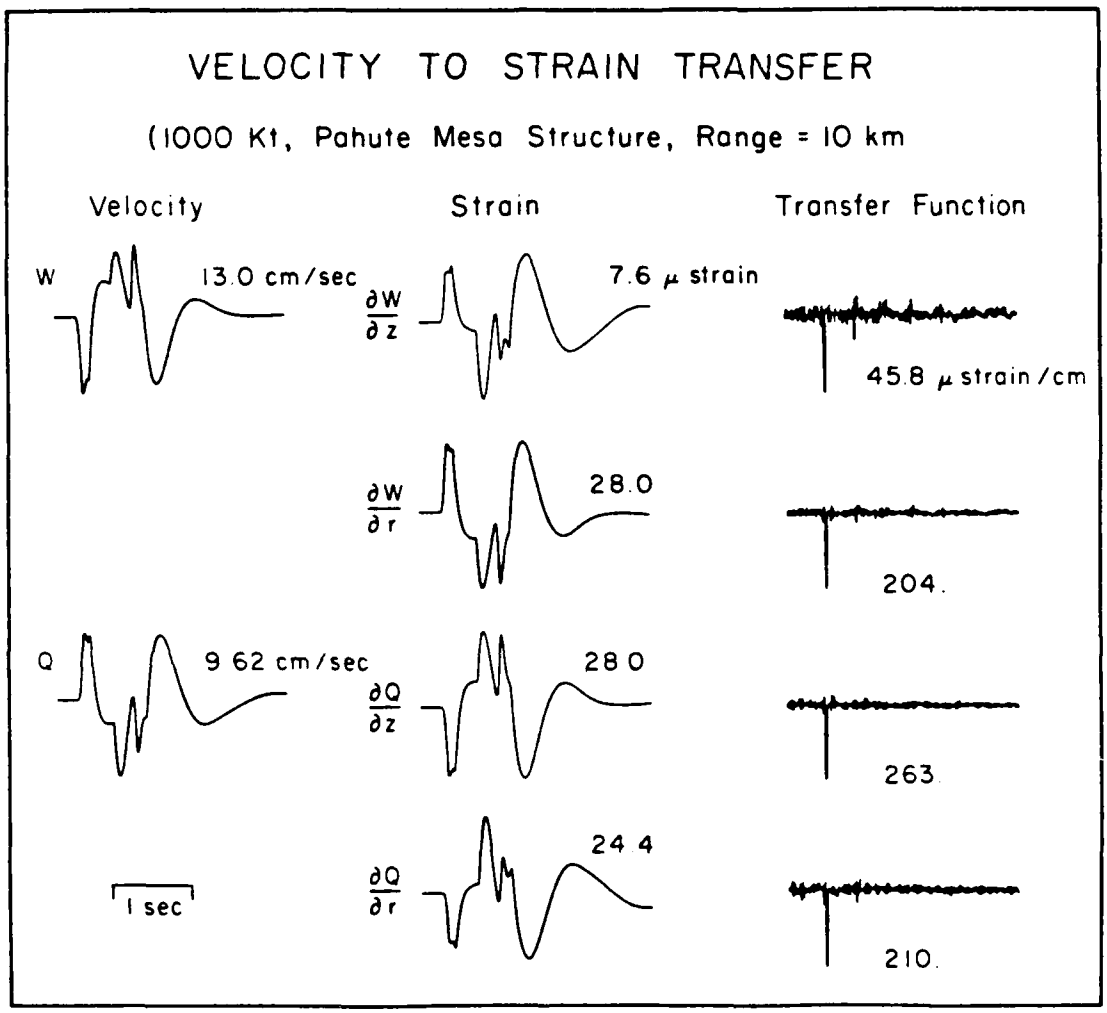

Figure 8. An example of the computation of the velocity to strain transfer functions for the Pahute Mesa structure. The velocity traces on the left are deconvolved from the strain traces in the center to produce the transfer operators on the right.

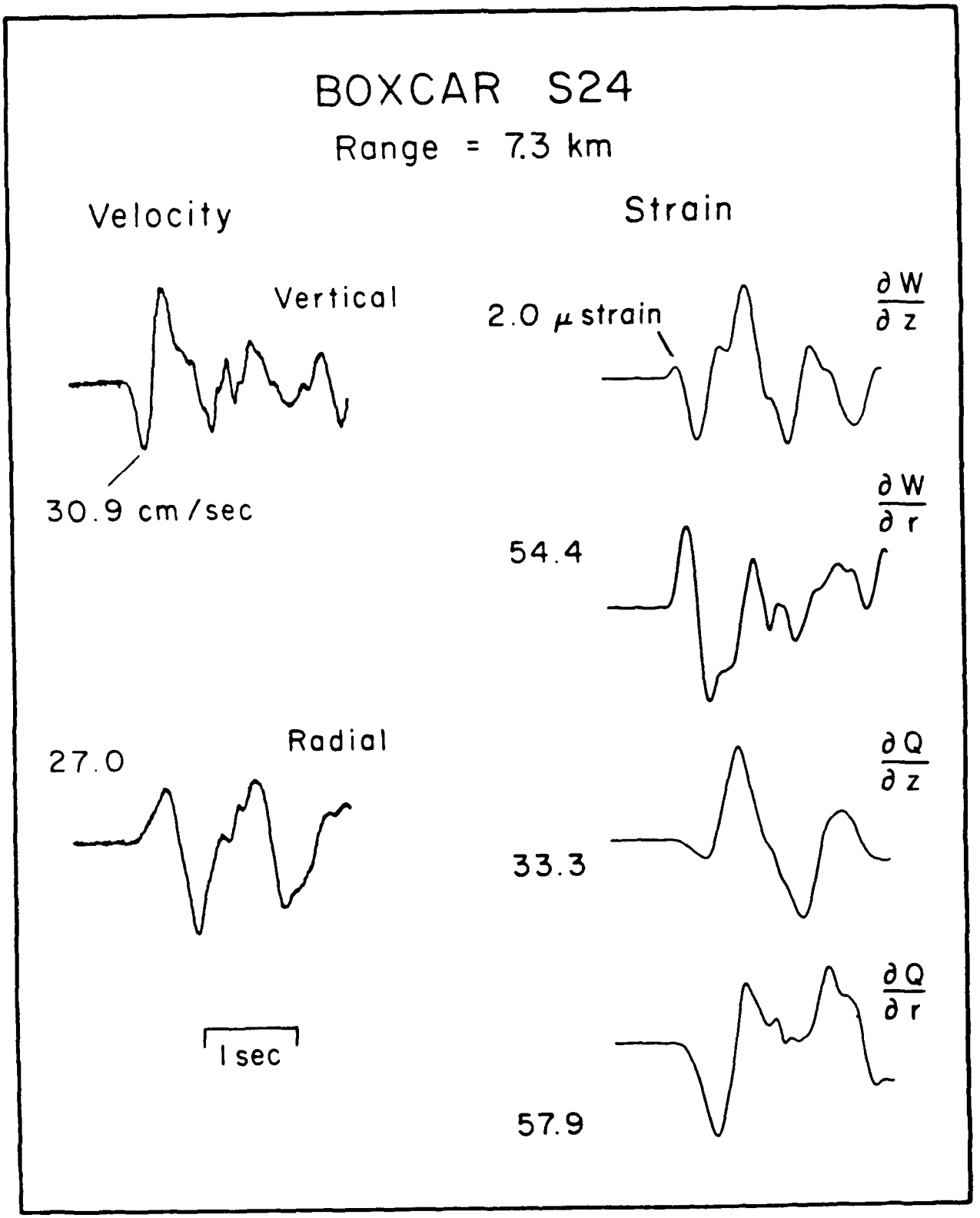

Figure 9. An example of the velocity to strain transfer for one of the stations from the event BOXCAR. The velocity pulses are shown on the left and the estimated strain pulses on the right. The amplitude values refer to the first positive peak.

$\partial W/\partial z$ is strongly reduced with respect to the later peaks. This is the component in which the phase shifting by the strain receiver function is generally the strongest. Its amplitude is also usually the lowest as it is in this example. The top trace is E_{ZZ}, the center two are combined to produce E_{ZR} and the bottom is E_{RR}. If the free surface condition is to be satisfied exactly, the center two traces should cancel. This clearly will not occur in the example shown. In order for this delicate cancellation to take place, the vertical and radial traces both need to be transfered into time series which are exactly proportional. The synthetics are never really exact, and generally the vertical component of motion is predicted better than the radial. The radial is presumably much more sensitive to lateral velocity variations directly under the instrument. In the following, we will force the free surface condition to be satisfied by using only the more reliable vertical records. In order for the stress P_{zz} to remain zero

$$E_{zz} = -\left(1 - 2\beta^2/\alpha^2\right)E_{rr} \tag{8}$$

Thus, we can generate one nonzero strain from the other in such a way that the free surface condition is satisfied.

Figure 10 shows the strains along with the trace of the strain tensor next to the bottom and the maximum shear strain as a function of time at the bottom. The maximum shear strain is defined as the absolute value of the difference between the largest and smallest diagonal elements in the diagonalized strain tensor. The event BOXCAR appears to have generated a peak shear of 74 μstrain at 7.3 km and presumably higher at closer ranges. The laboratory data in Figure 2 extends up to only 70 μstrain. This figure shows that if the waves from BOXCAR propagated through a material like sandstone, they would be strongly attenuated indeed. Figure 11 shows the corresponding stresses. The pressure in the next to bottom row is the negative of 1/3 the

trace of the stress tensor and the bottom trace is the maximum shear stress. The sixteen processed records are presented in Appendix 1 in the same format as Figures 10 and 11.

The decay rate of the peak shear strain with range is shown in Figure 12. Theoretical curves are shown for event BOXCAR which is the largest in the data set and for SCOTCH which is the smallest. The curves are computed assuming elastic theory is appropriate and using the same velocity structure as in the calculation of transfer functions. Note in Figure 7 that this structure is consistant with models derived using a variety of different approaches. The observed values from the processed records are shown as data points. The 70 μstrain level is only half way up the vertical scale. The theoretical curve for the smallest event does not drop below 1 μstrain by 25 km. Thus the entire data set is within the strain regime in which the nonlinear process observed in the laboratory is believed to be significant. It is interesting that the observations show the same rate of decay as the theoretical curve. The curve was computed using a theory which assumes linear elasticity holds. The nonlinear effects, if they are indeed significant, should have dropped the observed values below the elastic curves with range. However, it is important to remember that the nonlinearity associated with sliding on cracks (see Figure 2) probably only occurs very near to the surface. All of the generalized rays important to the P pulse dive downward into the crust and only enter the region where they might be attenuated as they emerge under the receiver. In other words, all of the signals in the data from a given event might be attenuated by more or less the same amount. The reduction in amplitude by the nonlinearity would then be reflected in an underestimate of the absolute size of the event.

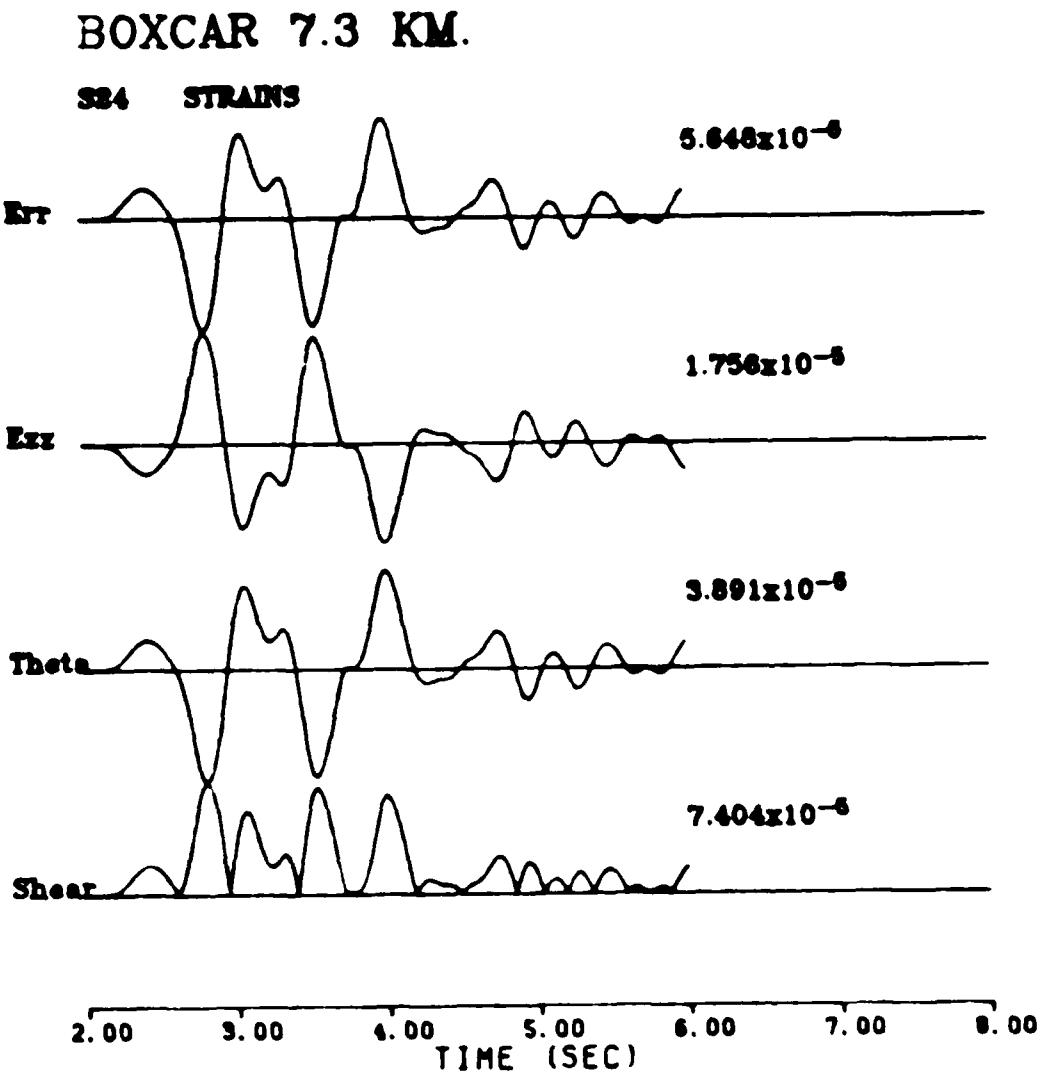

Figure 10. Strains from a typical BOXCAR station. The top two traces are the nonzero strains in a cylindrical coordinate system assuming that the free surface condition holds. The third trace is the trace of the strain tensor, and the bottom trace is the peak shear strain.

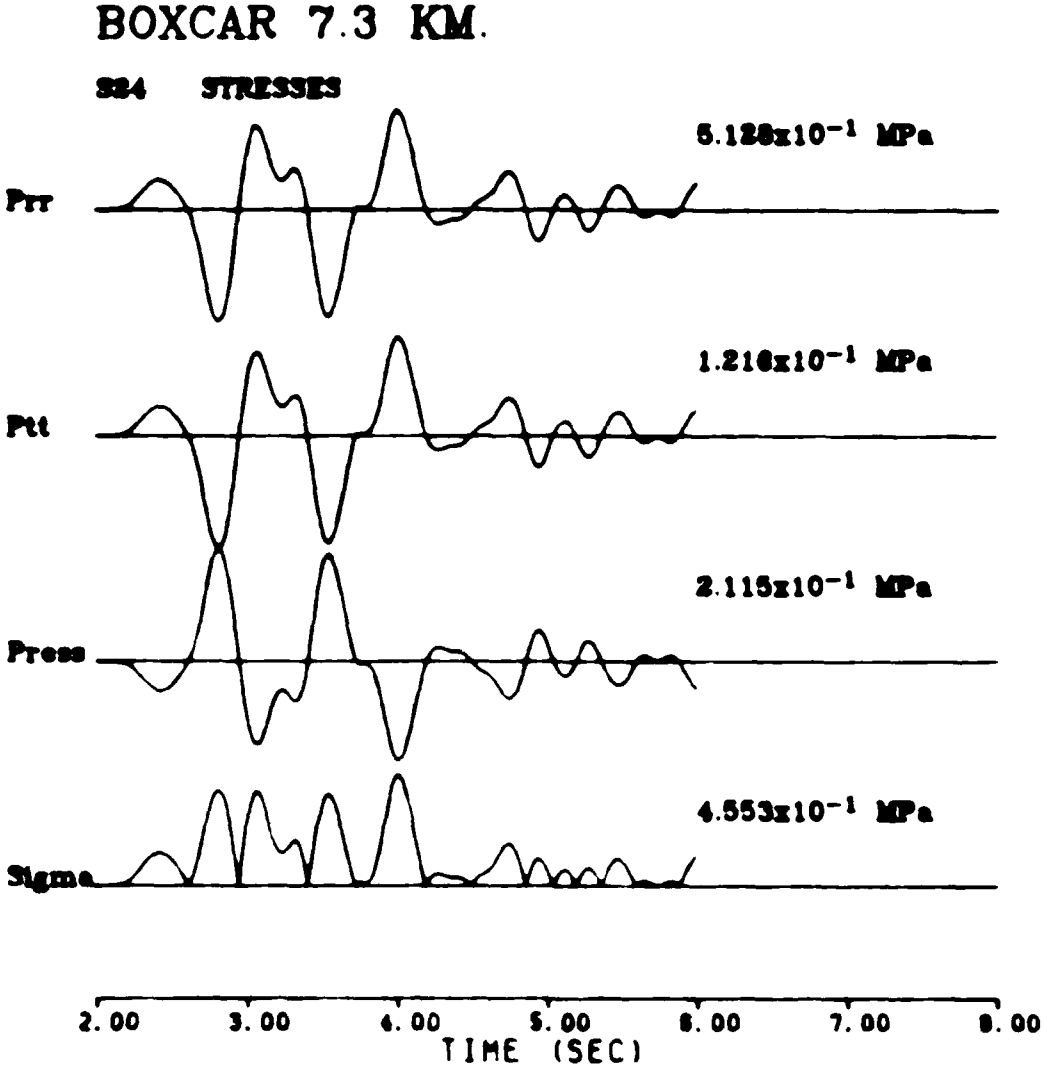

Figure 11. Stresses from a typical BOXCAR station. The top two traces are the nonzero stresses in a cylindrical coordinate system. The third trace is pressure and the fourth is peak shear stress.

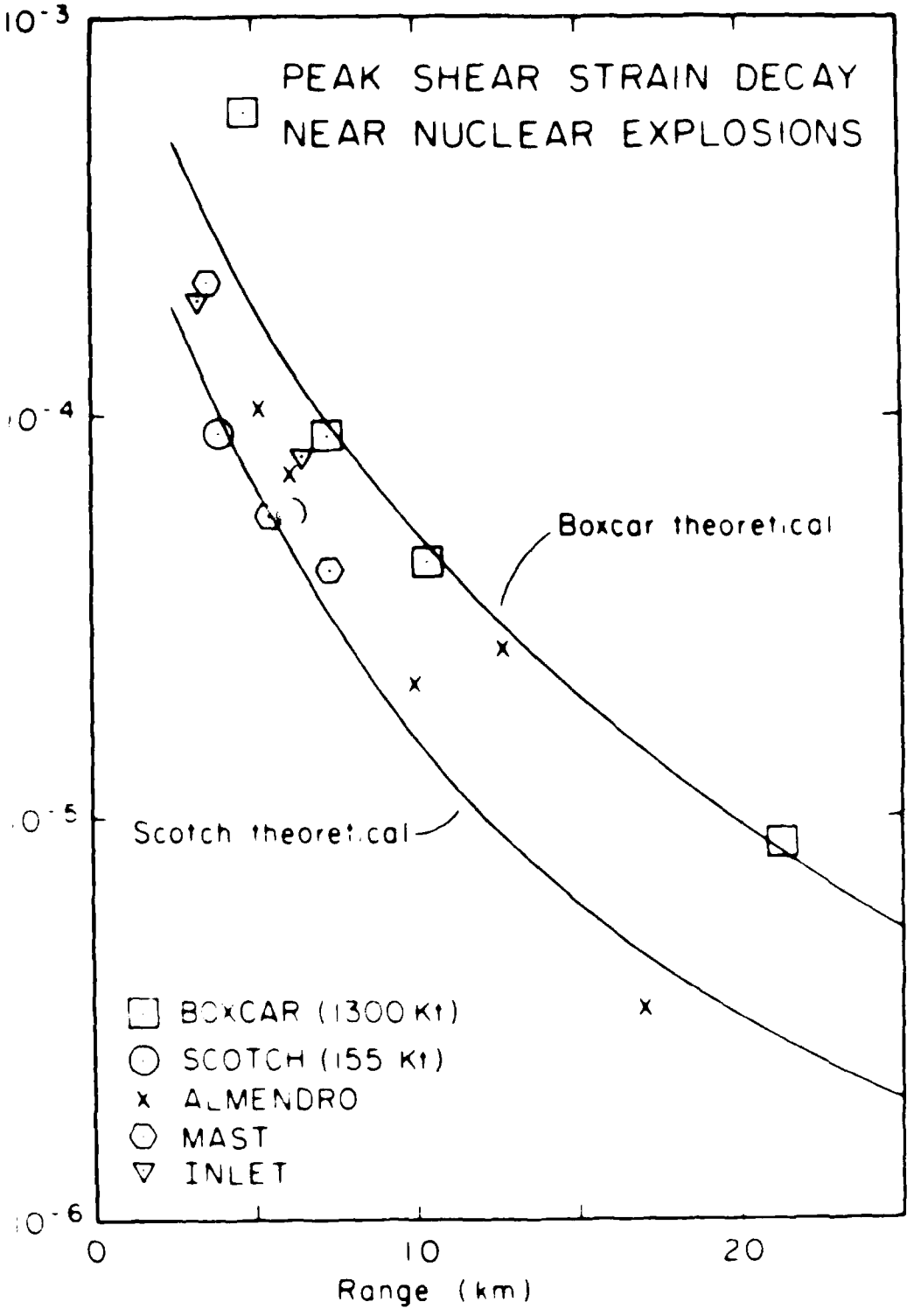

Figure 12. The decay of peak shear strain near to nuclear explosions. The largest observed value of shear strain is 10^{-3}. Theoretical curves are shown for the largest and smallest events studied. The observations appear to follow the theoretical predictions.

STRAINS AND STRESSES NEAR TO EARTHQUAKES

The next records to which we will apply our velocity to strain transformation procedure are from a small aftershock of the 15 October 1979 Imperial Valley earthquake. The aftershock was studied in some detail by Liu and Helmberger (1985) who provided a mechanism, moment and time function for it. They reported the event depth as 9.5 km. Figure 13 shows the strong motion recordings from it. A map of the stations, the aftershock location and the mainshock location is shown in an inset. The strong, clear pulse is the direct S wave. The P wave was only recorded in its entirety at a few stations and was too complex to model. Several polarity changes are apparent in the data. Liu and Helmberger (1985) used this information to infer that the event had a vertical strike slip mechanism. They reported a moment of 1.0×10^{24} dyne-cm and a triangular time function with a rise of 0.1 sec and a fall of 0.1 sec. From our modeling studies, however, we conclude that a moment value of 0.6×10^{24} dyne-cm and a source with a rise of 0.3 sec and a fall of 0.1 sec is more accurate.

Certain unusual characteristics of the strong motion records will guide how we will proceed to estimate strain from velocity in this instance. Figure 14 shows the three components of motion observed at four of the stations at a representative set of ranges. HOLT is the closest station and BRAW the farthest. HOLT, ELCE and BNCR were three of the six stations that recorded the complete P as well as the S waves. Note in these records that the P wave is smaller and much less coherent than the S wave. The peak strains are carried by the S wave pulse, so we will transform the S waves alone and not attempt to process the P waves. Also note that there is no clear SV arrival on the vertical records. In some cases there is a burst of incoherent energy, but there is no clear long period pulse as on the radial component. The fact that the SV pulse is so small on the vertical component can be explained by the fact that the shear velocity near the surface in Imperial valley is very

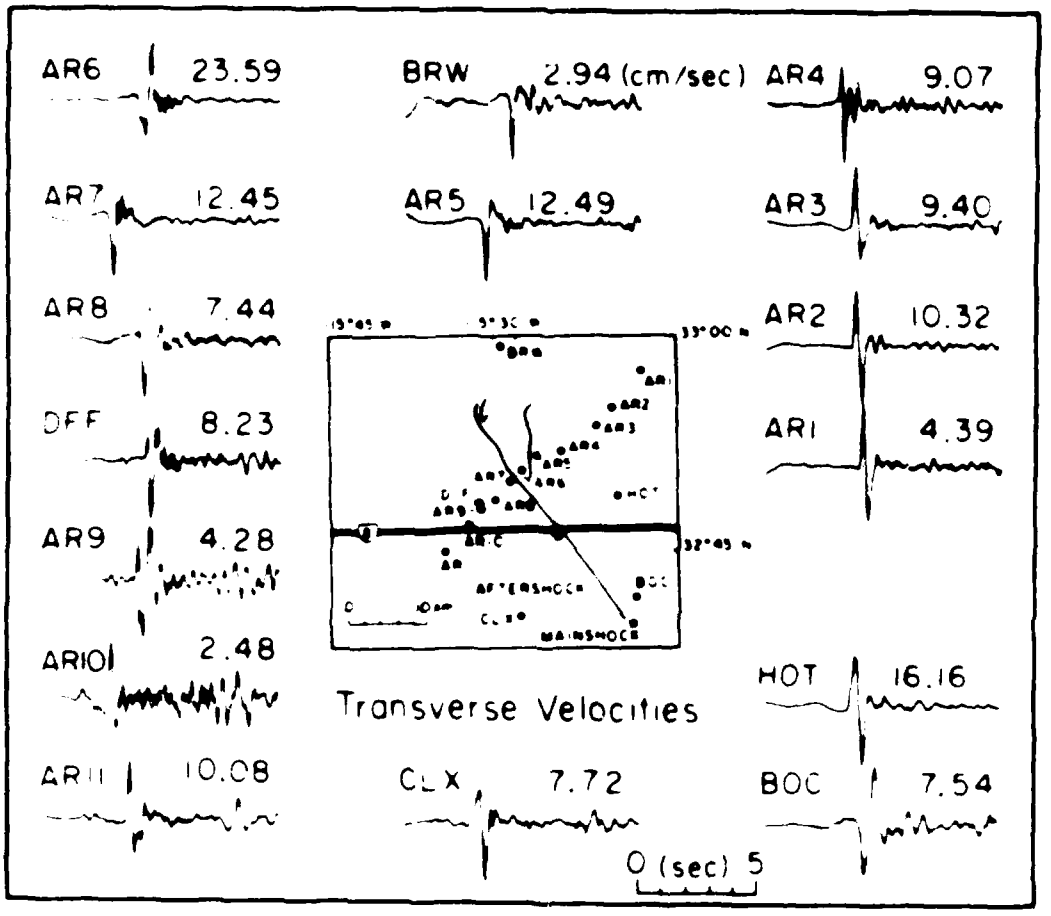

Figure 13a. The transverse ground velocities from the 23 19, 15 October 1979 Imperial Valley aftershock

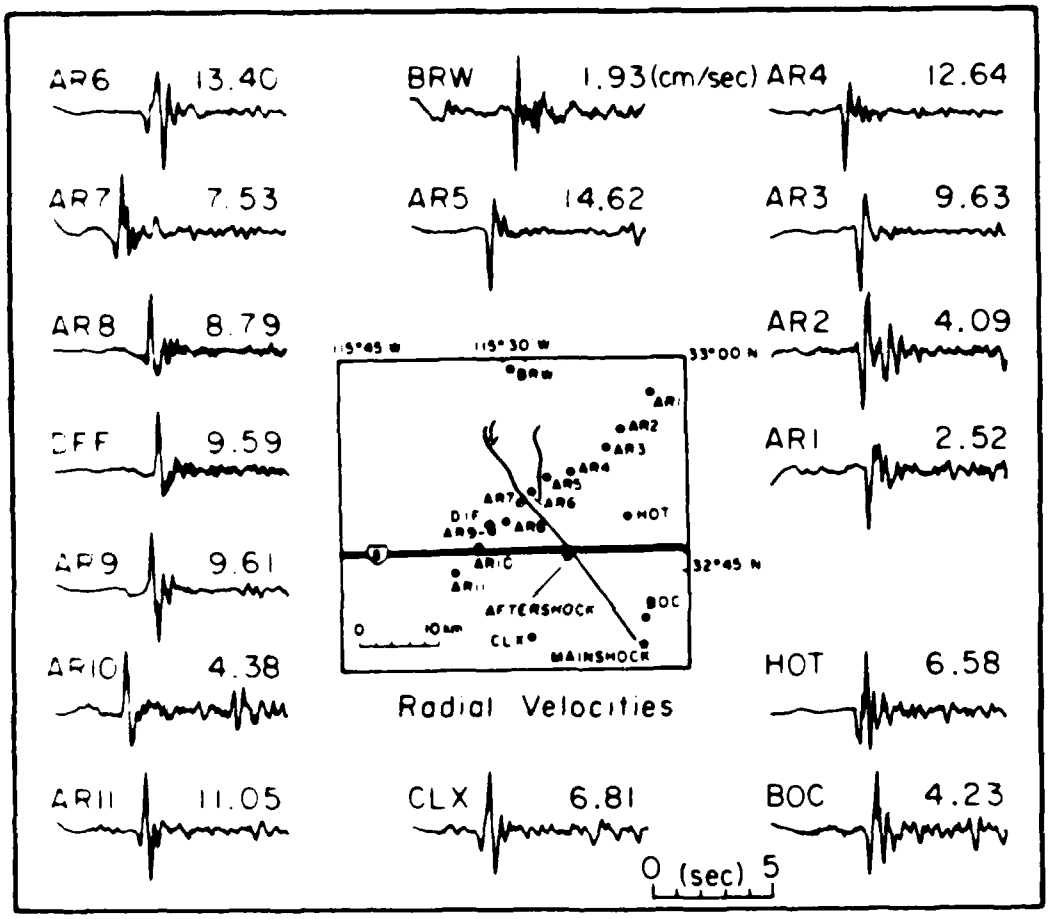

Figure 13b. The radial ground velocities from the 23:19, 15 October 1979 Imperial Valley aftershock.

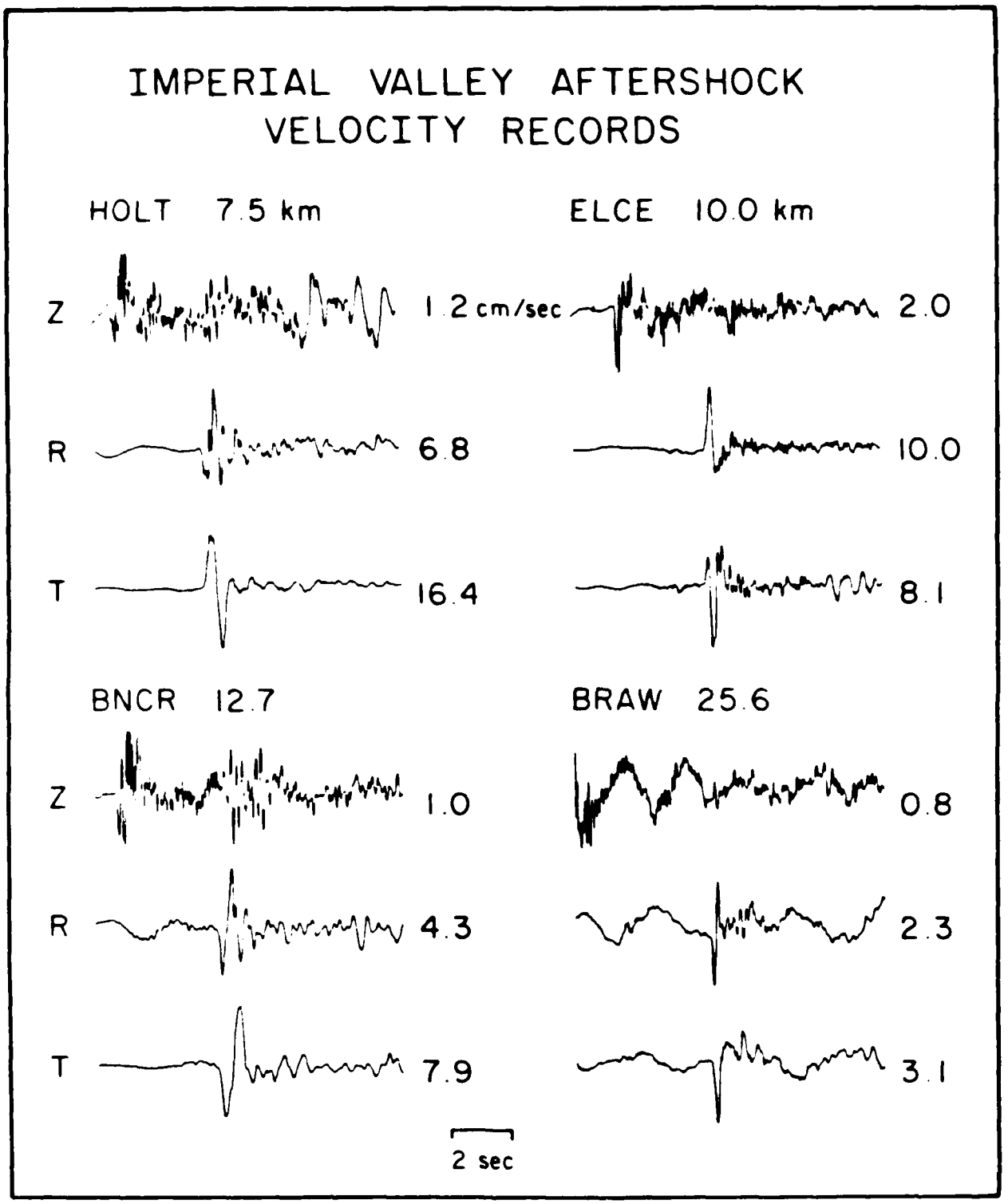

Figure 14. Four typical three component record sets from the Imperial Valley aftershock. The P wave is more complex and much higher frequency than the S wave. The vertical S wave component is small.

low. Thus the SV ray emerges almost vertically and the wave produces little vertical motion. We wish to avoid using the noisy vertical signals in our processing since they will probably only degrade the accuracy of our strain estimate.

The nonzero strains generated by an incident SV wave are E_{zz}, E_{rr} and E_{rz}. As before, we could use the vertical velocity record to generate the first of these and the radial to generate the other two. Instead, we again will use relation 8 to generate the information we need regarding E_{zz} from E_{rr}, and do it in such a way that the free surface condition is automatically satisfied. In essence, we generate an estimate of the vertical signal from the radial signal instead of using the noisy vertical channel itself. One other point worth noting about Figure 14 is the clear shift in frequency content between P and S waves. Liu and Helmberger (1985) attribute this shift to a low effective shear Q in the Imperial Valley. The value they used for shear Q in the top layer of their crustal model was only 6.2. This results in a relatively distance independent t^* of .132 sec. In the calculations shown in the following, we use this value along with the crustal model they presented (see Table 1). A value for shear Q as low as 6.2 is surely atypical and could easily be interpreted as an indication that nonlinear processes like those suggested by the laboratory data shown in Figure 2 might be taking place.

An example of the velocity to strain transfer operators for the earthquake case is given in Figure 15. As in Figure 8, the relevant theoretical velocity traces are shown on the left, the spatial derivatives of them in the center and the transfer operators on the right. In this instance, the velocity traces are Q (radial) and V (tangential). The transfer operators are shown with the gaussian filter (cutoff 5 hz) convolved through. Of the four partial derivatives shown, only two are actually used in the calculations that follow. The top one would be used to generate E_{rz}, but the other term in E_{rz} would always cancel it to satisfy the free surface condition. The third

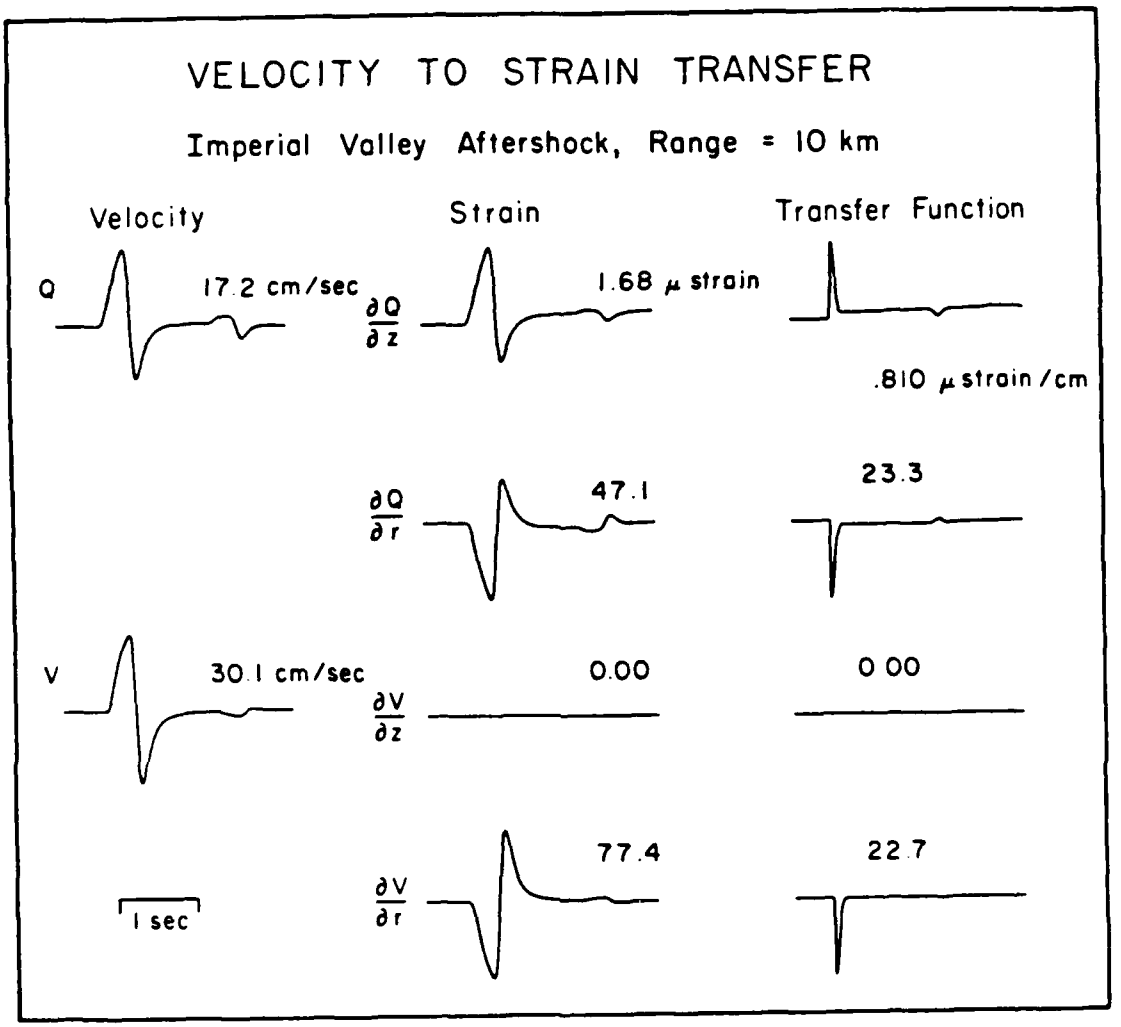

Figure 15. An example of the computation of the velocity to strain transfer functions for the Imperial Valley structure. The velocity traces on the left are deconvolved from the strain traces in the center to produce the transfer operators on the right.

transfer function is always zero because the corresponding receiver coefficient is zero in Table 2. The second and fourth transfer functions generate nonzero strain components E_{rr} and $E_{r\theta}$. The range for the calculations shown in Figure 15 is 10 km just as in Figure 8. The strains for the earthquake are slightly larger than for the megaton explosion. This is not true at all ranges because, as we shall show in the following, the earthquake strains decay at a much slower rate. Also, because different components of the strain tensor are nonzero, the peak shear strains are somewhat larger in the explosion case. The transfer operators for the earthquake source are generally simpler than for the explosion case meaning that we are probably obtaining a more reliable estimate of dynamic strain for the earthquake.

Figure 16 shows the transfer of the HOLT velocity record into strain. The strain traces on the right are not strongly altered from the velocity traces on the left. The changes in polarity that do or do not occur are just as predicted in Table 2. The smoothing out of the detail is primarily caused by the gaussian filter used in the deconvolution. The two nonzero strains are shown at the top of Figure 17 along with the trace of the strain tensor and the maximum shear. It is of interest to compare the peak strains for the HOLT record to those of the SCOTCH record from 6.1 km. The peak shear for SCOTCH is about twice as large and the peak compressive strain about three times as large. It is important to note, however, that the SCOTCH source is actually much closer to the station than the earthquake source. The depth of the earthquake is 9.5 km while that of SCOTCH is 0.97 km. A theoretical calculation of the strain for an earthquake source at the same depth and range as the SCOTCH record predicts that the strains from the earthquake would be slightly higher. Figure 18 shows the stresses associated with the HOLT strains. Stresses and strains from all 16 stations are given in Appendix 2. Figure 19 shows the decay of peak shear strain with range. The observations are shown as data points and the theoretical prediction of the model as a smooth curve. The theoretical curve was computed for the particular

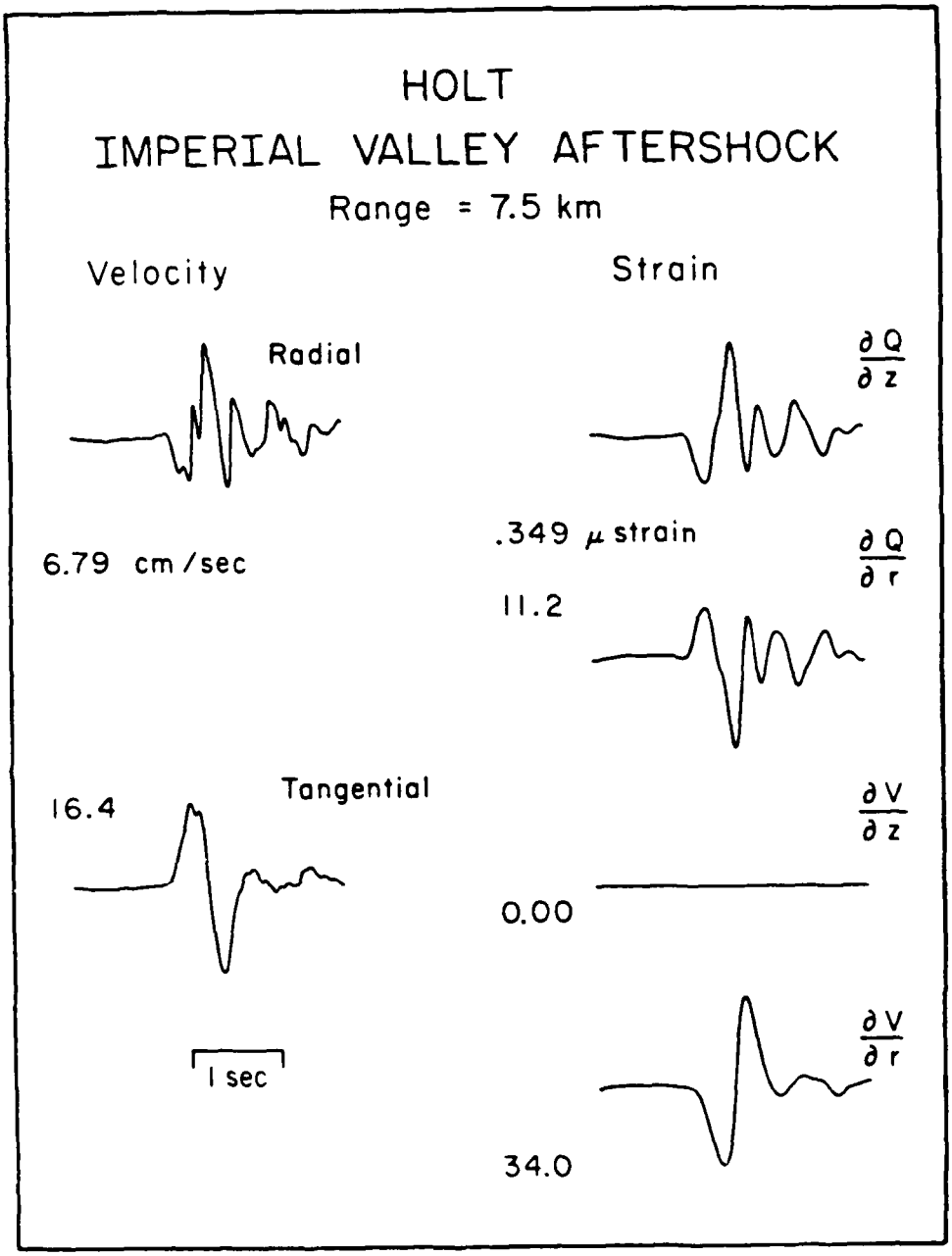

Figure 16. An example of the velocity to strain transfer for station HOLT from the Imperial Valley aftershock. The velocity pulses are shown on the left and the estimated strain pulses on the right.

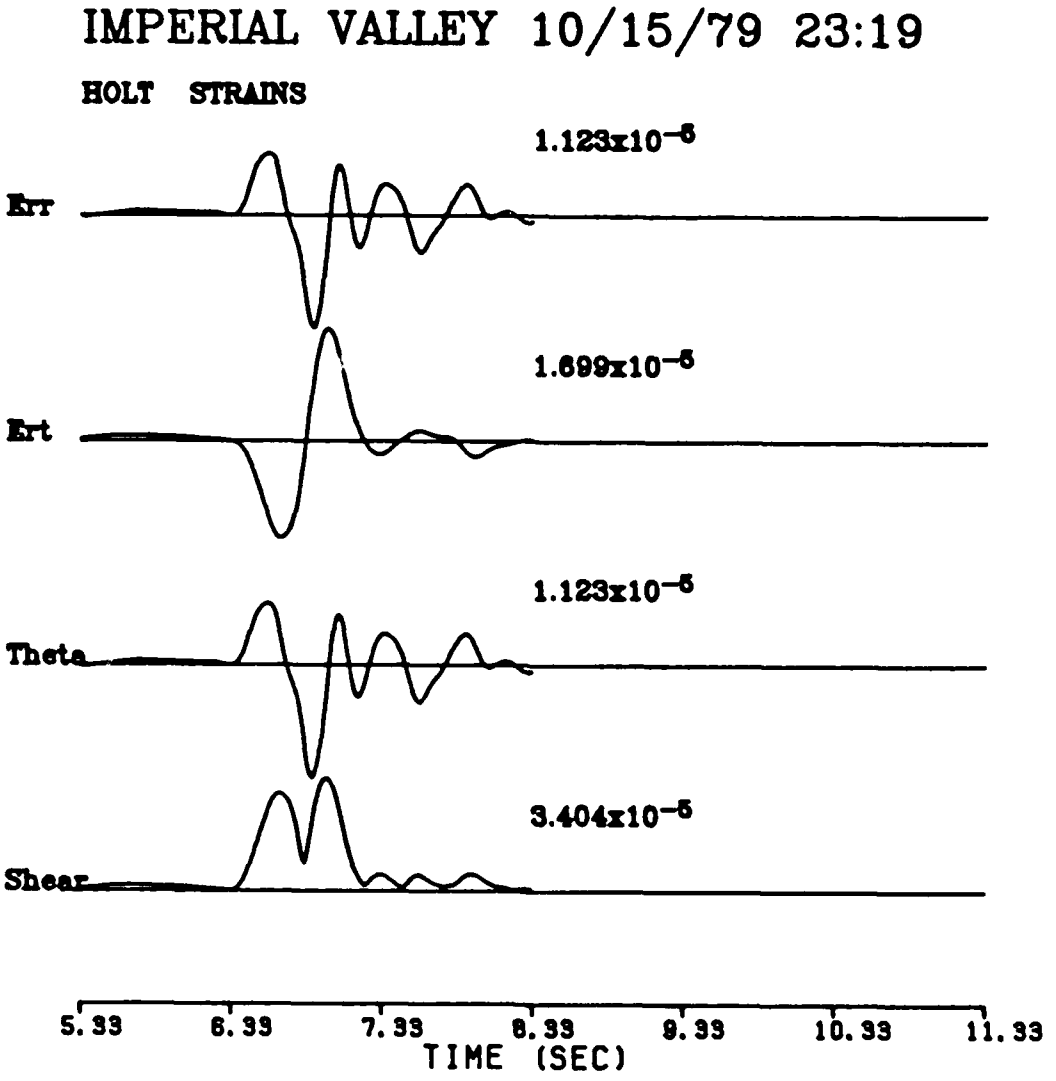

Figure 17. Strains from station HOLT from the Imperial valley aftershock. The top two traces are the nonzero strains in a cylindrical coordinate system. The third trace is the trace of the strain tensor. The bottom trace is the peak shear strain.

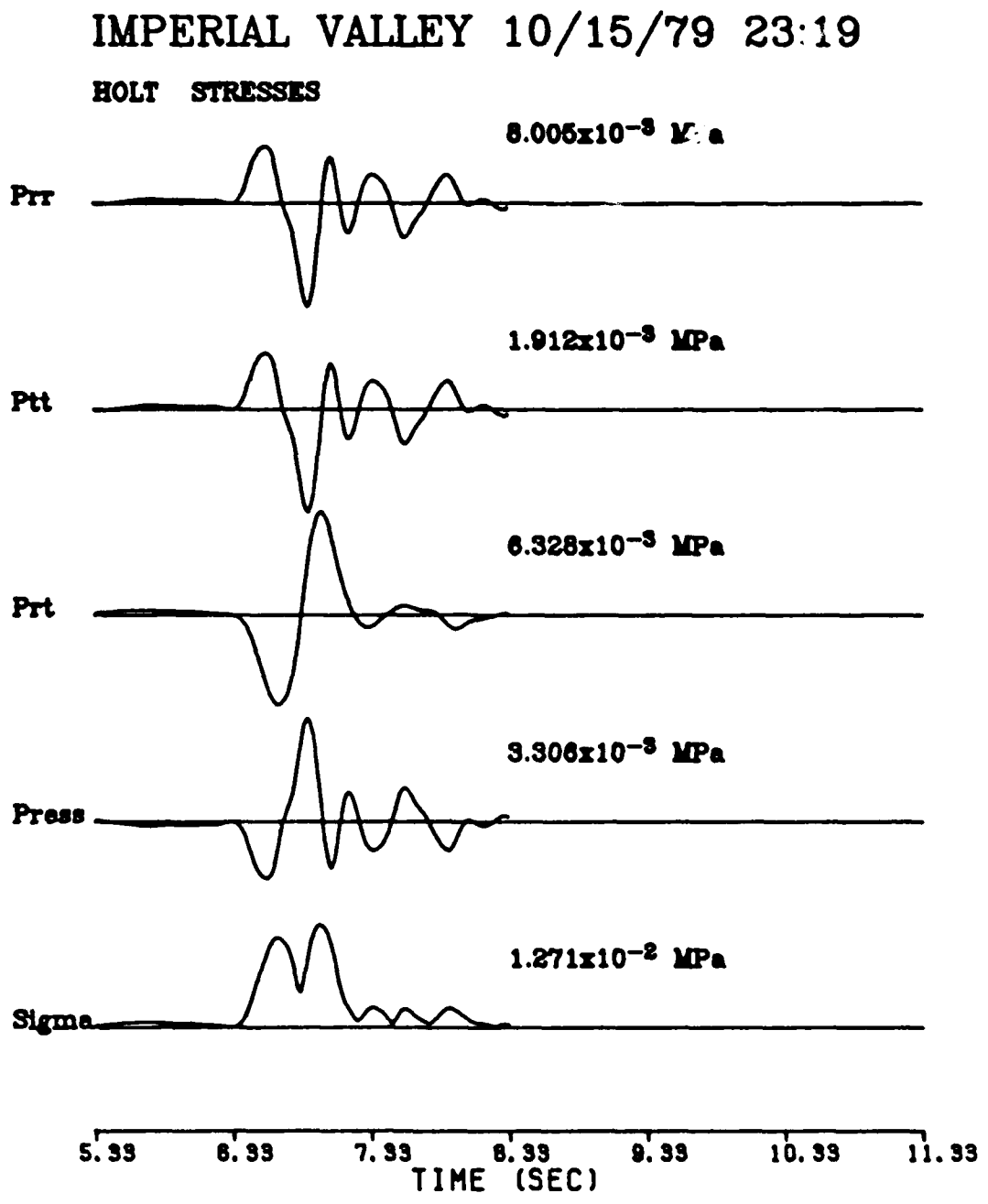

Figure 18. Stresses from station HOLT from the Imperial Valley aftershock. The top three traces are the nonzero stresses in a cylindrical coordinate system. The fourth trace is pressure and the fifth is peak shear stress.

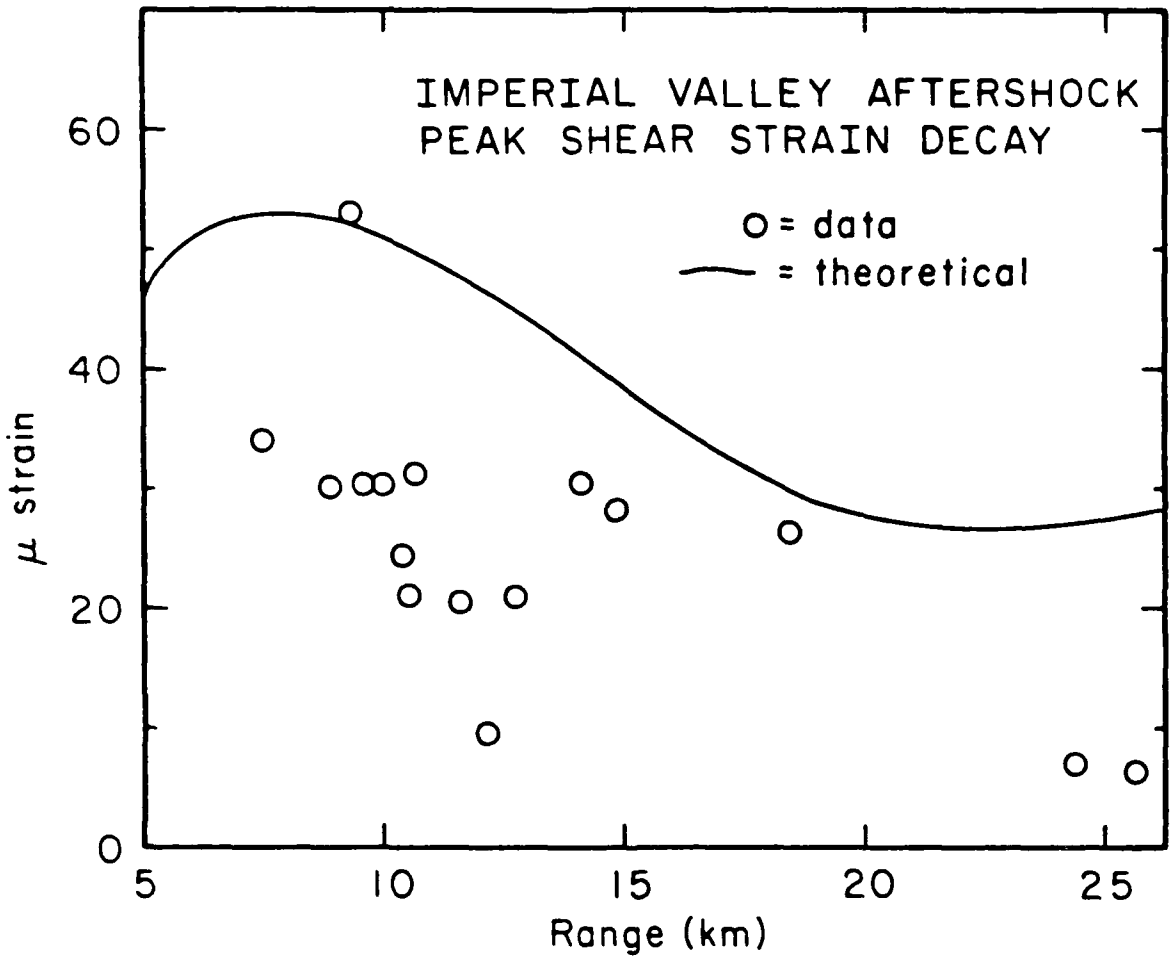

Figure 19. The decay of peak shear strain near to the Imperial Valley aftershock.

azimuth of 45° Here the SH and SV waves are equal amplitude and the peak shear strain is relatively high The data come from a variety of azimuths which is why many of the data points fall under the curve Also, the source model of Liu and Helmberger (1985) fails to correctly predict the ratio of SV to SH. The SH data alone suggest a moment of .42 x 10^{24} dyne-cm and the SV .73 x 10^{24} dyne-cm. The SH wave apparently has a more important effect in determining the peak shear strain in many cases. The peak shear for the earthquake at the surface of the earth is lower than for the explosions but decays much less rapidly with range. This is because of the vertical radiation pattern of the source and because the earthquake source is deeper The strains generated by the earthquake are large enough so that the nonlinear effects illustrated in Figure 2 are potentially significant.

DISCUSSION

The bulk of all seismic observations have been very successfuly explained using linear elastic theory. It seems doubtful that nonlinear processes could be of great importance without having been noted previously. On the other hand, the science is still evolving and new types of data are being studied Very high frequencies (5 to 20 hz) are being studied for potential use in discrimination between earthquakes and explosions. A thin, shallow layer with nonlinear response might have an effect on the generation of such energy but would be of no significance to 1 hz or lower frequency energy. If the nonlinear zone has different characteristics for explosions and earthquakes, it might alter how regional phases are initiated in the two cases Such a layer would obviously also be important to the generation of free surface phases such as pP. At low frequency such phases would appear as elastic reflections, whereas at very high frequency they would appear to be strongly attenuated. Some observations of nuclear explosions suggest that this is the

case Another piece of evidence that some nonlinear losses are occurring is the strong motion data of Liu and Helmberger (1985) which does suggest that effective Q in the near field of the Imperial Valley earthquake was very low

It is important to note that even if the nonlinear process indicated by the laboratory data does occur in the earth and is significant, it is not clear exactly how it would manifest itself. At one level of approximation effective Q could be considered to be a function of time with a value dictated by the strain wave field. It is difficult to imagine exactly what effect this would have. Stewart et al. (1983) have suggested a model for how the nonlinearity would depend on the density of cracks in the medium and the overburden pressure presuming that it is indeed related to frictional sliding on cracks. They proposed that

$$Q = P^{4/3}/k\lambda E \qquad (9)$$

where P is the overburden pressure, k is a constant function of the material's elastic parameters, λ is the crack density and E is the strain amplitude. Day and Minster (1986) suggest an equivalent linear method for solving wave propagation problems in materials behaving in a weakly nonlinear fashion, but their method does not adapt easily to realistic media. Much additional progress will be needed before the role played by high strain nonlinearity in seismic wave propagation is understood.

CONCLUSIONS

The close relationship between velocity and strain wave pulses in a whole space appears to be maintained for the most part in a layered half space. The large data bases of near field velocity records which have been collected over the years can thus be transformed into a data base of near field dynamic stress and strain records. Near field strains for a large explosion appear to be as high as 10^{-3} at the surface of the earth. Those near to a small

earthquake appear to be about 10^{-5} at the surface, though the source is much deeper. These strains are large enough so that they may induce a nonlinear response from near surface materials.

REFERENCES

Burdick, L. J., T. Wallace and T. Lay, Modeling the near field and teleseismic observations from the Amchitka test site, *J. Geophys. Res.*, **89**, 4373-4388, 1984.

Burger, R. W., T. Lay, and L. J. Burdick, Average Q and yield estimates from the Pahute Mesa test site, *Bull. Seism. Soc. Am.*, (in press), 1987.

Day, S. M. and J. B. Minster, Decay of wave fields near to an explosive source due to high strain nonlinear attenuation, *J. Geophys. Res.*, **91**, 2113-2122, 1986.

Carroll, R. D., Preliminary interpretation of geophysical logs, UE2OF, Pahute Mesa, Nevada Test Site, technical letter: special studies-I-37, supplement 1, *U. S. Geol Survey Open File Report*, 1966.

Haskell, N. A., Analytic approximation for the elastic radiation from a contained underground explosion, *J. Geophys. Res.*, 7, 2583-2587, 1967.

Hamilton, R. M. and J. H. Healy, Aftershocks of the BENHAM nuclear explosion, *Bull. Seism. Soc. Am.*, **59**, 2271-2281, 1969.

Heaton, T. H. and D. V. Helmberger, Predictability of strong ground motion in the Imperial Valley: modeling the M4.9, November 4, 1976 Brawley Earthquake, *Bull. Seism. Soc. Am.*, **68**, 31-48, 1978.

Helmberger, D. V., Generalized ray theory for shear dislocations, *Bull. Seism. Soc. Am.*, **64**, 45-64, 1974.

Helmberger, D. V. and D. M. Hadley, Seismic source functions and teleseismic observations of the NTS events Jorum and Handley, *Bull. Seism. Soc. Am.*, 71, 51-67, 1981.

Langston, C. A. and D. V. Helmberger, A procedure for modeling shallow dislocation sources, *Geophys. J. R. astr. Soc.*, **42**, 117-130, 1975.

Liu, H. and D. V. Helmberger, The 23:19 aftershock of the 15 October 1979 Imperial Valley earthquake: more evidence for an asperity, *Bull. Seism. Soc. Am.*, 75, 689-708, 1985.

Mavko, G. M., Frictional attenuation:and inherent amplitude dependence, *J. Geophys. Res.*, **84**, 4765-4775, 1979.

Stewart, R. R. , M. N. Toksoz and A. Timur, Strain dependent attenuation: observations and a proposed mechanism, *J. Geophys. Res.*, **88**, 546-554, 1983.

Wiggins, R. A., and D. V. Helmberger, Synthetic seismogram computation through expansion in generalized rays, *Geophys. J. R. astr Soc.*, 37, 73-90, 1974.

APPENDIX 1.

PROCESSED NUCLEAR EXPLOSION RECORDS

ALMENDRO 5.1 KM.

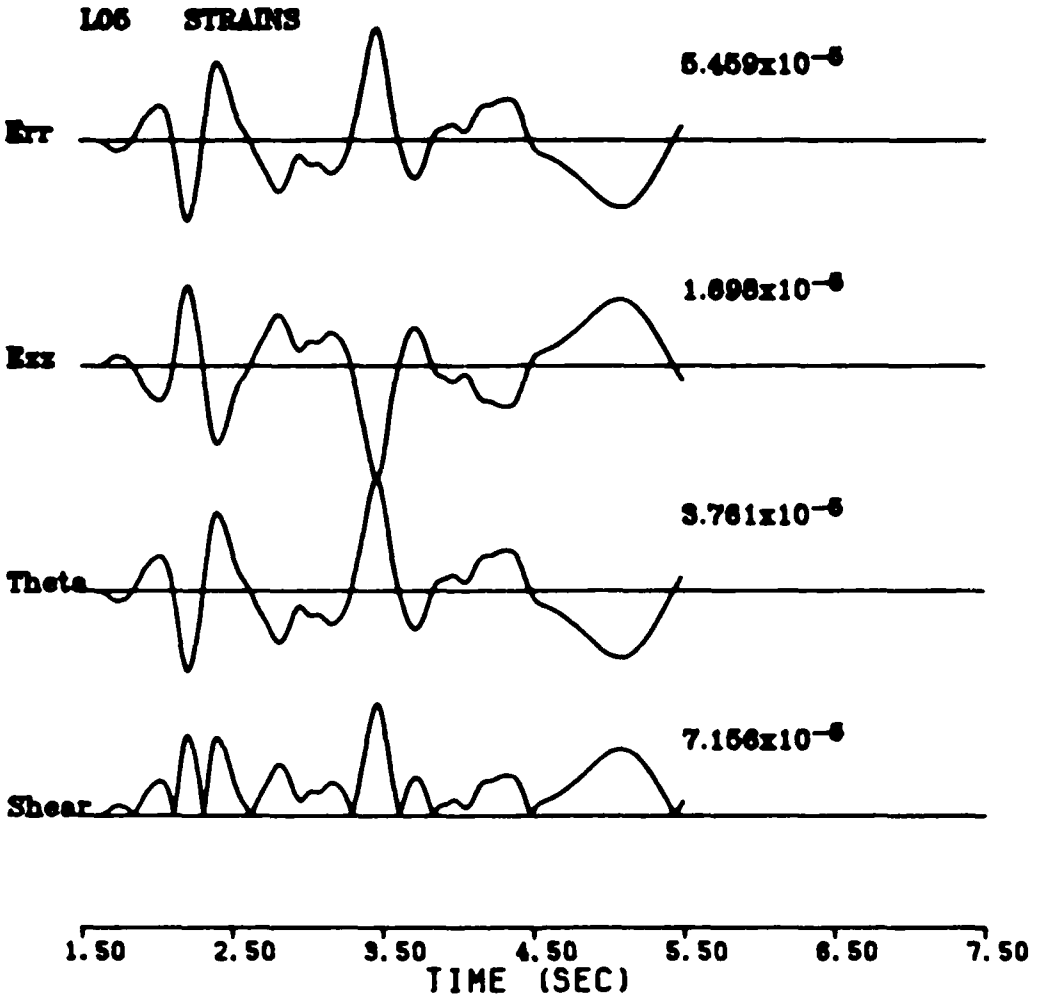

ALMENDRO 5.1 KM.

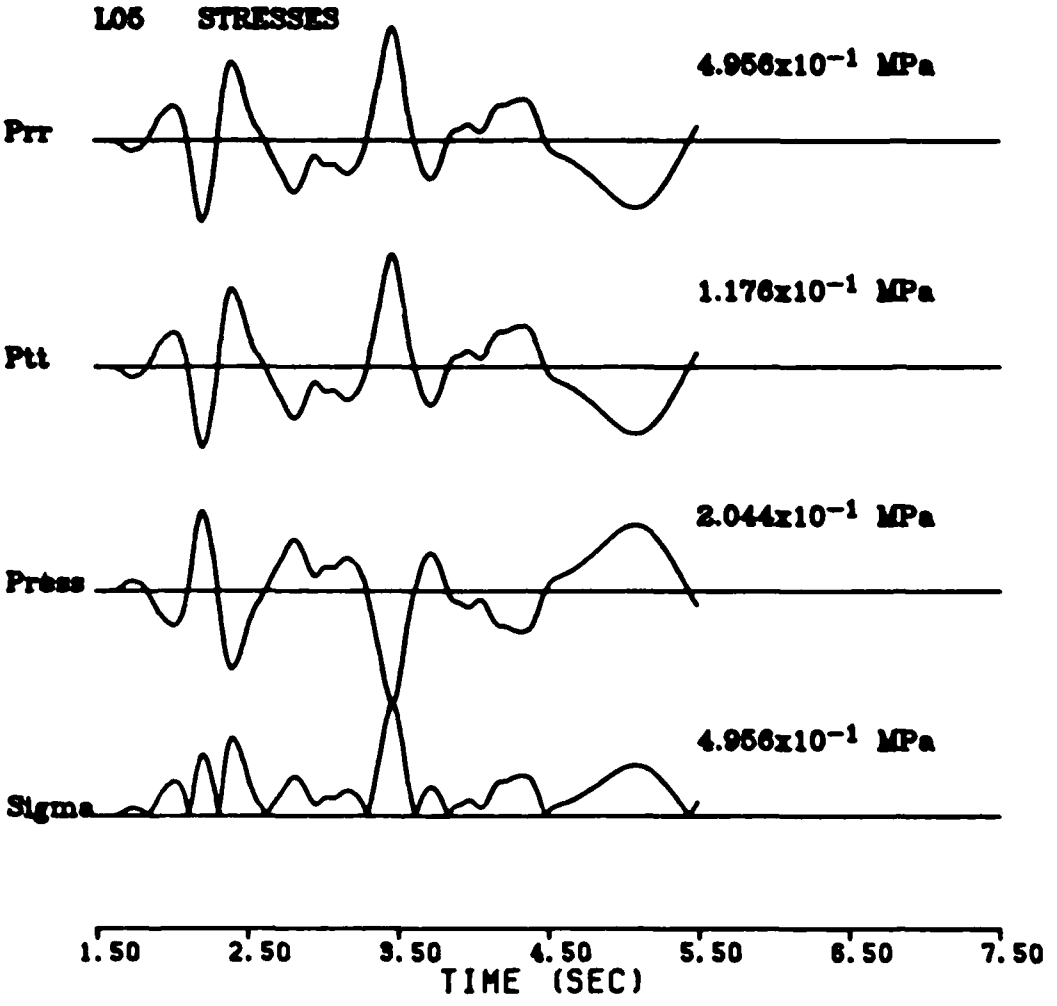

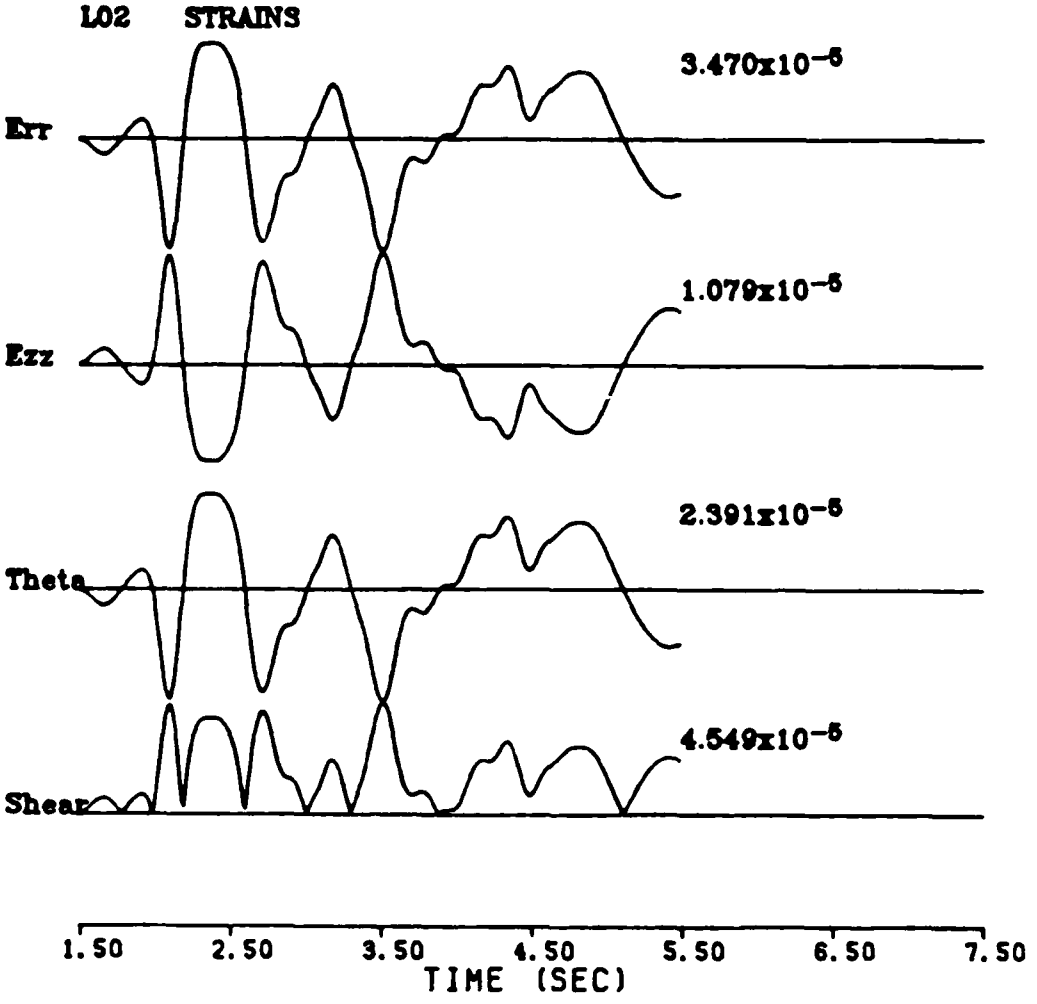
ALMENDRO 6.1 KM
L02 STRAINS
Err
3.470x10⁻⁶
Ezz
1.079x10⁻⁶
Theta
2.391x10⁻⁶
Shear
4.549x10⁻⁶
1.50
2.50
3.50
4.50
5.50
6.50
7.50
TIME (SEC)

ALMENDRO 6.1 KM

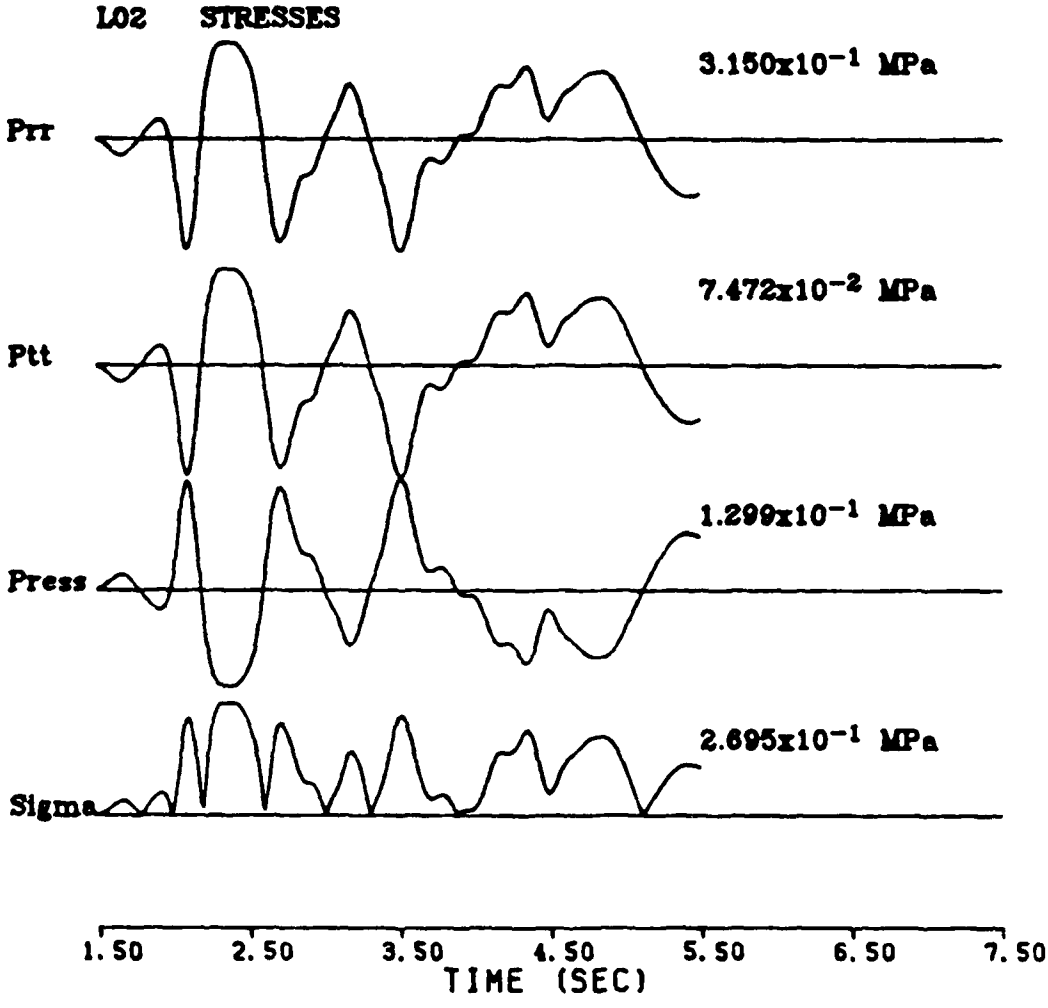

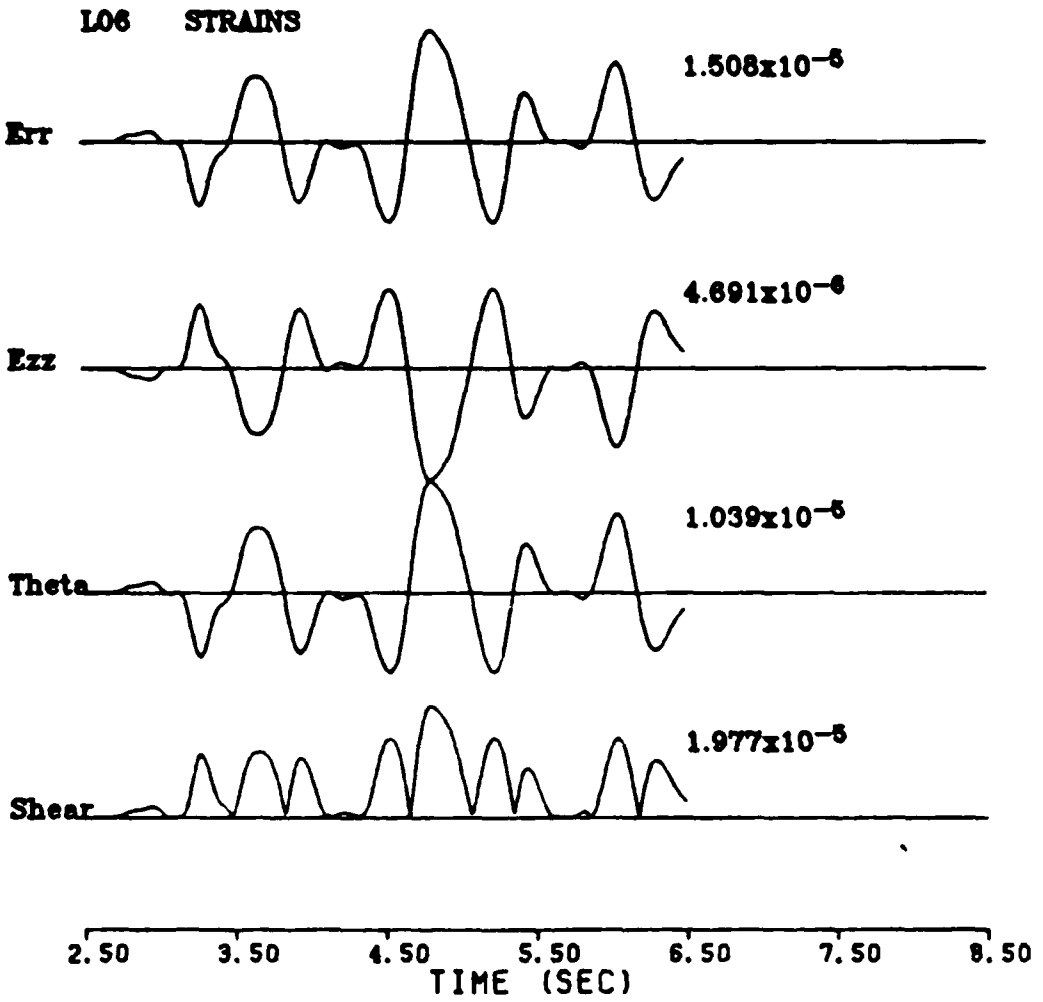
ALMENDRO 10.0 KM
LOG STRAINS
Err
1.508x10⁻⁵
Ezz
4.691x10⁻⁶
Theta
1.039x10⁻⁵
Shear
1.977x10⁻⁵
2.50
3.50
4.50
5.50
6.50
7.50
8.50
TIME (SEC)

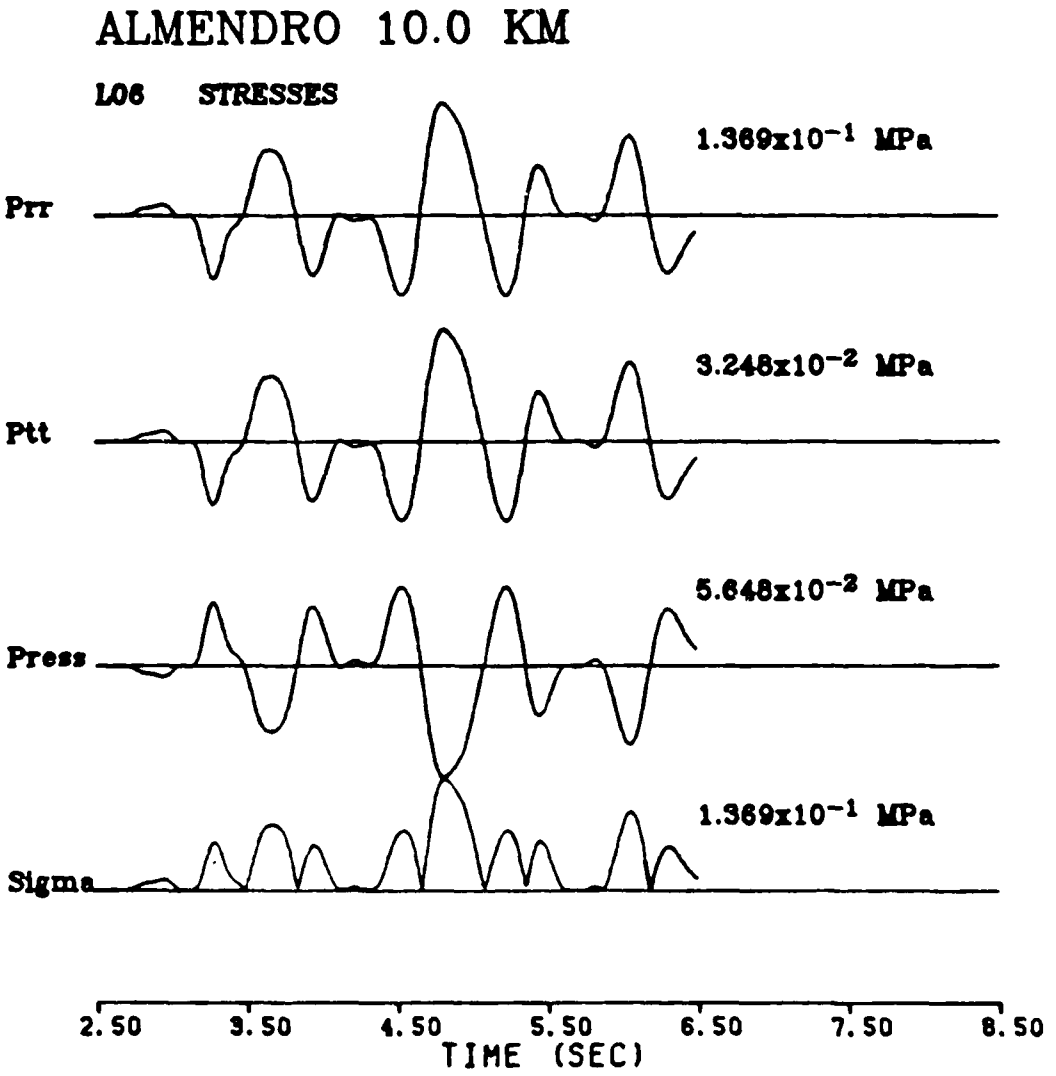
ALMENDRO 10.0 KM
L06 STRESSES
Prr
1.369x10⁻¹ MPa
Ptt
3.248x10⁻² MPa
Press
5.648x10⁻² MPa
Sigma
1.369x10⁻¹ MPa
2.50
3.50
4.50
5.50
6.50
7.50
8.50
TIME (SEC)

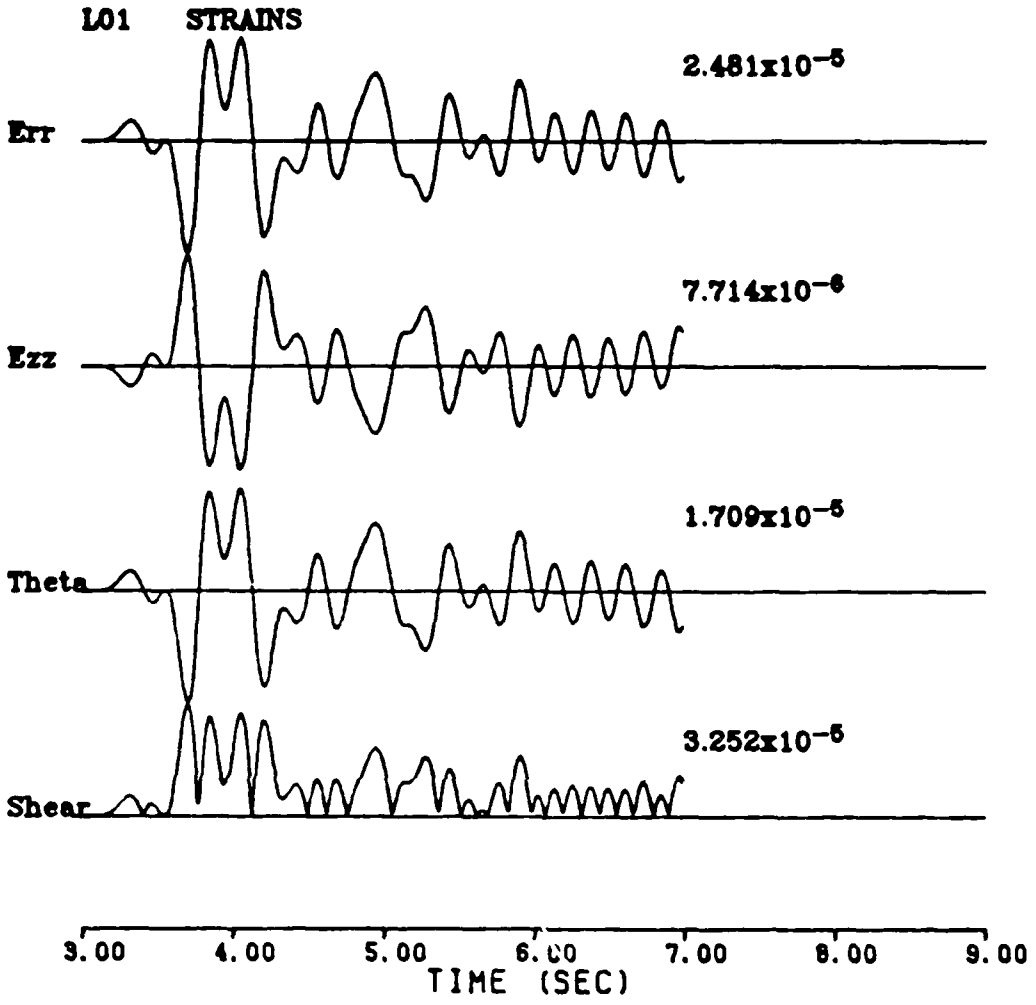
ALMENDRO 12.6 KM
L01 STRAINS
2.481x10⁻⁵
Err
7.714x10⁻⁶
Ezz
1.709x10⁻⁵
Theta
3.252x10⁻⁵
Shear
3.00
4.00
5.00
6.00
7.00
8.00
9.00
TIME (SEC)

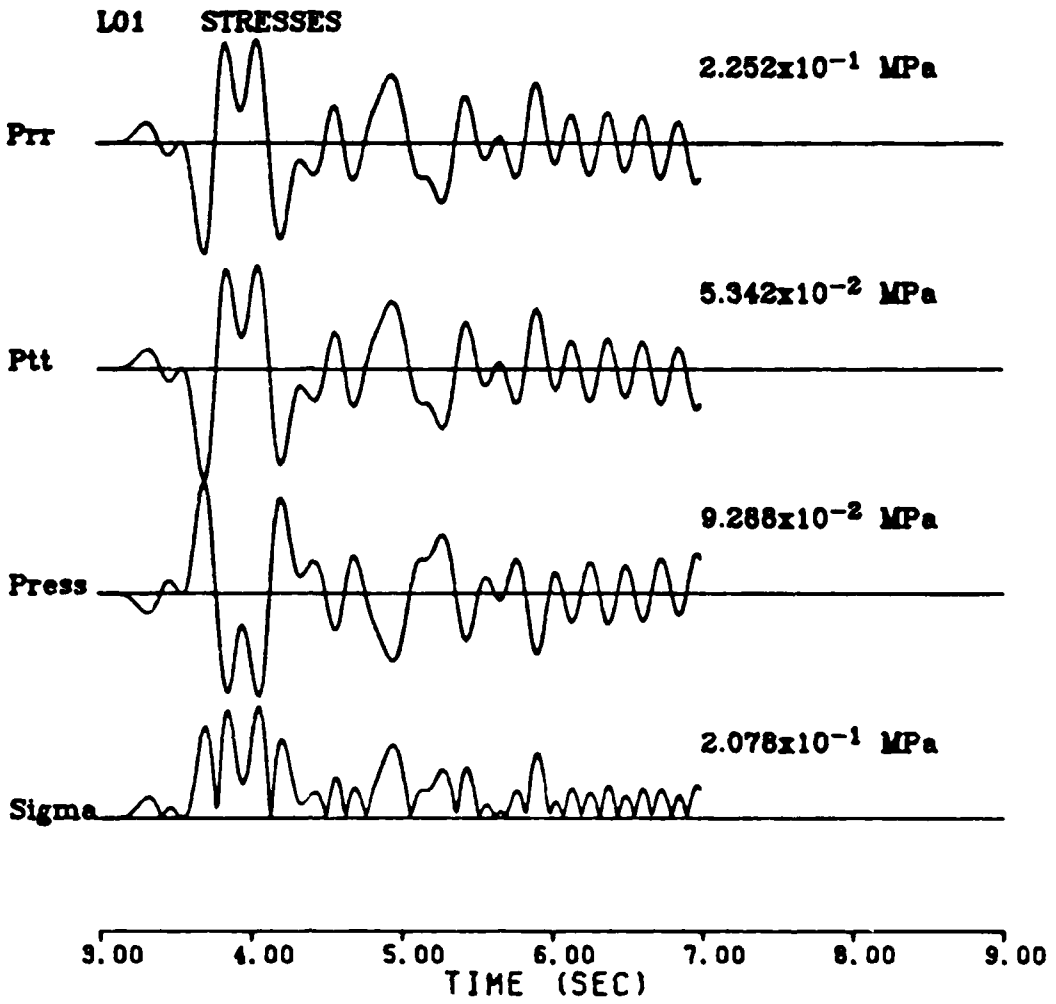
ALMENDRO 12.6 KM
L01 STRESSES
2.252x10⁻¹ MPa
Prr
5.342x10⁻² MPa
Ptt
9.288x10⁻² MPa
Press
2.078x10⁻¹ MPa
Sigma
3.00
4.00
5.00
6.00
7.00
8.00
9.00
TIME (SEC)

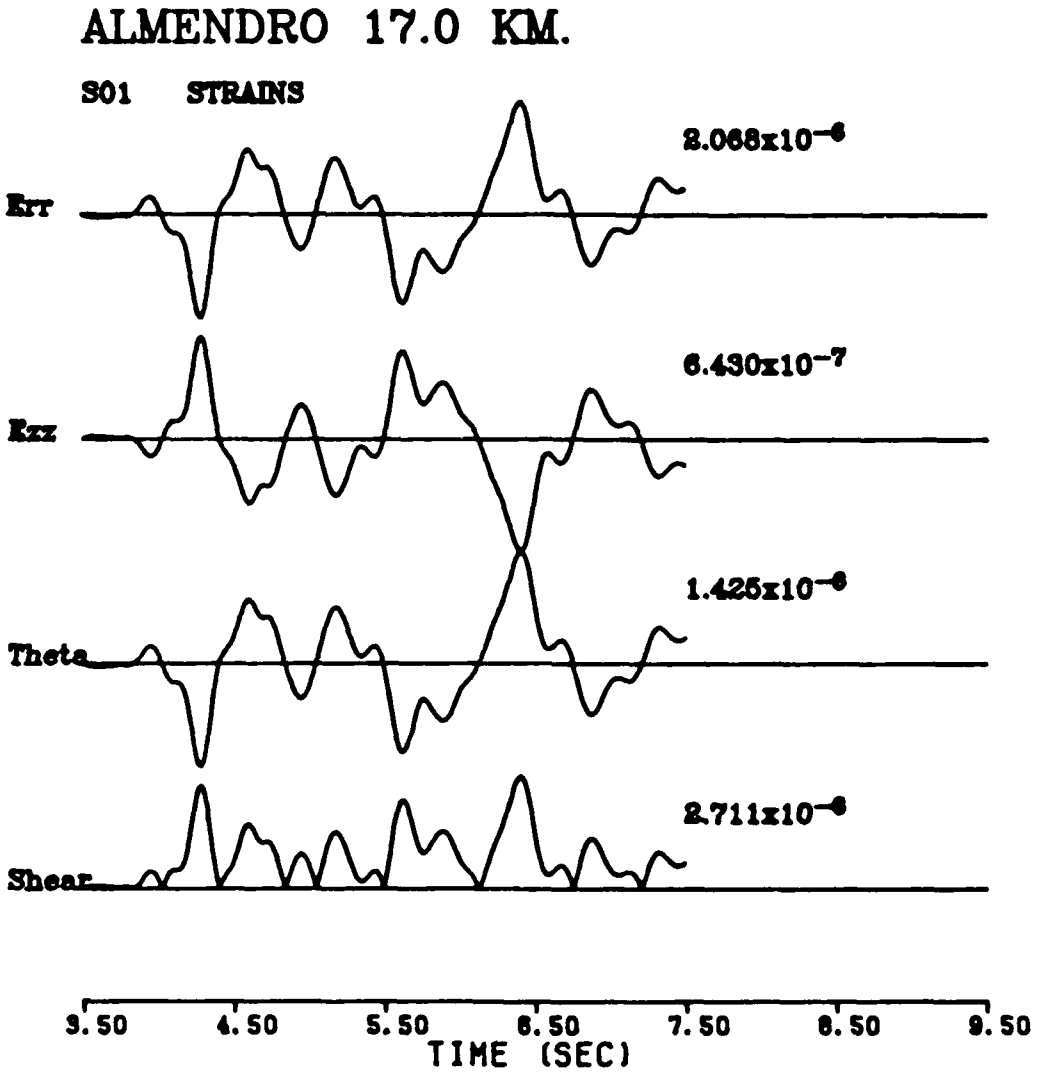
ALMENDRO 17.0 KM.
S01 STRAINS
2.068x10⁻⁶
Err
6.430x10⁻⁷
Ezz
1.425x10⁻⁶
Theta
2.711x10⁻⁶
Shear
3.50
4.50
5.50
6.50
7.50
8.50
9.50
TIME (SEC)

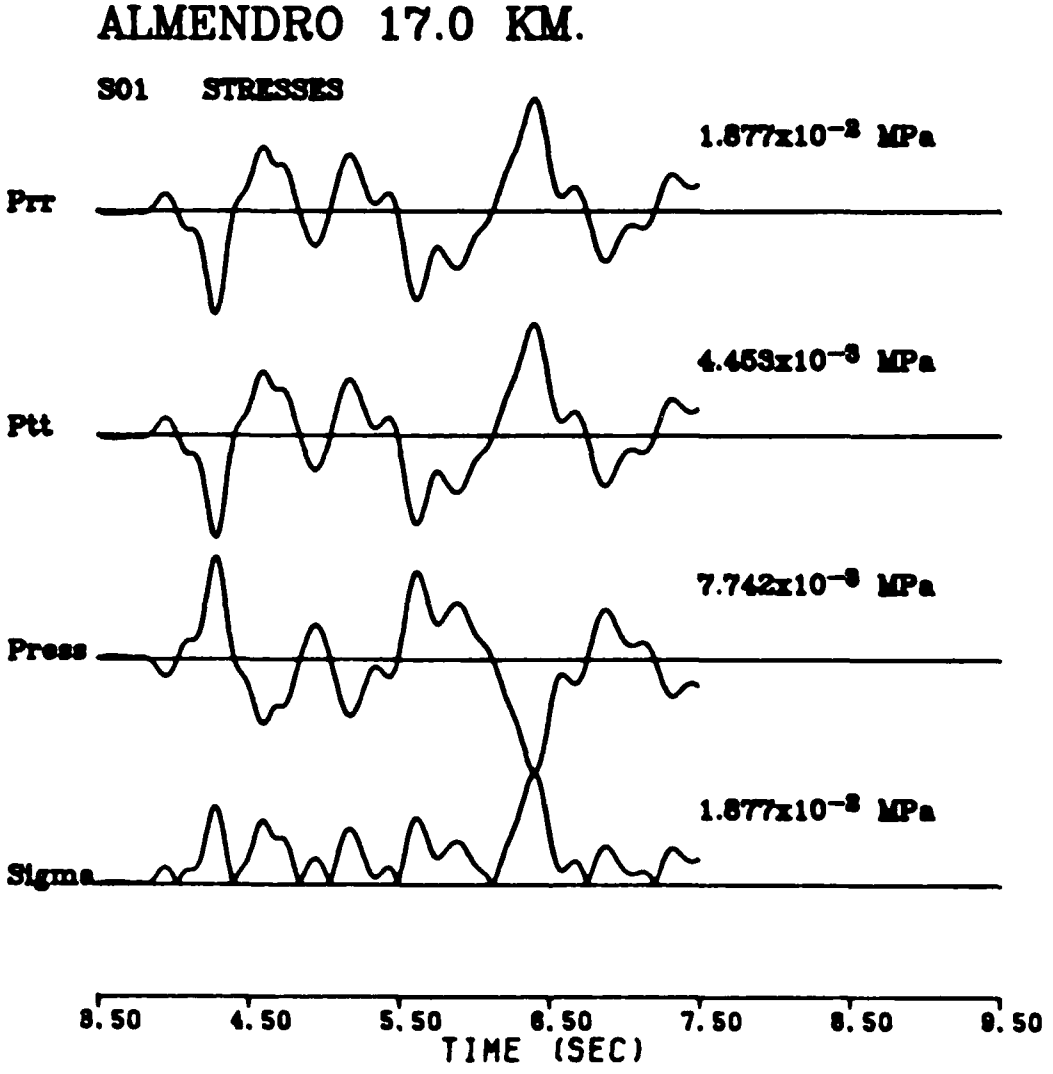
ALMENDRO 17.0 KM.
S01 STRESSES
Prr
1.877x10⁻² MPa
Ptt
4.453x10⁻³ MPa
Press
7.742x10⁻³ MPa
Sigma
1.877x10⁻² MPa
3.50
4.50
5.50
6.50
7.50
8.50
9.50
TIME (SEC)

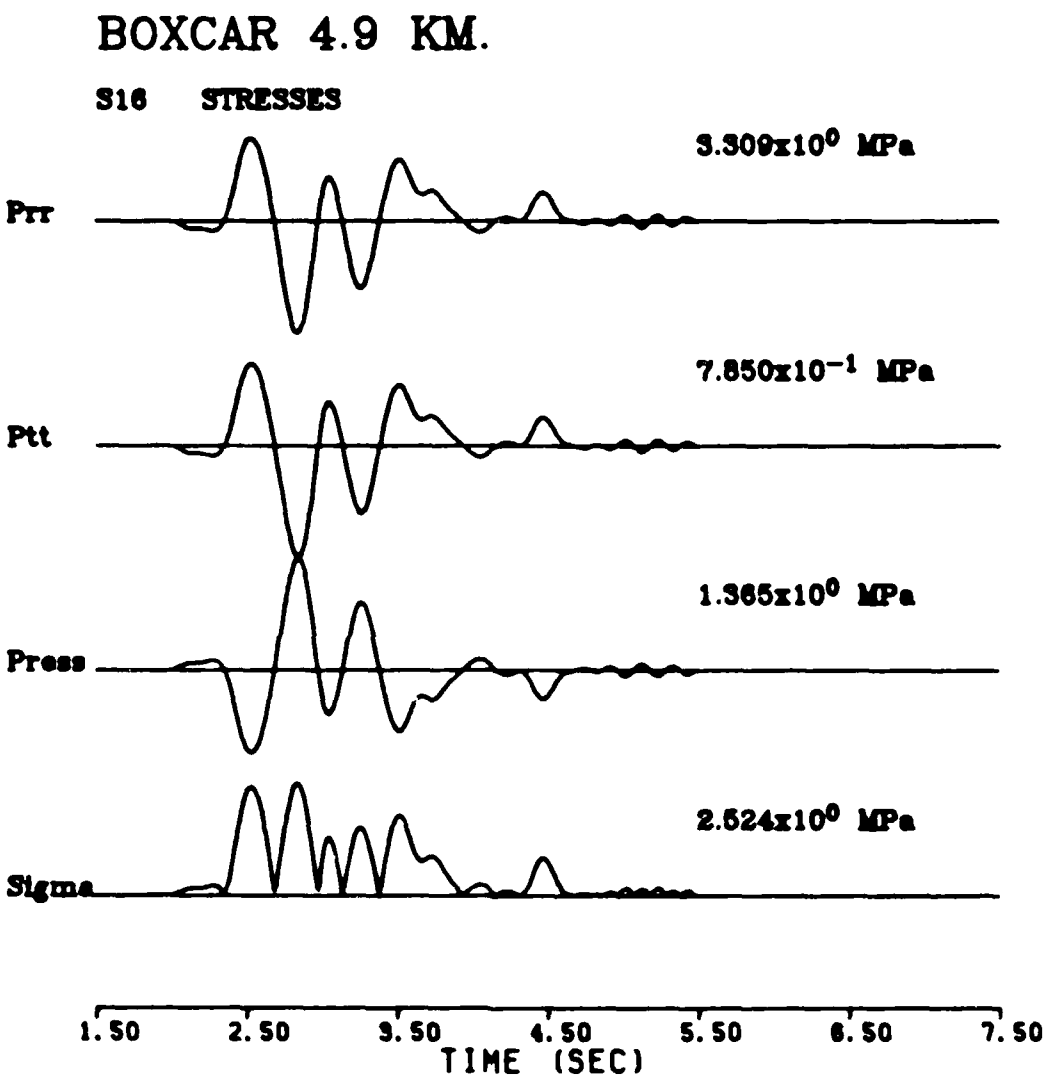
BOXCAR 4.9 KM.
S16 STRESSES
3.309x10^0 MPa
Prr
7.850x10^-1 MPa
Ptt
1.365x10^0 MPa
Press
2.524x10^0 MPa
Sigma
1.50
2.50
3.50
4.50
5.50
6.50
7.50
TIME (SEC)

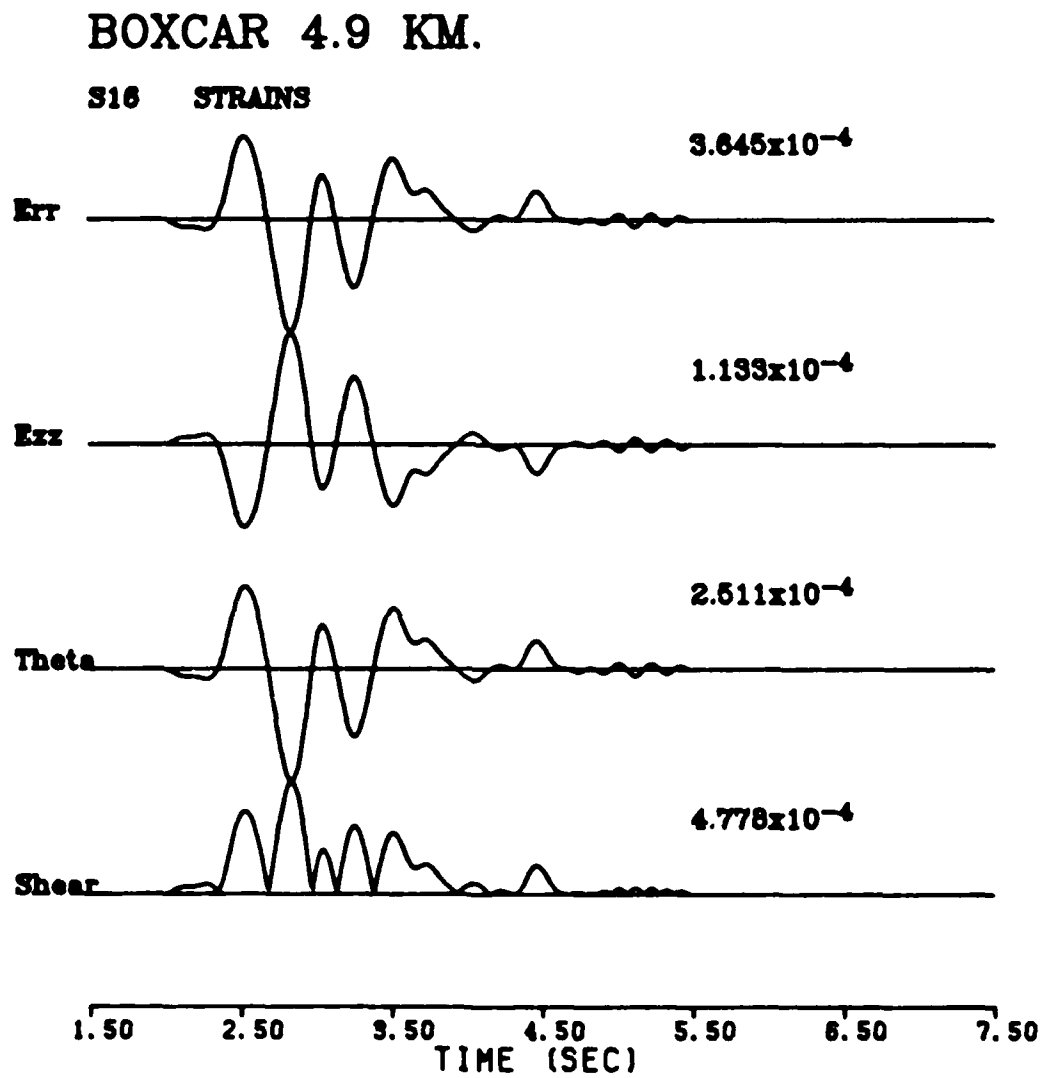
BOXCAR 4.9 KM.
S16 STRAINS
3.645x10⁻⁴
Err
1.133x10⁻⁴
Ezz
2.511x10⁻⁴
Theta
4.778x10⁻⁴
Shear
1.50
2.50
3.50
4.50
5.50
6.50
7.50
TIME (SEC)

BOXCAR 7.3 KM.

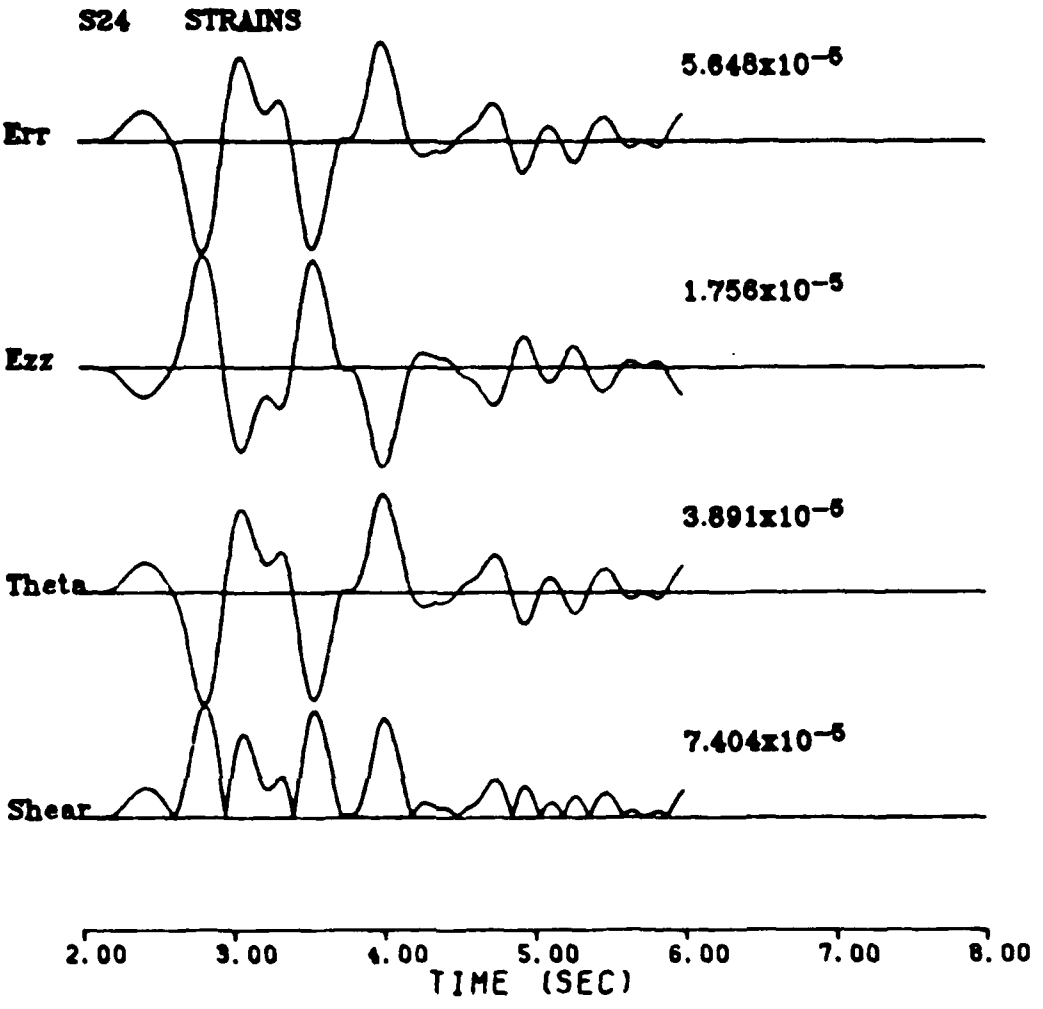
S24 STRAINS
5.648x10⁻⁵
Err
1.756x10⁻⁵
Ezz
3.891x10⁻⁵
Theta
7.404x10⁻⁵
Shear
2.00
3.00
4.00
5.00
6.00
7.00
8.00
TIME (SEC)

BOXCAR 7.3 KM.

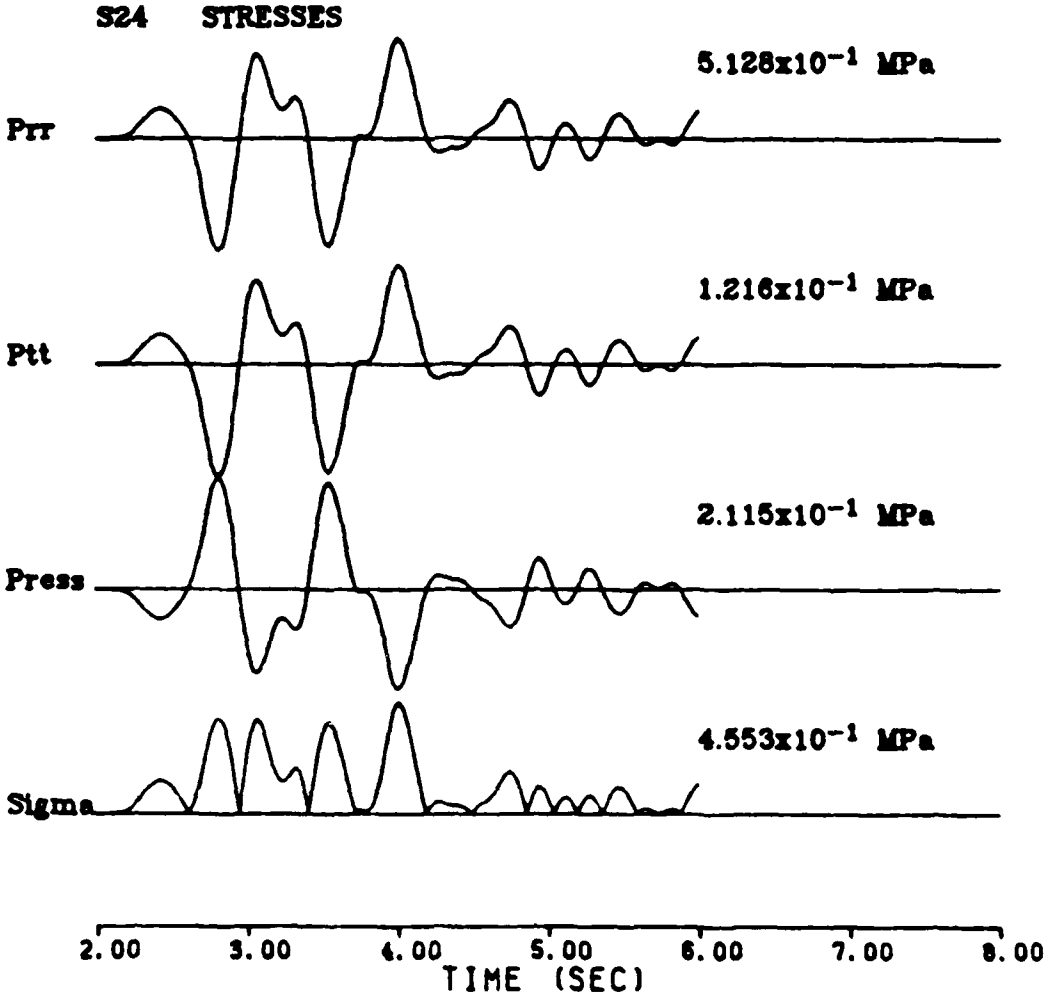
S24 STRESSES
5.128x10⁻¹ MPa
Prr
1.216x10⁻¹ MPa
Ptt
2.115x10⁻¹ MPa
Press
4.553x10⁻¹ MPa
Sigma
2.00
3.00
4.00
5.00
6.00
7.00
8.00
TIME (SEC)

BOXCAR 10.4 KM.

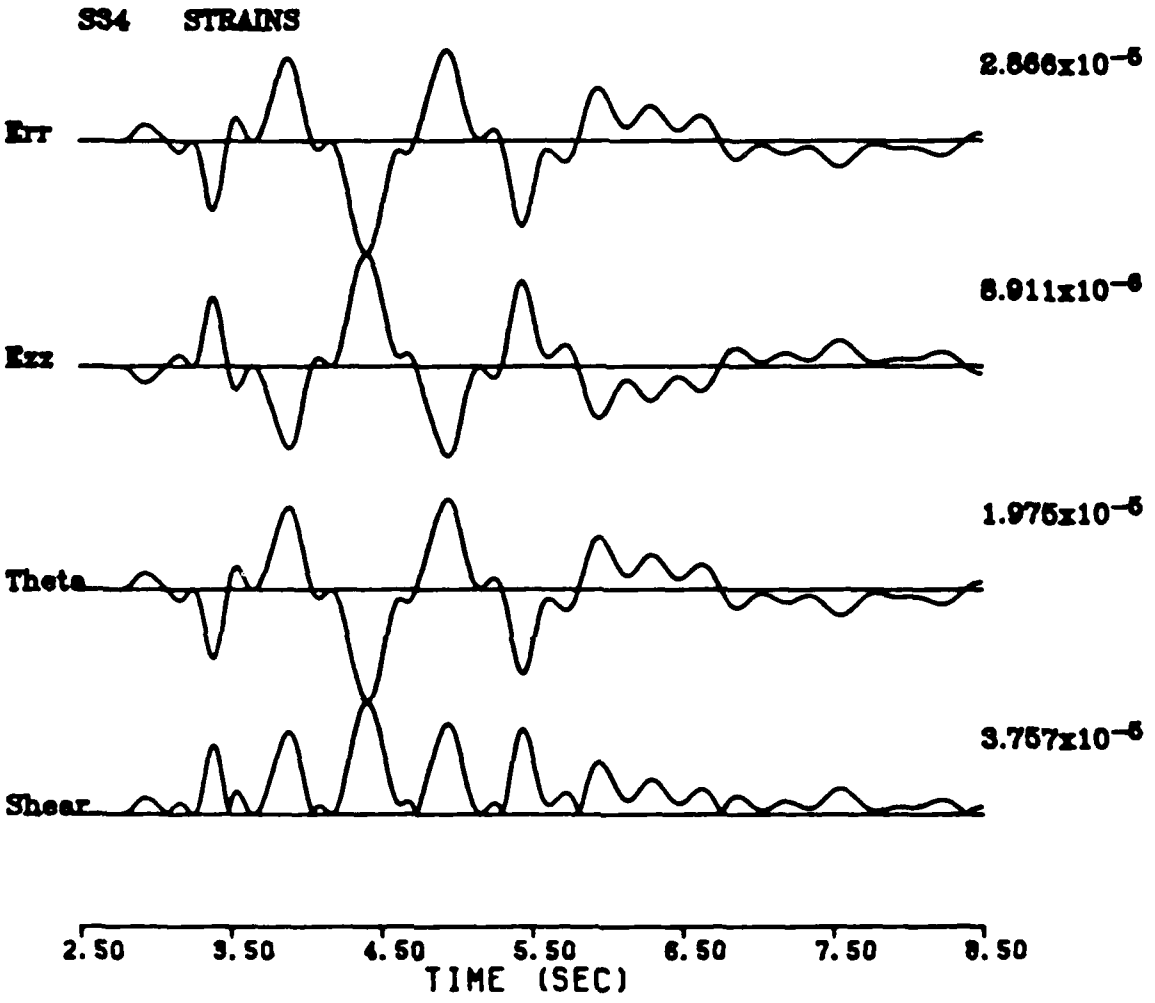

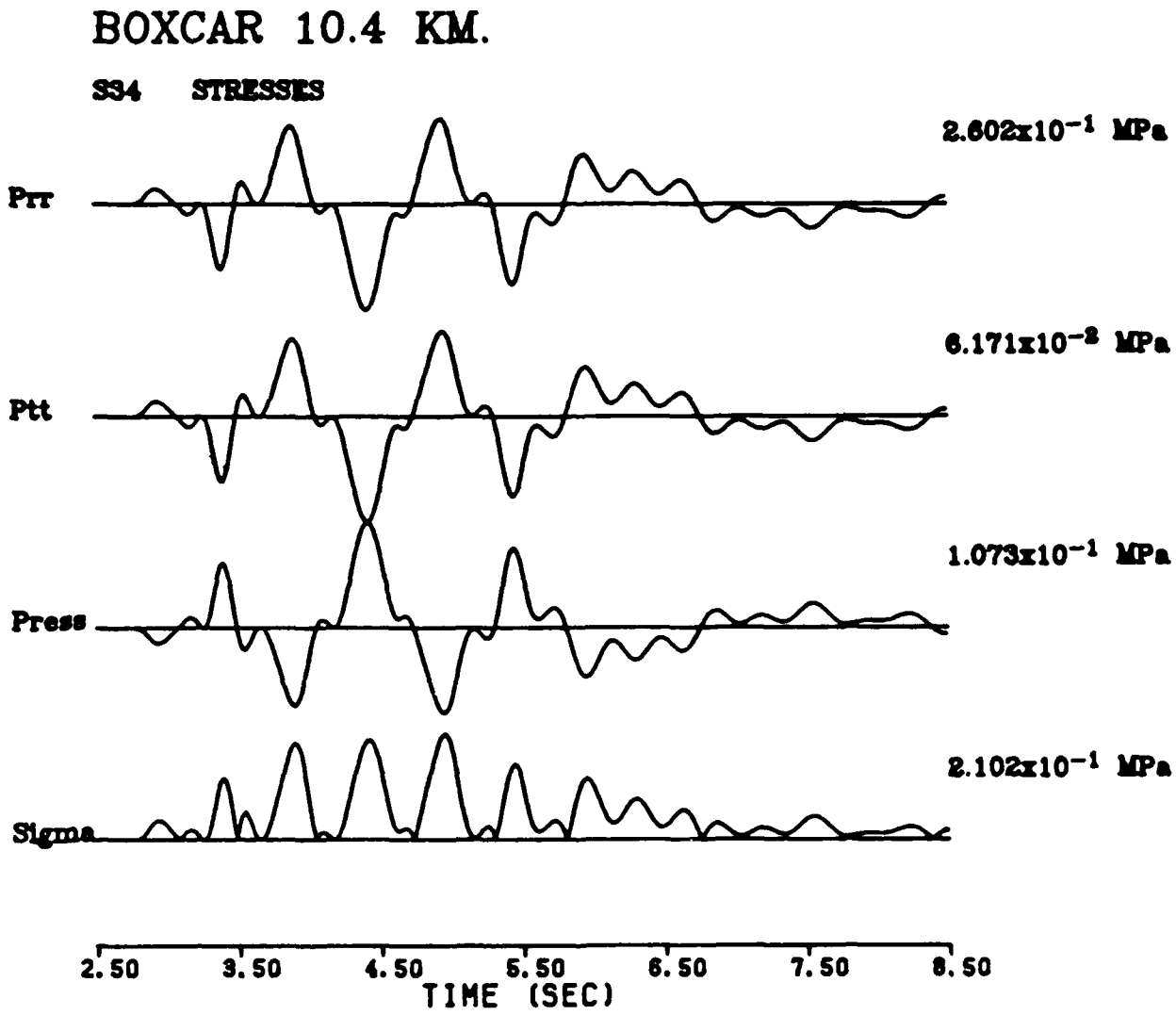
BOXCAR 10.4 KM.
S34 STRESSES
2.602x10-1 MPa
Prr
6.171x10-2 MPa
Ptt
1.073x10-1 MPa
Press
2.102x10-1 MPa
Sigma
2.50
3.50
4.50
5.50
6.50
7.50
8.50
TIME (SEC)

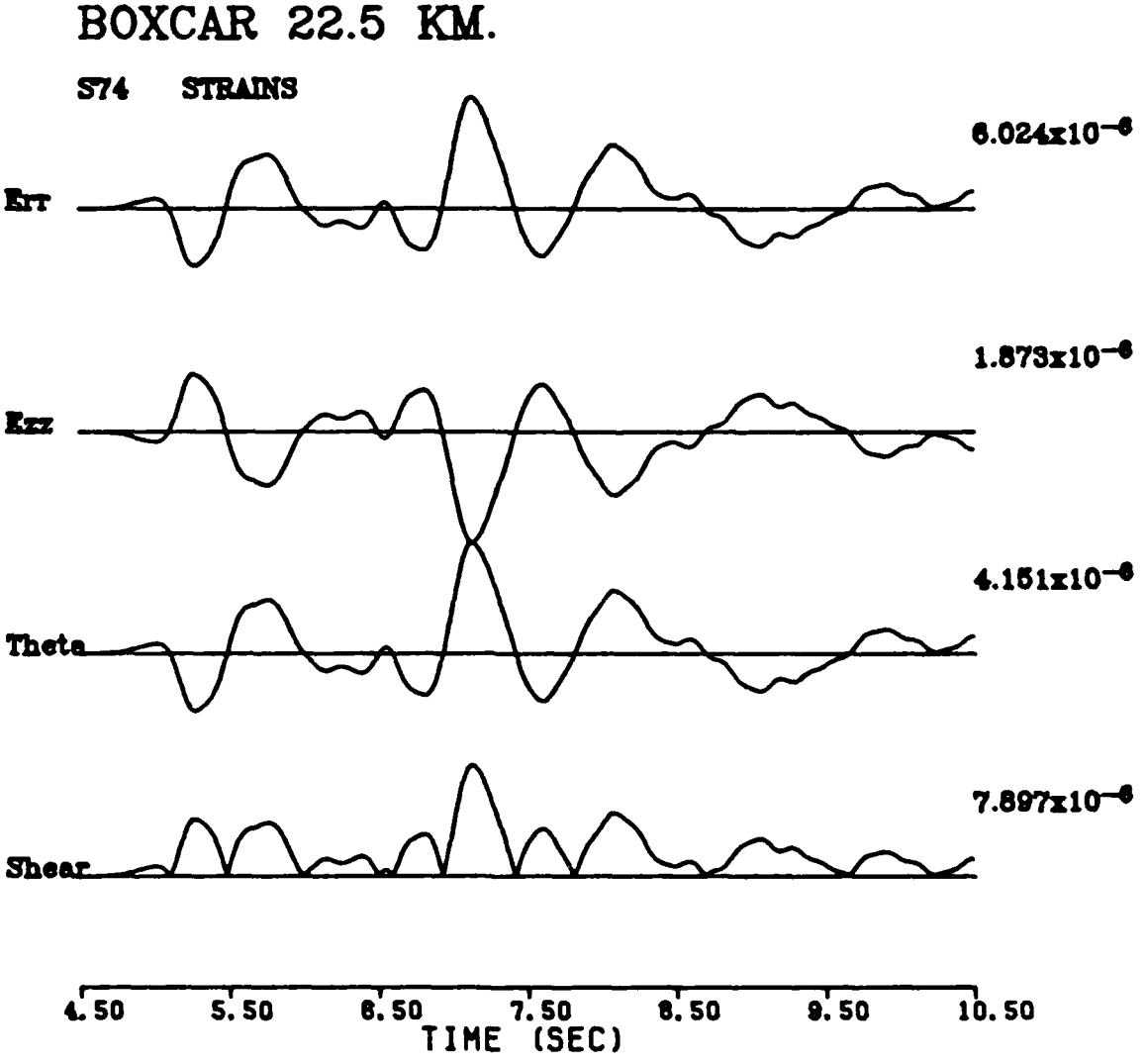
BOXCAR 22.5 KM.
S74 STRAINS
6.024x10⁻⁶
Err
1.873x10⁻⁶
Ezz
4.151x10⁻⁶
Theta
7.897x10⁻⁶
Shear
4.50
5.50
6.50
7.50
8.50
9.50
10.50
TIME (SEC)

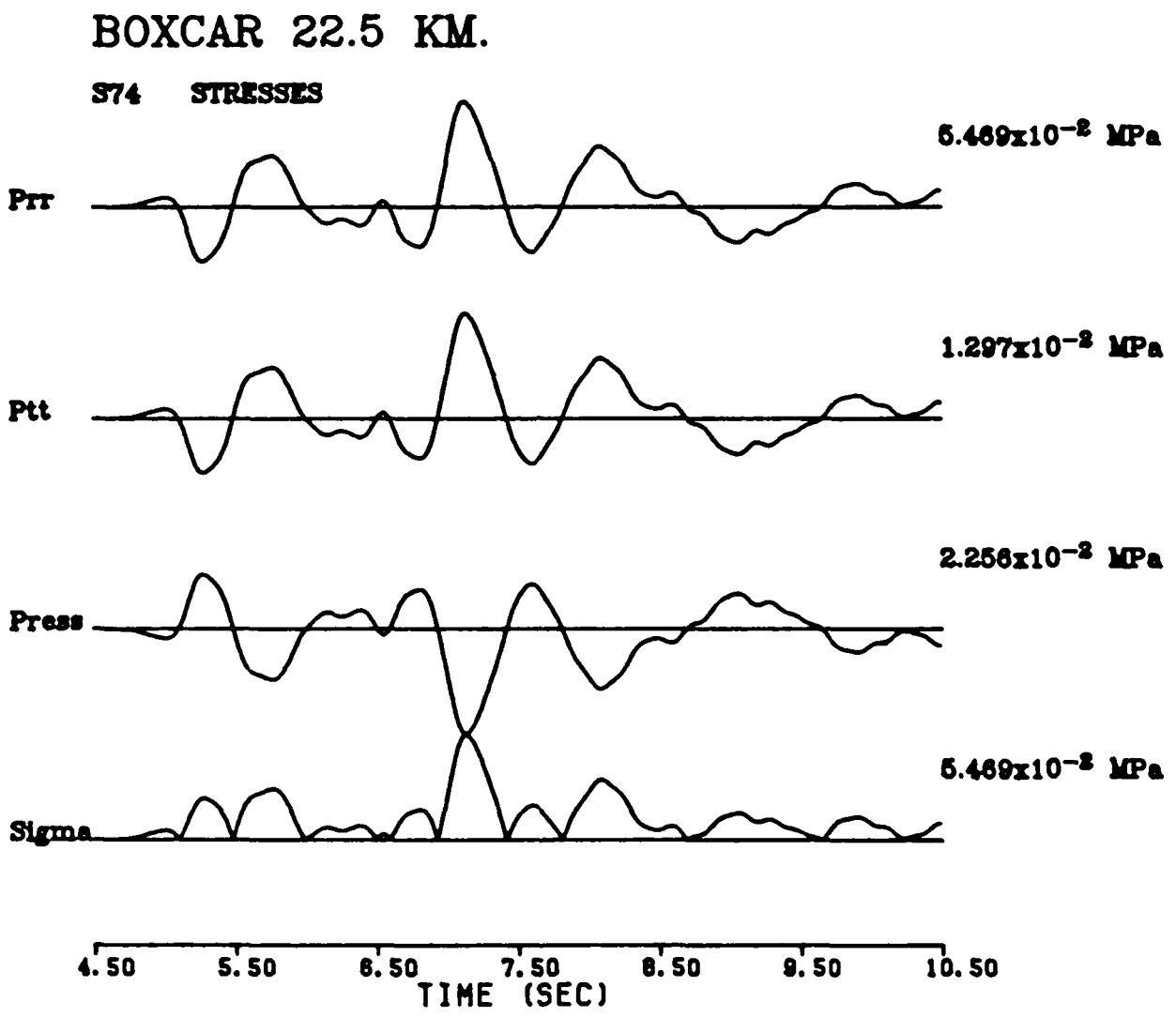
BOXCAR 22.5 KM.
S74 STRESSES
5.469x10-2 MPa
Prr
1.297x10-2 MPa
Ptt
2.256x10-2 MPa
Press
5.469x10-2 MPa
Sigma
4.50
5.50
6.50
7.50
8.50
9.50
10.50
TIME (SEC)

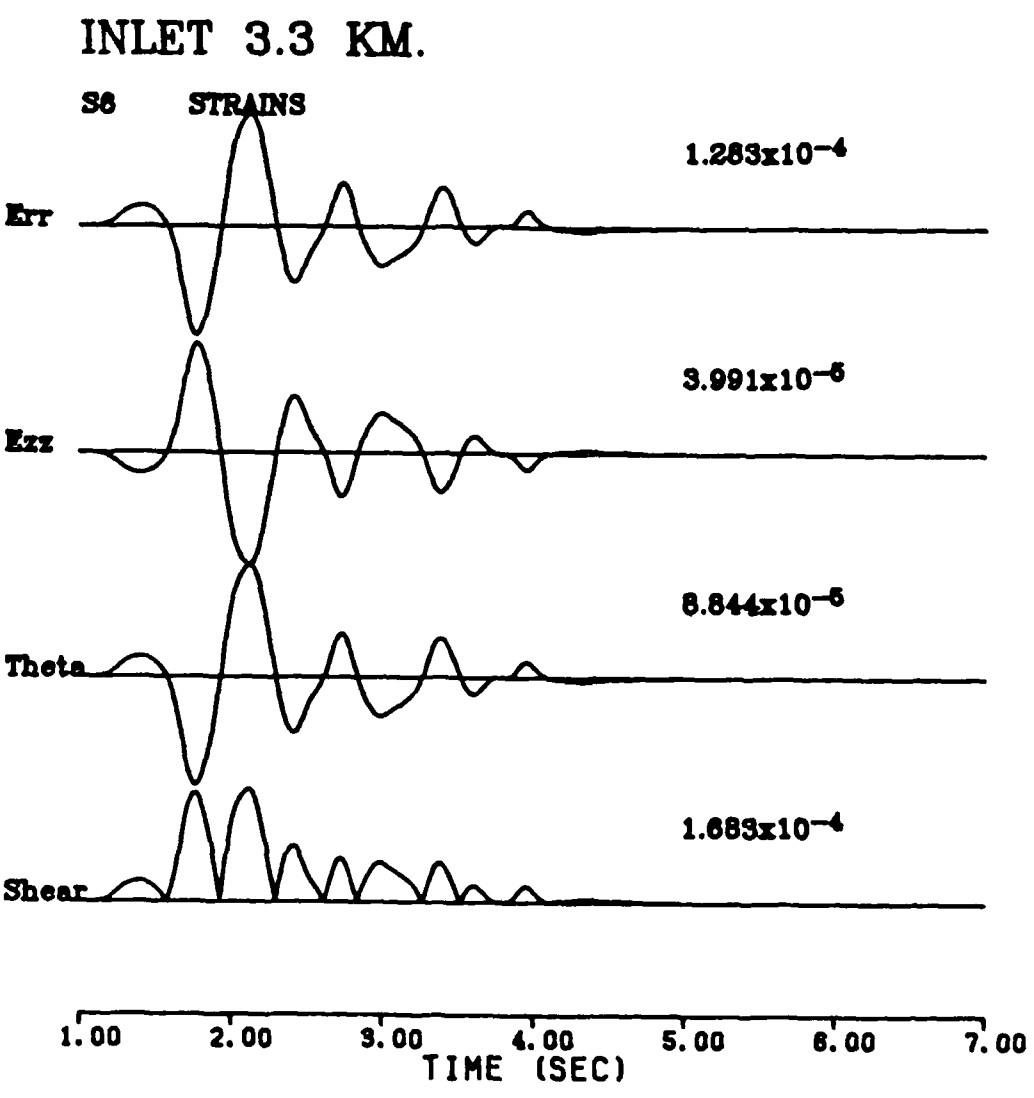
INLET 3.3 KM.
S8 STRAINS
1.283x10⁻⁴
Err
3.991x10⁻⁵
Ezz
8.844x10⁻⁵
Theta
1.683x10⁻⁴
Shear
1.00
2.00
3.00
4.00
5.00
6.00
7.00
TIME (SEC)

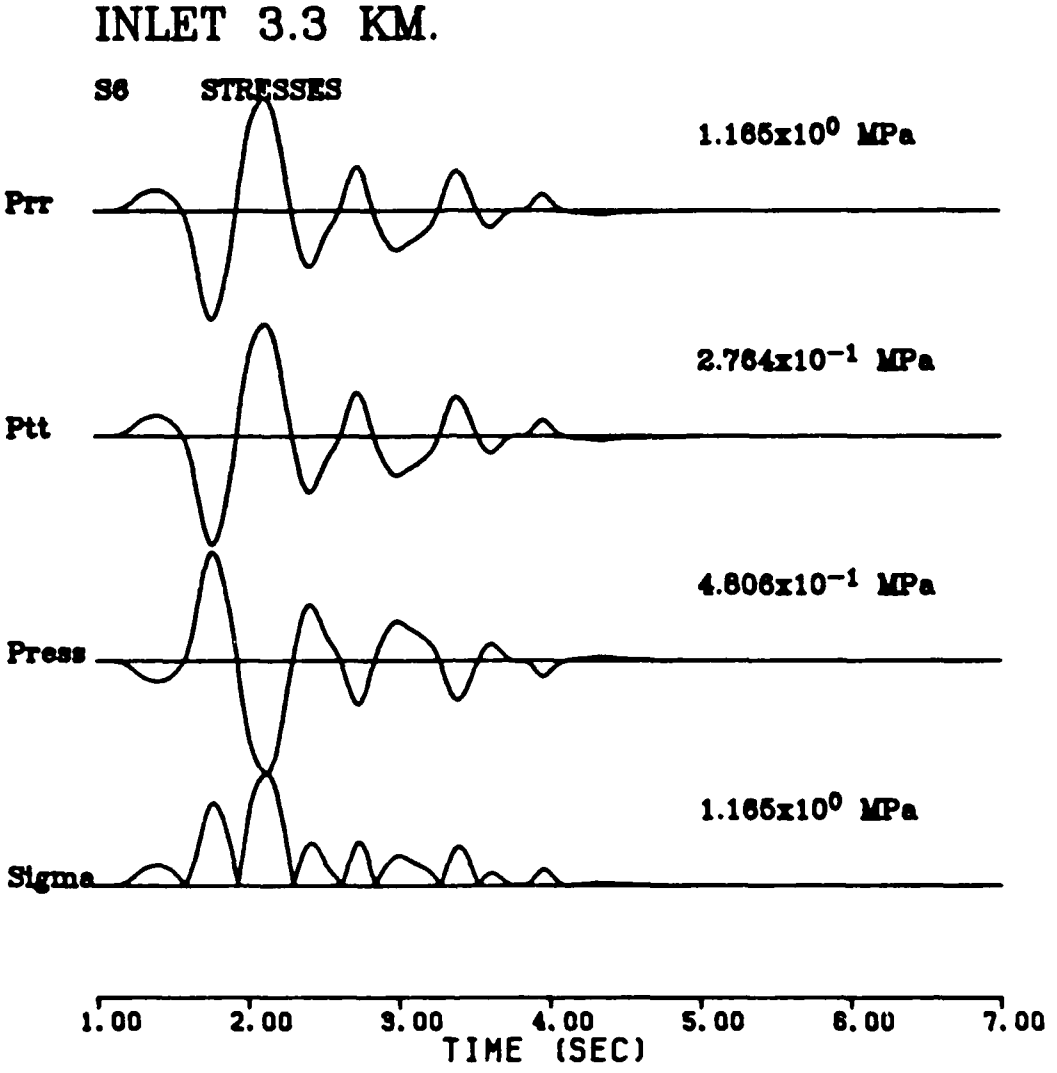
INLET 3.3 KM.
S6 STRESSES
1.165x10^0 MPa
Prr
2.764x10^-1 MPa
Ptt
4.606x10^-1 MPa
Press
1.165x10^0 MPa
Sigma
1.00
2.00
3.00
4.00
5.00
6.00
7.00
TIME (SEC)

INLET 6.5 KM.

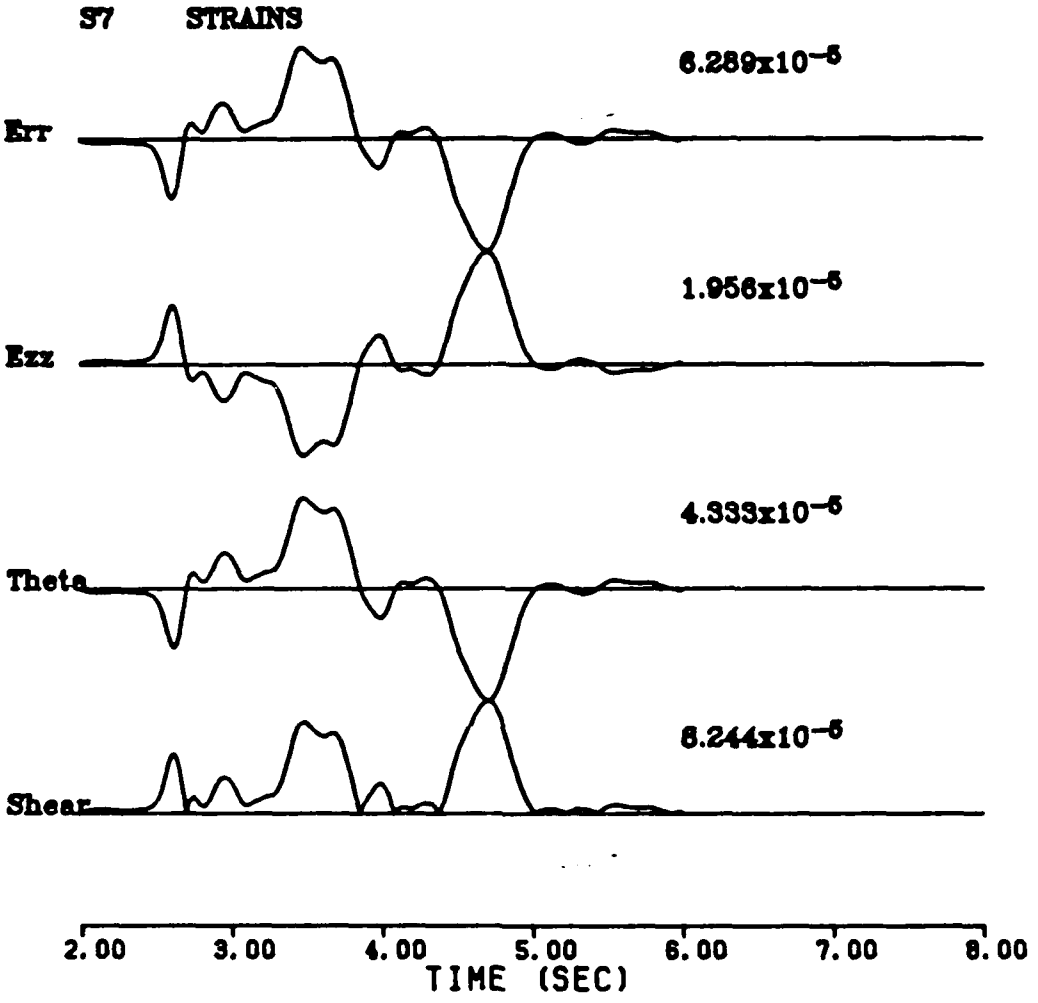
S7 STRAINS
6.289x10⁻⁵
Err
1.956x10⁻⁵
Ezz
4.333x10⁻⁵
Theta
6.244x10⁻⁵
Shear
2.00
3.00
4.00
5.00
6.00
7.00
8.00
TIME (SEC)

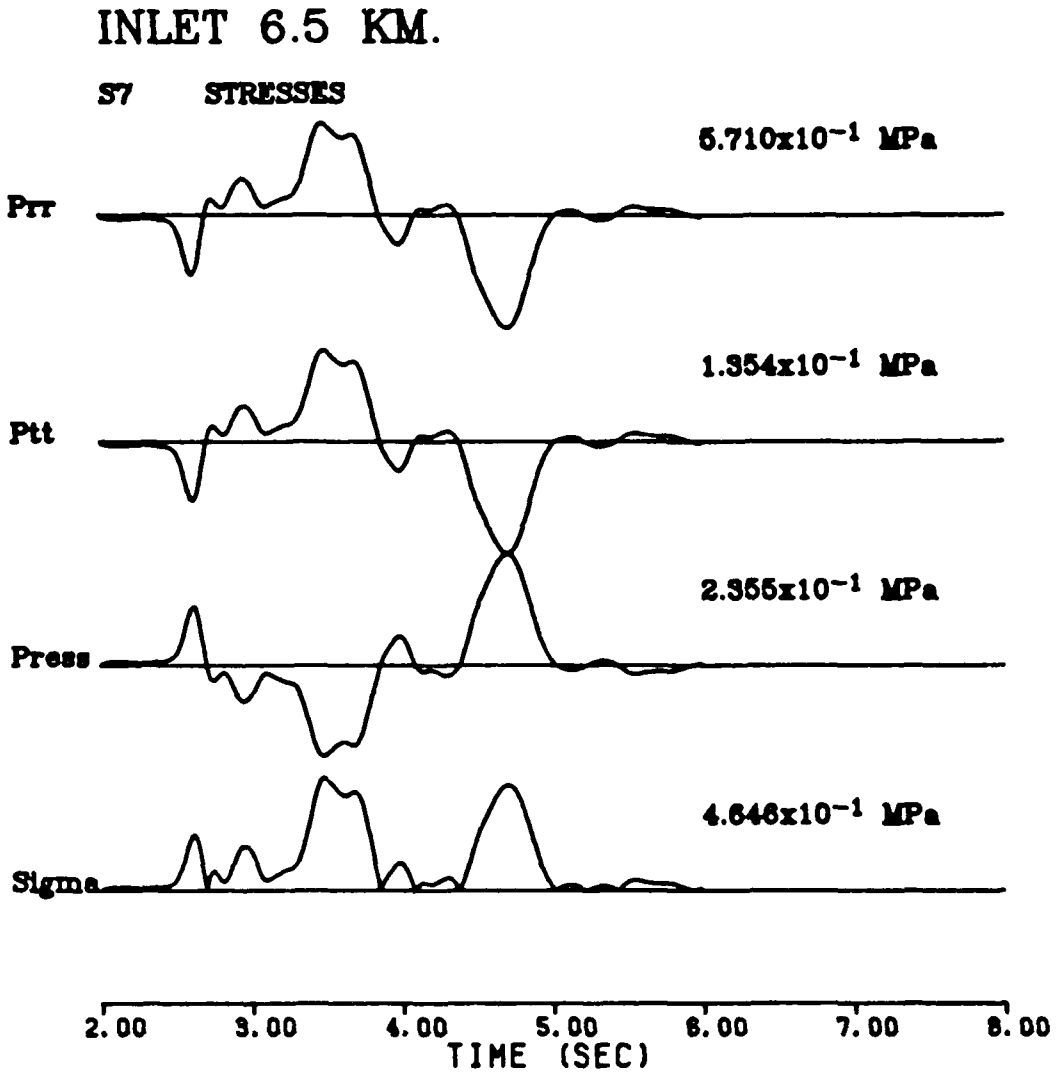
INLET 6.5 KM.
S7 STRESSES
5.710x10⁻¹ MPa
Prr
1.354x10⁻¹ MPa
Ptt
2.355x10⁻¹ MPa
Press
4.646x10⁻¹ MPa
Sigma
2.00
3.00
4.00
5.00
6.00
7.00
8.00
TIME (SEC)

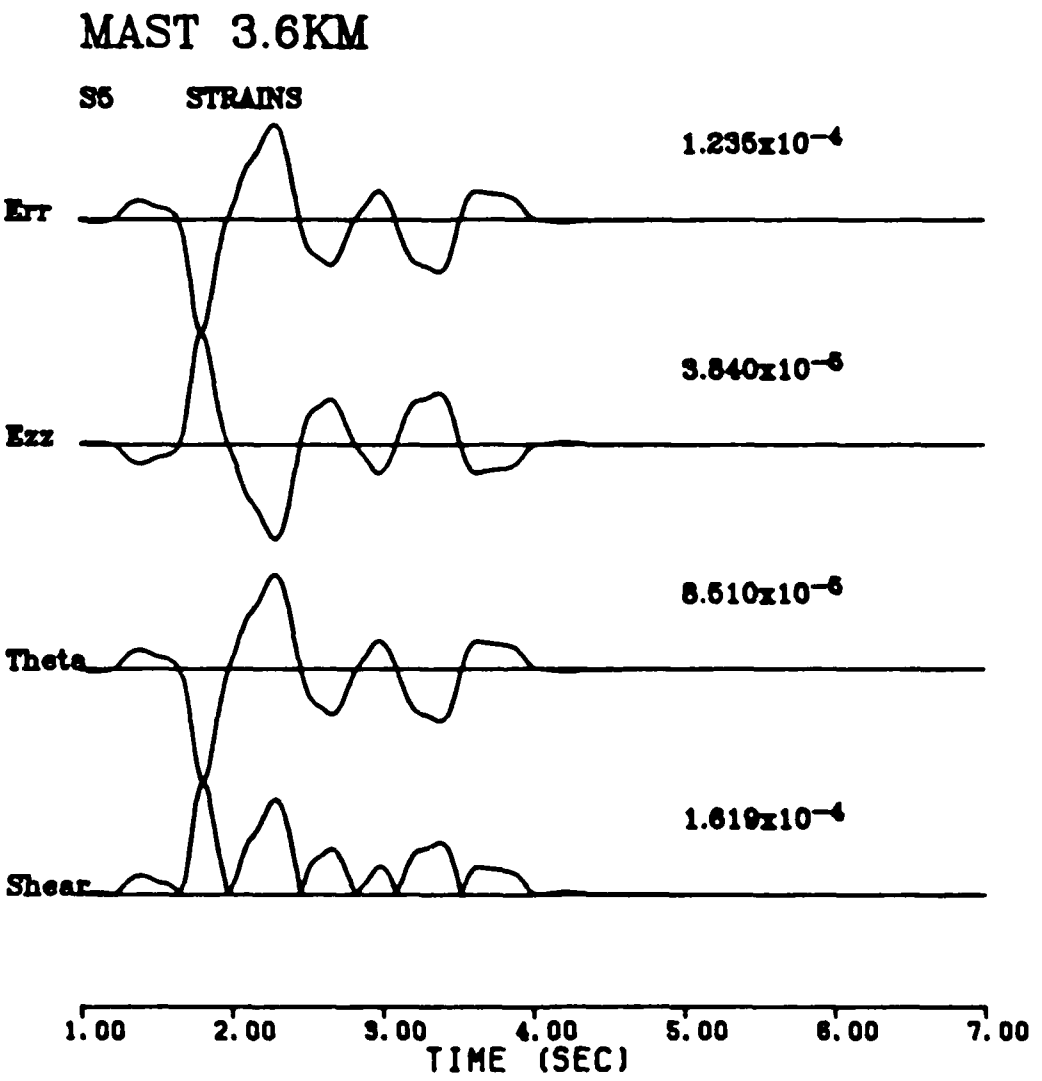
MAST 3.6KM
S6 STRAINS
1.236x10⁻⁴
Err
3.840x10⁻⁵
Ezz
8.510x10⁻⁵
Theta
1.619x10⁻⁴
Shear
1.00
2.00
3.00
4.00
5.00
6.00
7.00
TIME (SEC)

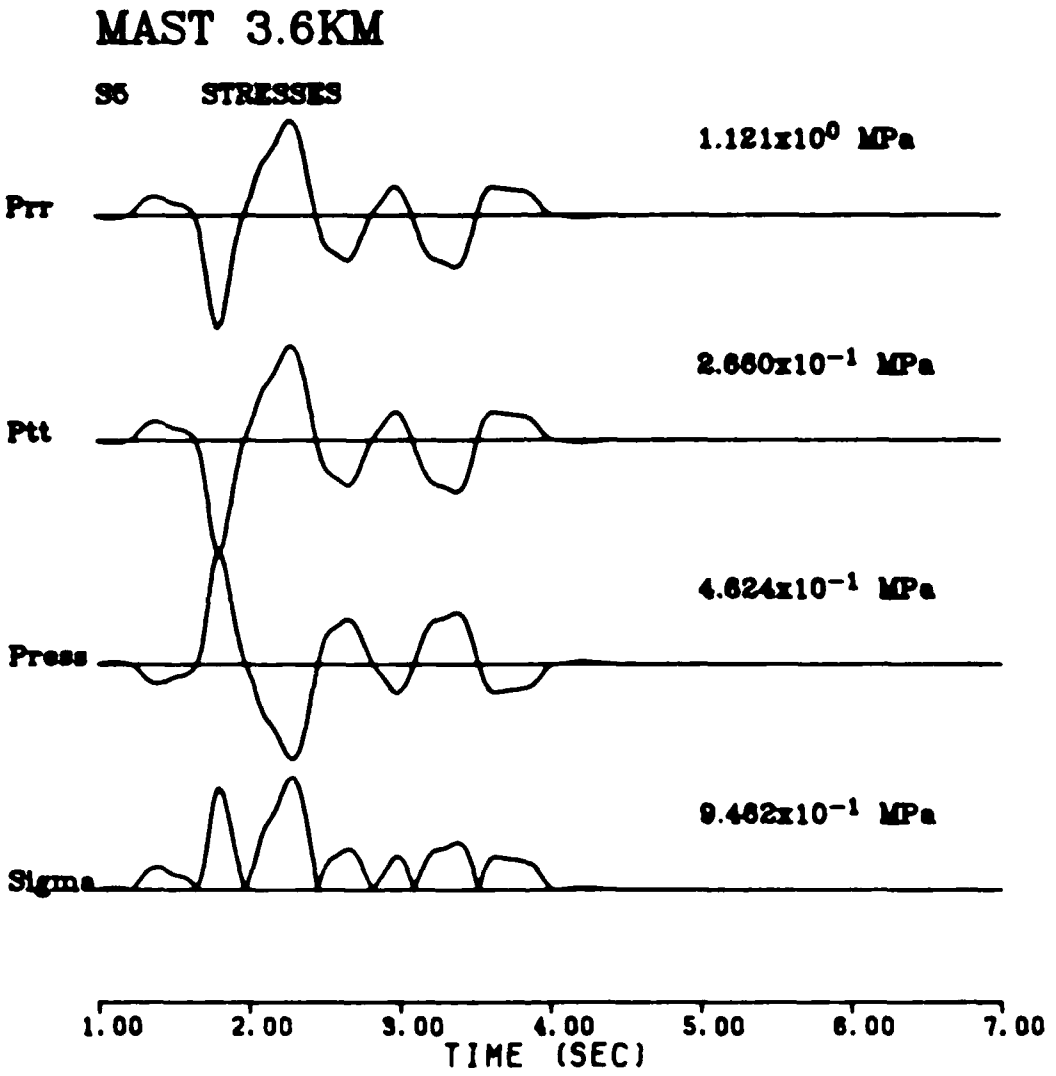
MAST 3.6KM
S6 STRESSES
1.121x10^0 MPa
Prr
2.660x10^-1 MPa
Ptt
4.624x10^-1 MPa
Press
9.462x10^-1 MPa
Sigma
1.00
2.00
3.00
4.00
5.00
6.00
7.00
TIME (SEC)

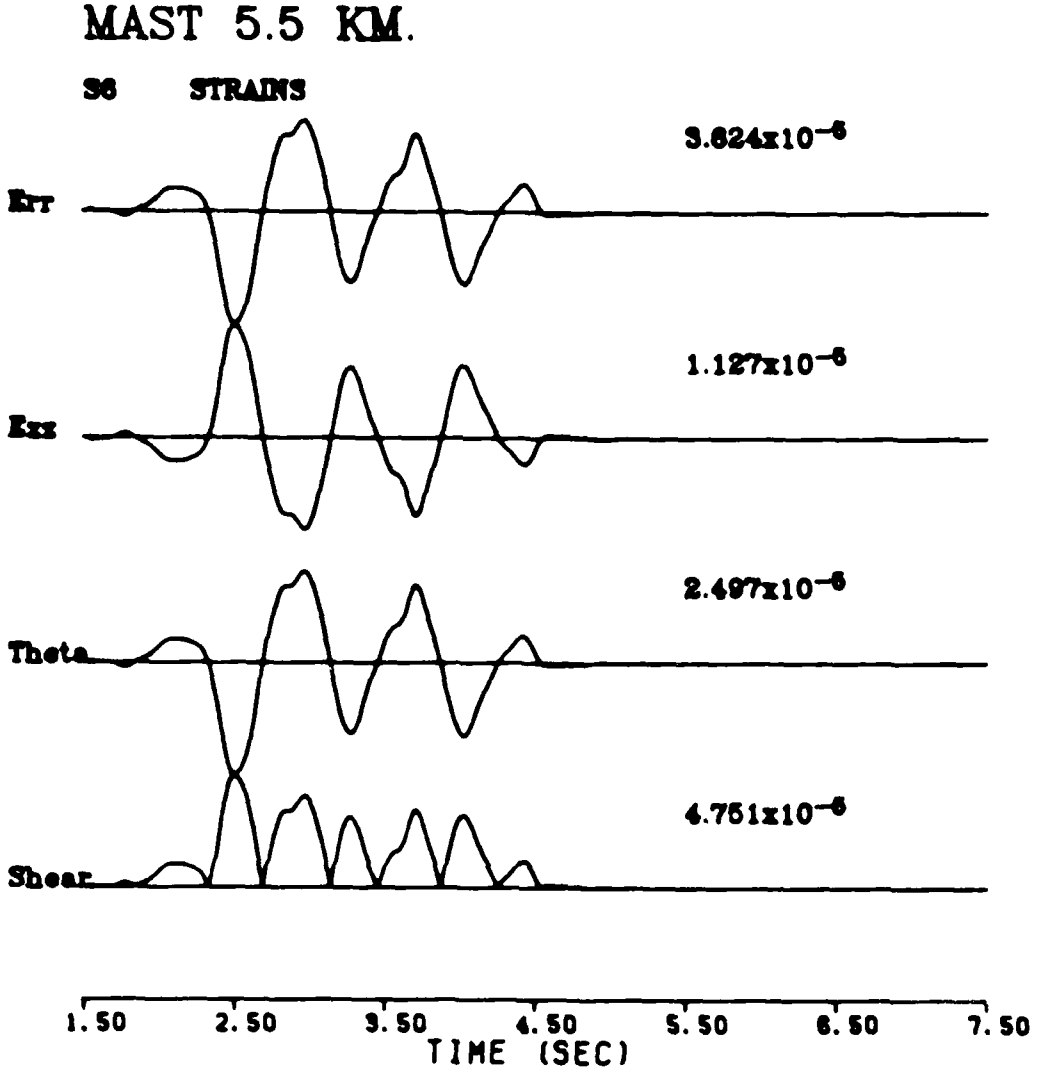
MAST 5.5 KM.
S6 STRAINS
3.624x10⁻⁶
Err
1.127x10⁻⁶
Exx
2.497x10⁻⁶
Theta
4.751x10⁻⁶
Shear
1.50
2.50
3.50
4.50
5.50
6.50
7.50
TIME (SEC)

MAST 5.5 KM.

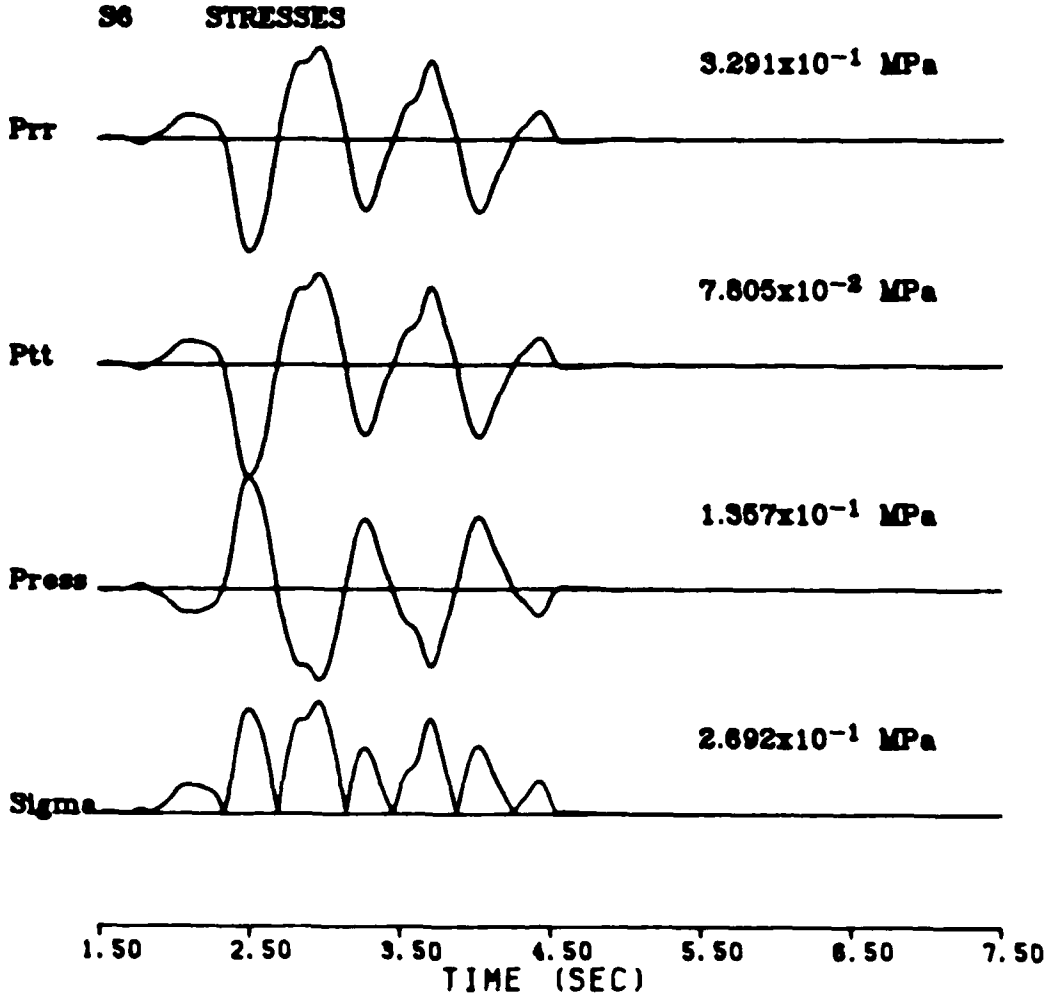
S6 STRESSES
3.291x10^{-1} MPa
Prr
7.805x10^{-2} MPa
Ptt
1.357x10^{-1} MPa
Press
2.692x10^{-1} MPa
Sigma
1.50
2.50
3.50
4.50
5.50
6.50
7.50
TIME (SEC)

MAST 7.3 KM.

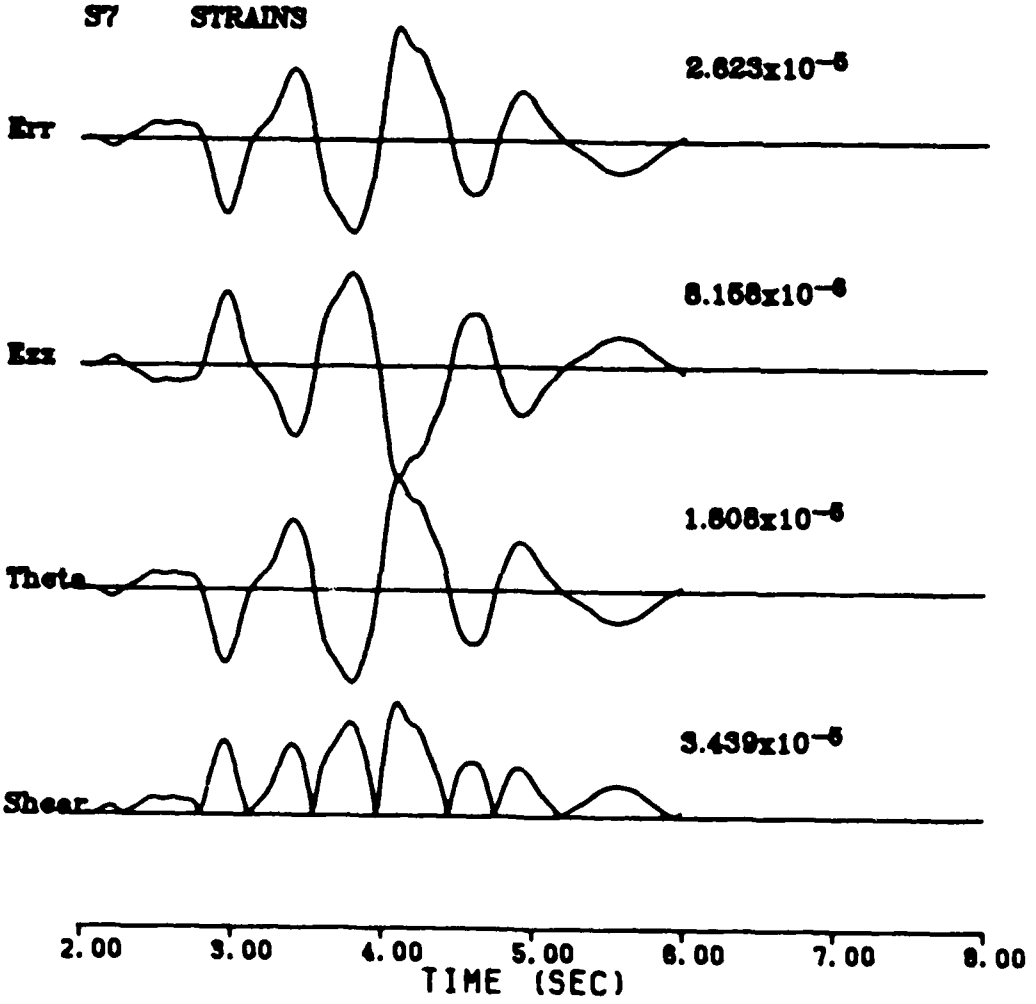
S7 STRAINS
Err
2.623x10⁻⁵
Exx
8.158x10⁻⁶
Theta
1.808x10⁻⁵
Shear
3.439x10⁻⁵
2.00
3.00
4.00
5.00
6.00
7.00
8.00
TIME (SEC)

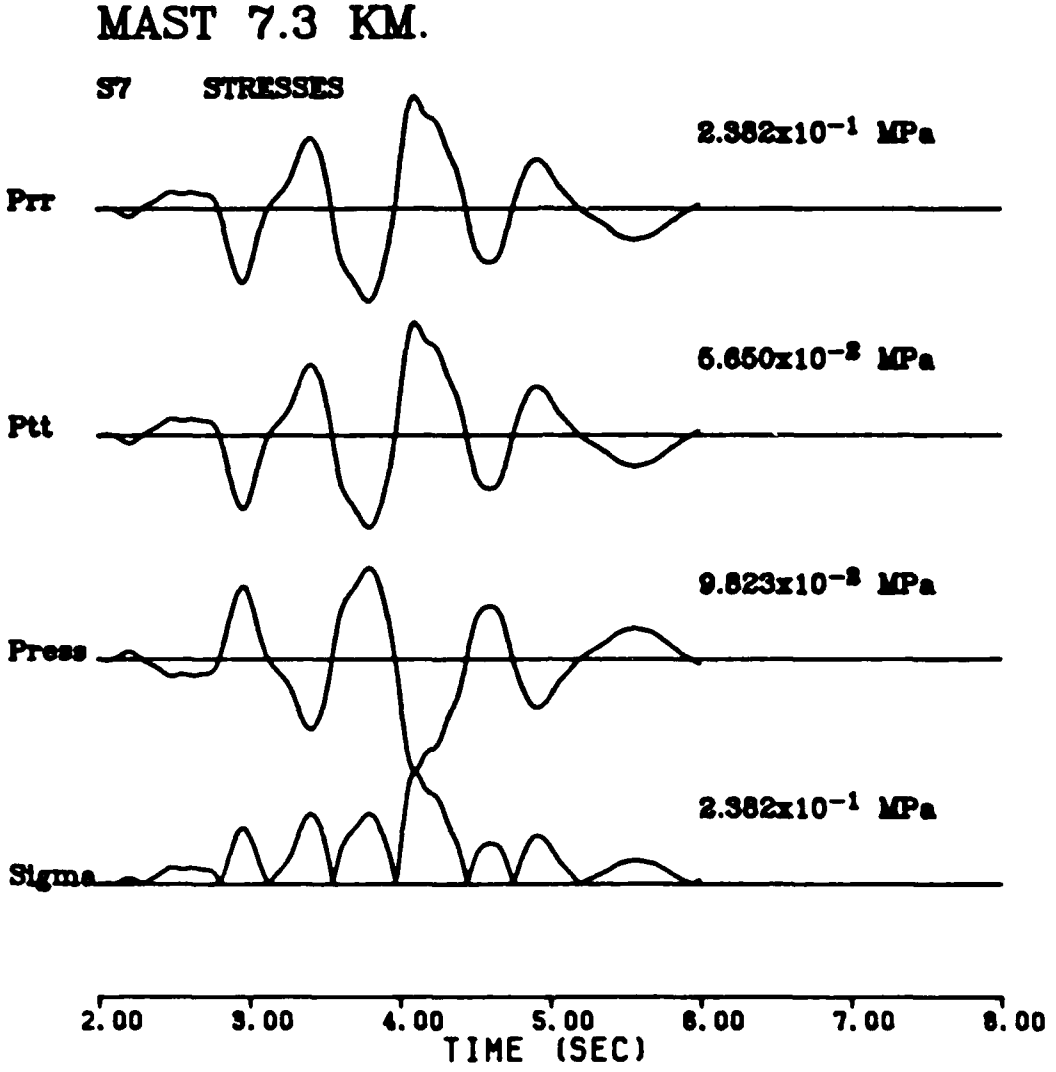
MAST 7.3 KM.
S7 STRESSES
2.382x10-1 MPa
Prr
6.650x10-2 MPa
Ptt
9.823x10-2 MPa
Press
2.382x10-1 MPa
Sigma
2.00
3.00
4.00
5.00
6.00
7.00
8.00
TIME (SEC)

SCOTCH 4.1 KM.

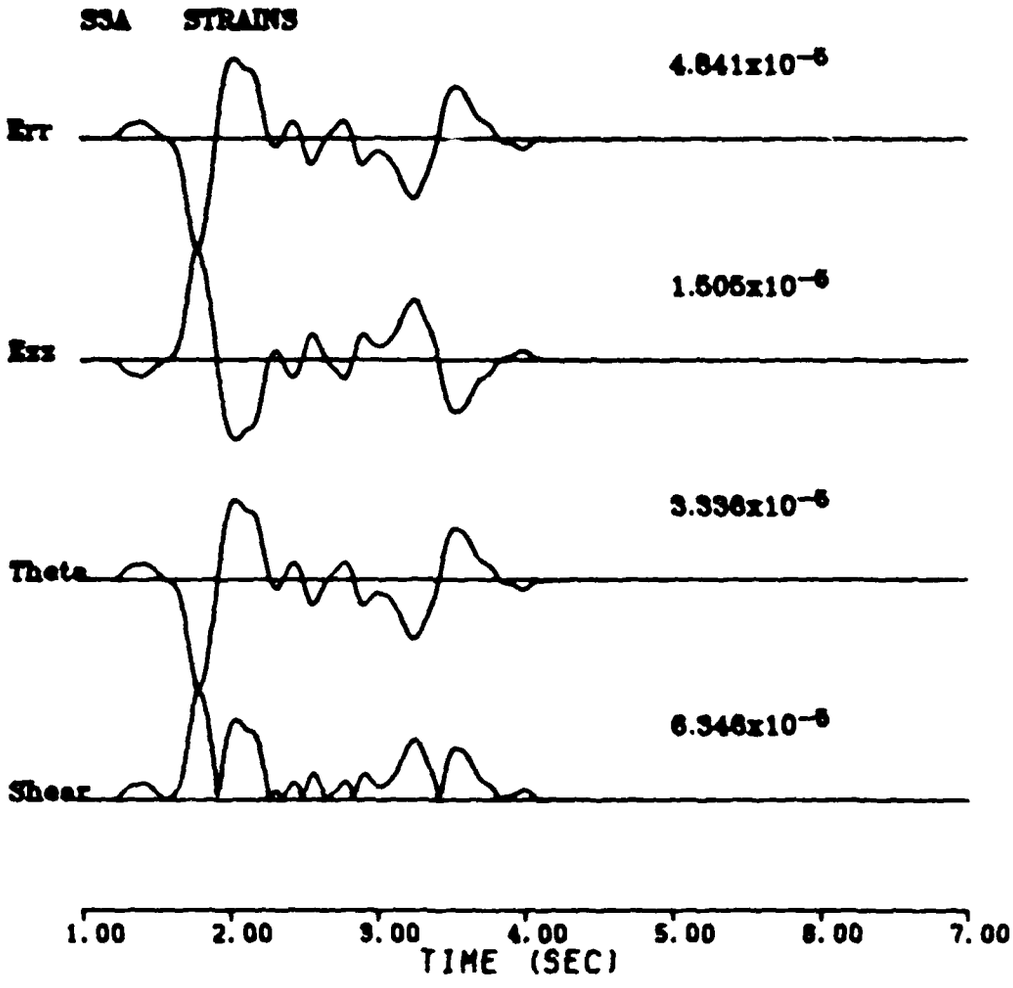
S5A STRAINS
4.841x10⁻⁶
Err
1.505x10⁻⁶
Ezz
3.336x10⁻⁶
Theta
6.346x10⁻⁶
Shear
1.00
2.00
3.00
4.00
5.00
6.00
7.00
TIME (SEC)

SCOTCH 4.1 KM.

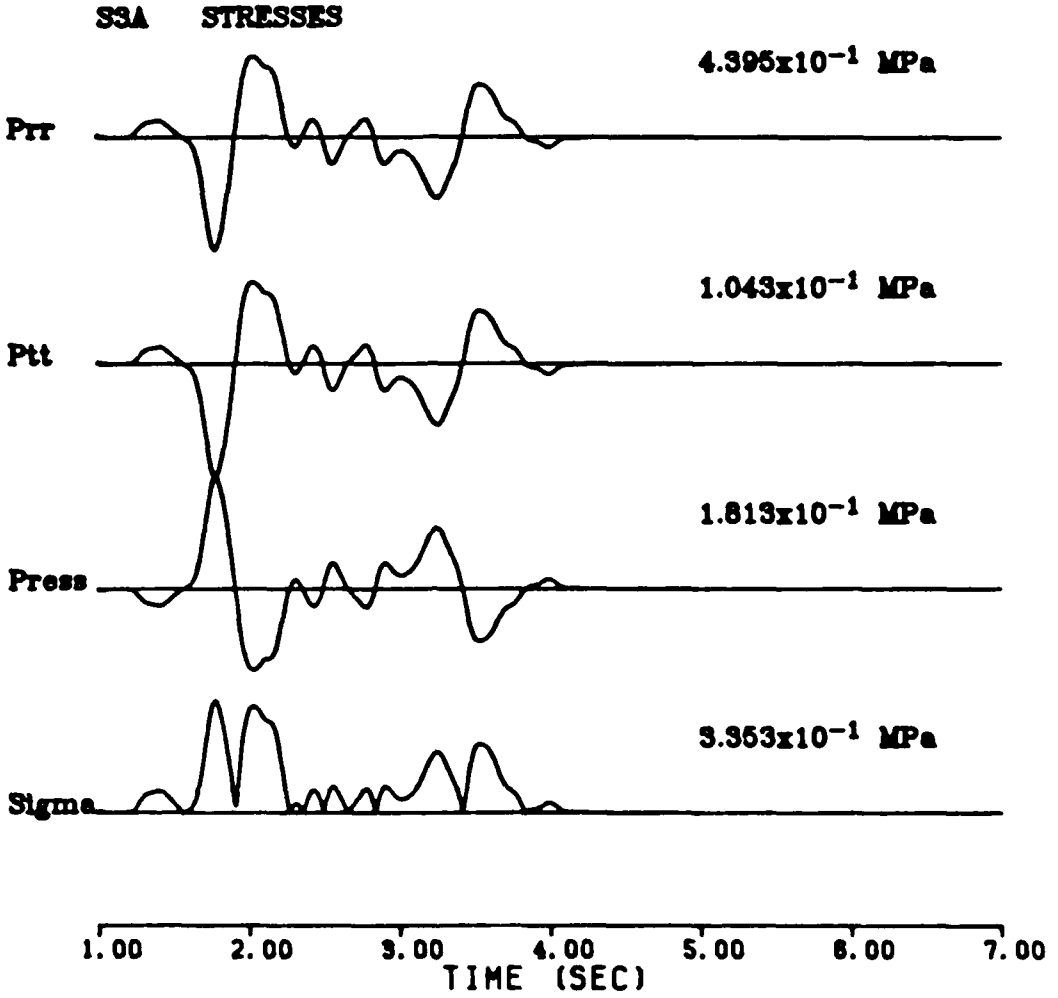
S3A STRESSES
4.395x10⁻¹ MPa
Prr
1.043x10⁻¹ MPa
Ptt
1.813x10⁻¹ MPa
Press
3.363x10⁻¹ MPa
Sigma
1.00
2.00
3.00
4.00
5.00
6.00
7.00
TIME (SEC)

SCOTCH 6.1 KM.

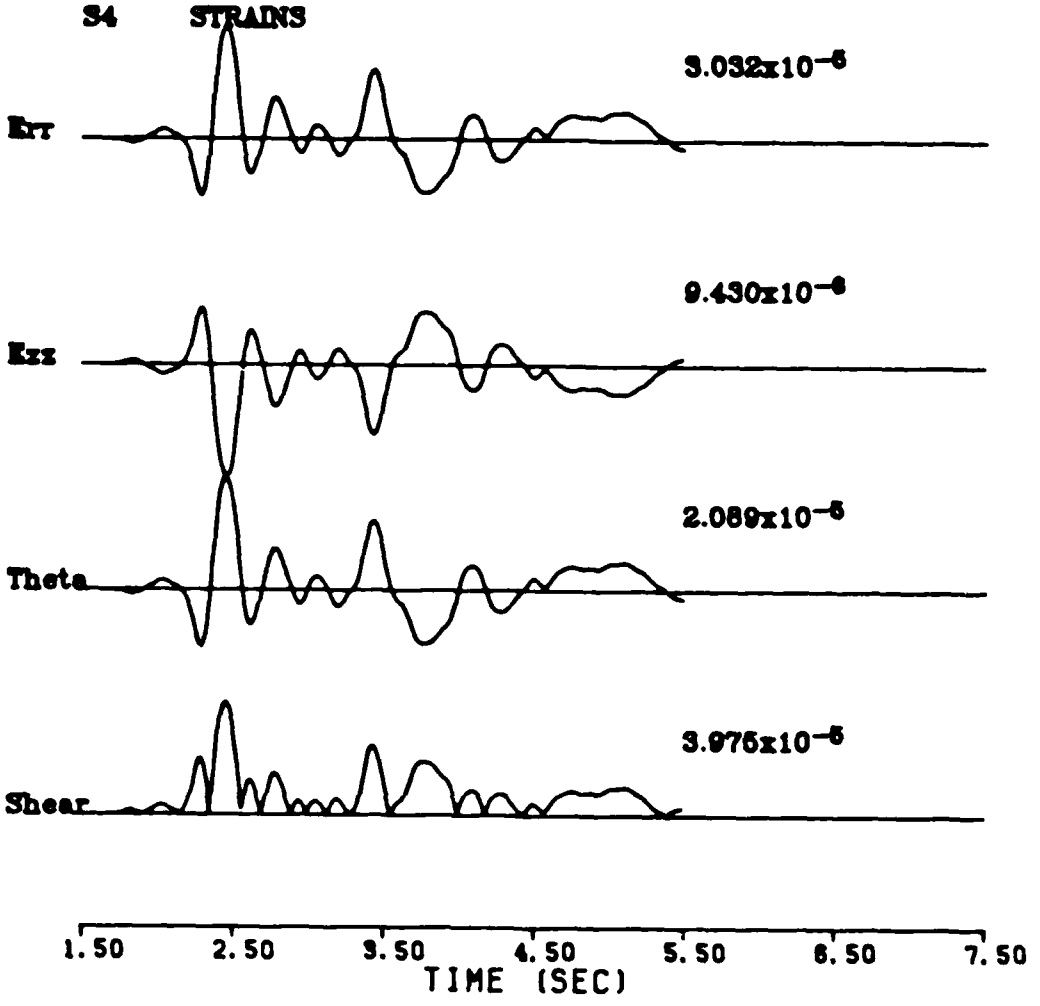
S4 STRAINS
3.032x10⁻⁶
Err
9.430x10⁻⁶
Ezz
2.089x10⁻⁶
Theta
3.976x10⁻⁶
Shear
1.50
2.50
3.50
4.50
5.50
6.50
7.50
TIME (SEC)

SCOTCH 6.1 KM.

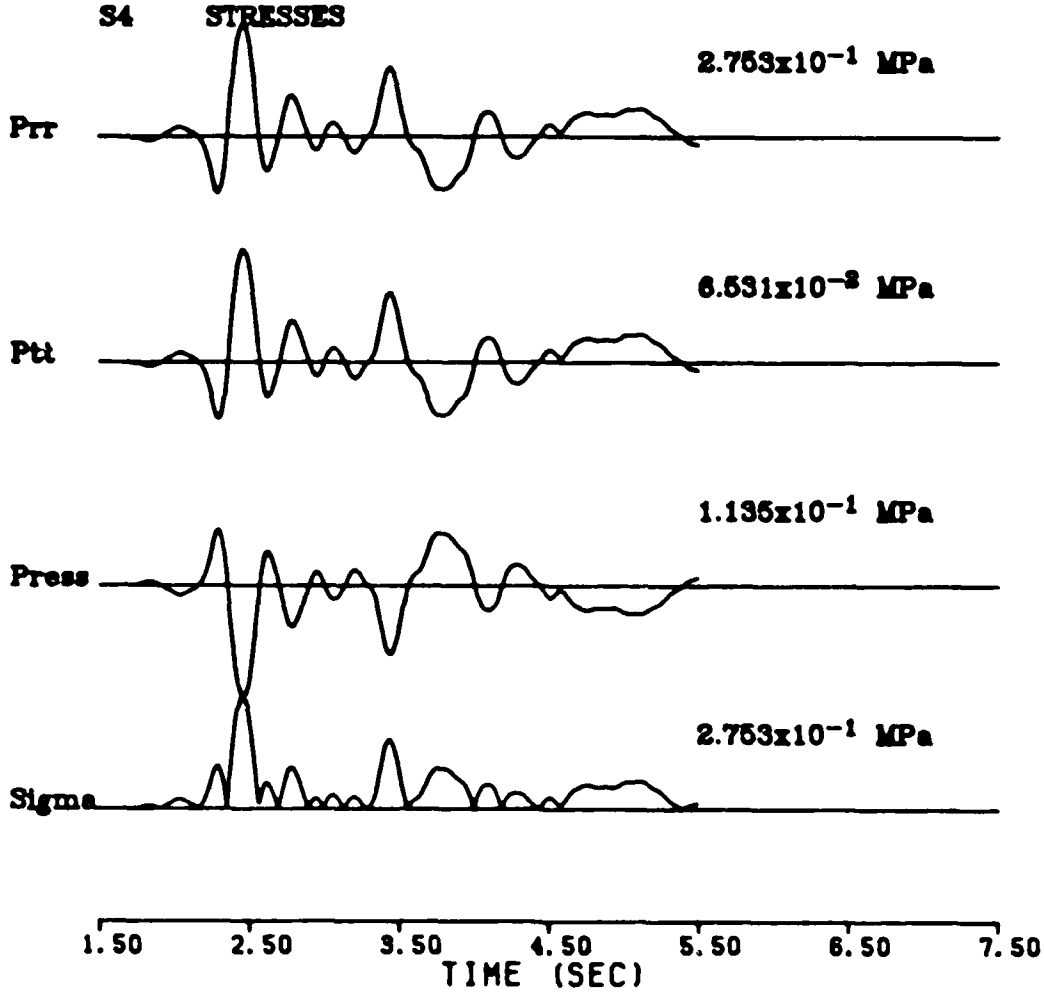
S4 STRESSES
2.763x10⁻¹ MPa
Prr
6.631x10⁻² MPa
Ptt
1.136x10⁻¹ MPa
Press
2.763x10⁻¹ MPa
Sigma
1.50
2.50
3.50
4.50
5.50
6.50
7.50
TIME (SEC)

APPENDIX 2.

PROCESSED EARTHQUAKE RECORDS

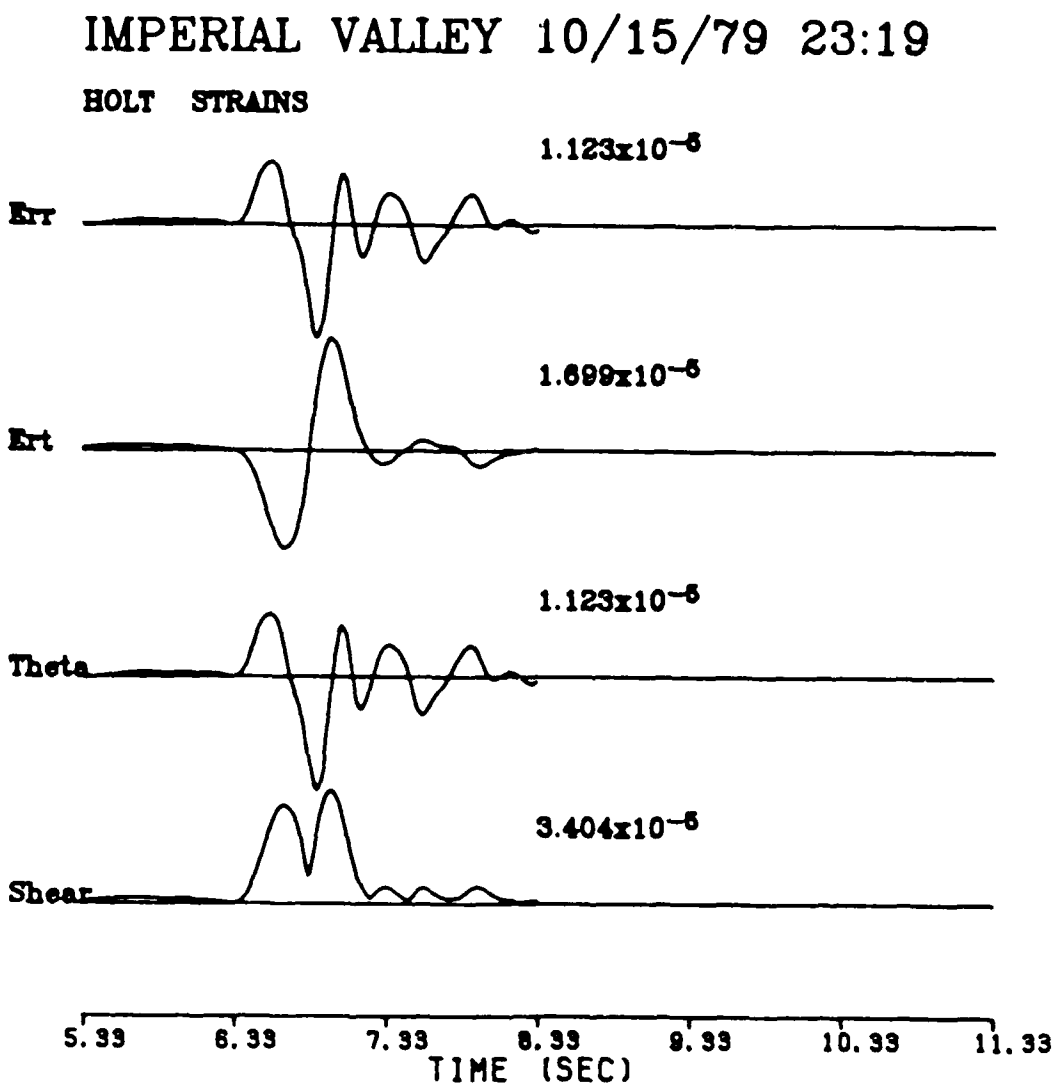
IMPERIAL VALLEY 10/15/79 23:19
HOLT STRAINS
1.123x10⁻⁶
Err
1.699x10⁻⁶
Ert
1.123x10⁻⁶
Theta
3.404x10⁻⁶
Shear
5.33
6.33
7.33
8.33
9.33
10.33
11.33
TIME (SEC)

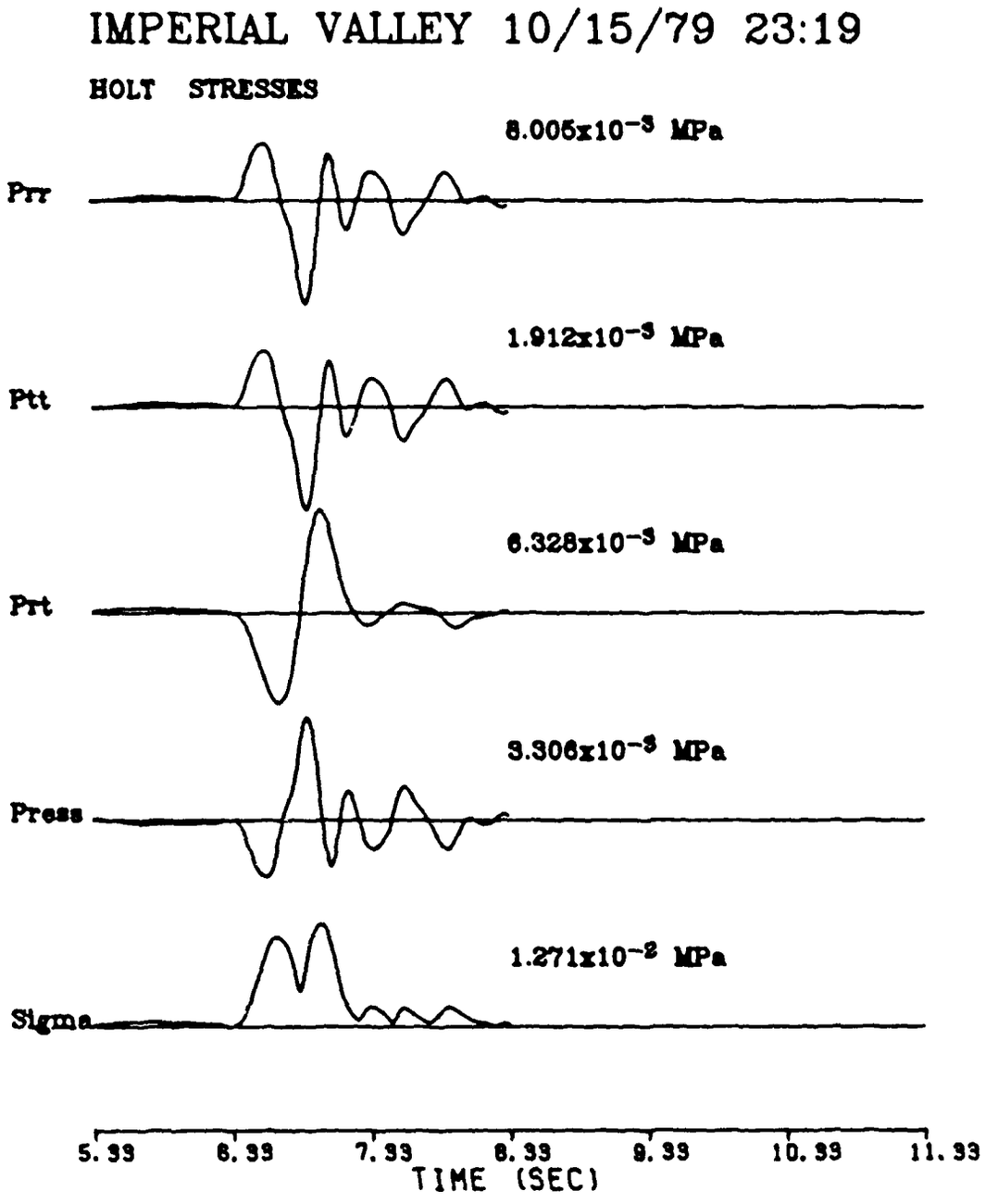
IMPERIAL VALLEY 10/15/79 23:19
HOLT STRESSES
8.005x10-3 MPa
Prr
1.912x10-3 MPa
Ptt
6.328x10-3 MPa
Prt
3.306x10-3 MPa
Press
1.271x10-2 MPa
Sigma
5.00
6.00
7.00
8.00
9.00
10.00
11.00
TIME (SEC)

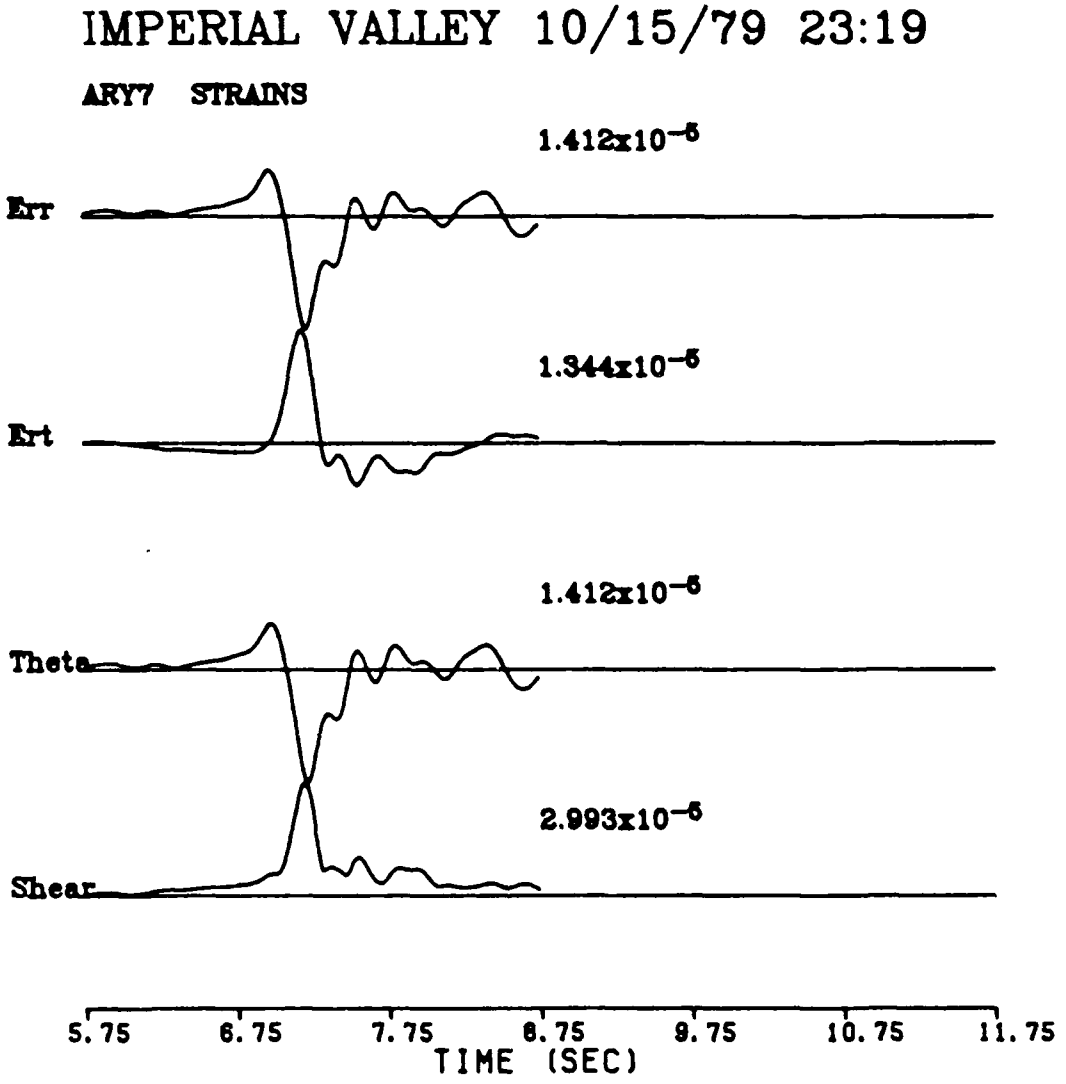
IMPERIAL VALLEY 10/15/79 23:19
ARY7 STRAINS
1.412x10⁻⁵
Err
1.344x10⁻⁵
Ert
1.412x10⁻⁵
Theta
2.993x10⁻⁵
Shear
5.75
6.75
7.75
8.75
9.75
10.75
11.75
TIME (SEC)

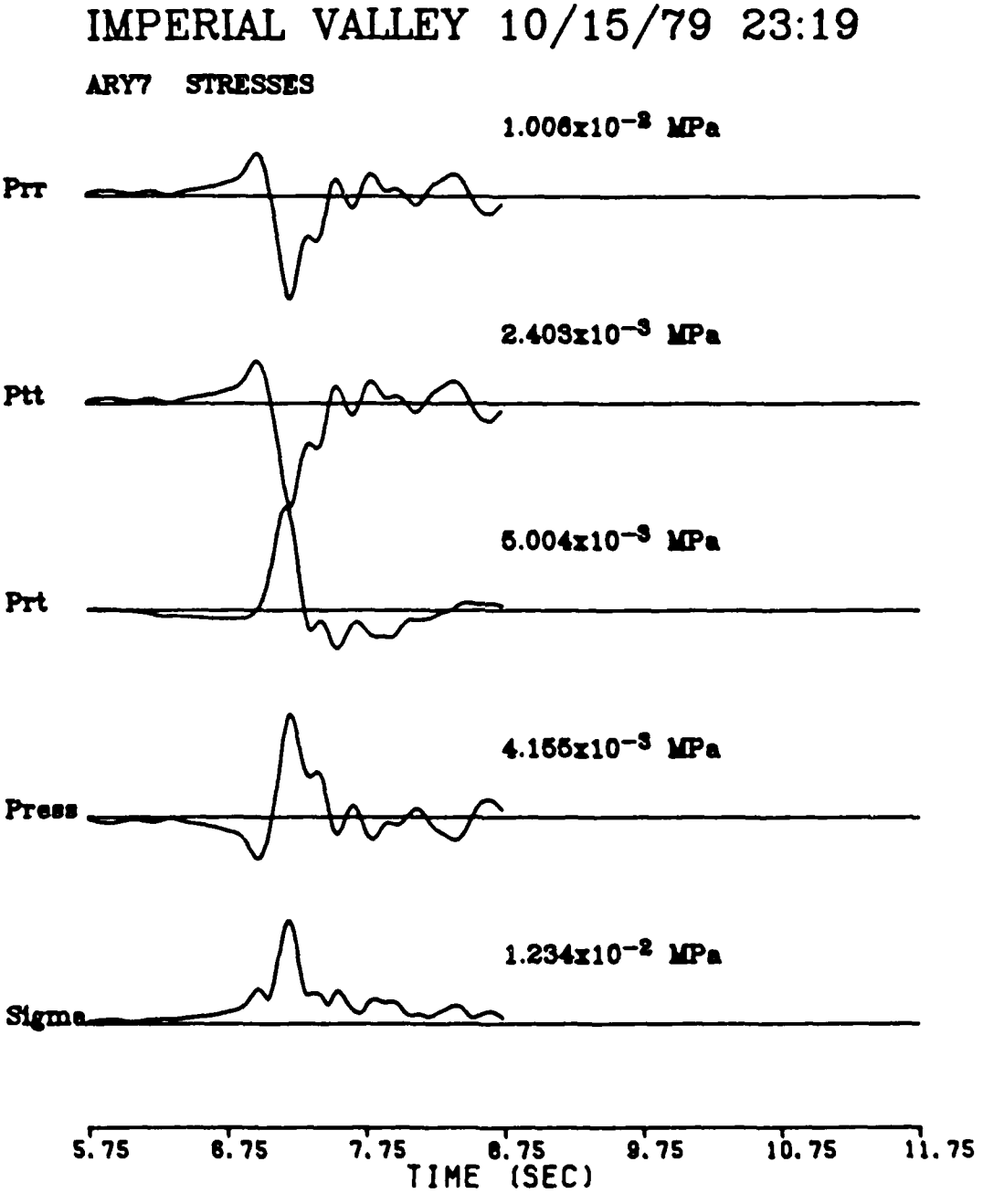
IMPERIAL VALLEY 10/15/79 23:19
ARY7 STRESSES
1.006x10-2 MPa
Prr
2.403x10-3 MPa
Ptt
5.004x10-3 MPa
Prt
4.155x10-3 MPa
Press
1.234x10-2 MPa
Sigma
5.75
6.75
7.75
8.75
9.75
10.75
11.75
TIME (SEC)

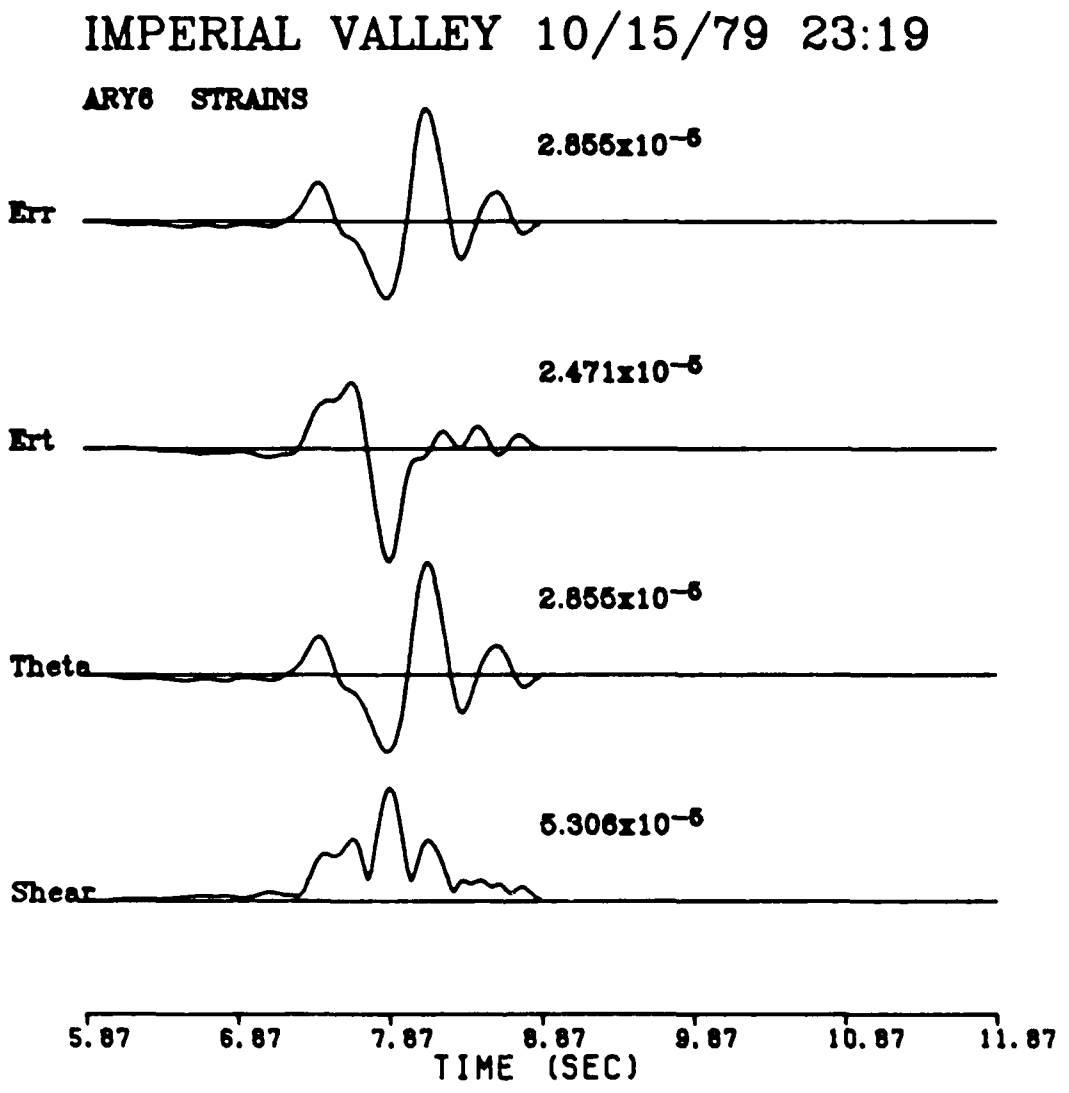
IMPERIAL VALLEY 10/15/79 23:19
ARY6 STRAINS
2.855x10⁻⁶
Err
2.471x10⁻⁶
Ert
2.855x10⁻⁶
Theta
5.306x10⁻⁶
Shear
5.87
6.87
7.87
8.87
9.87
10.87
11.87
TIME (SEC)

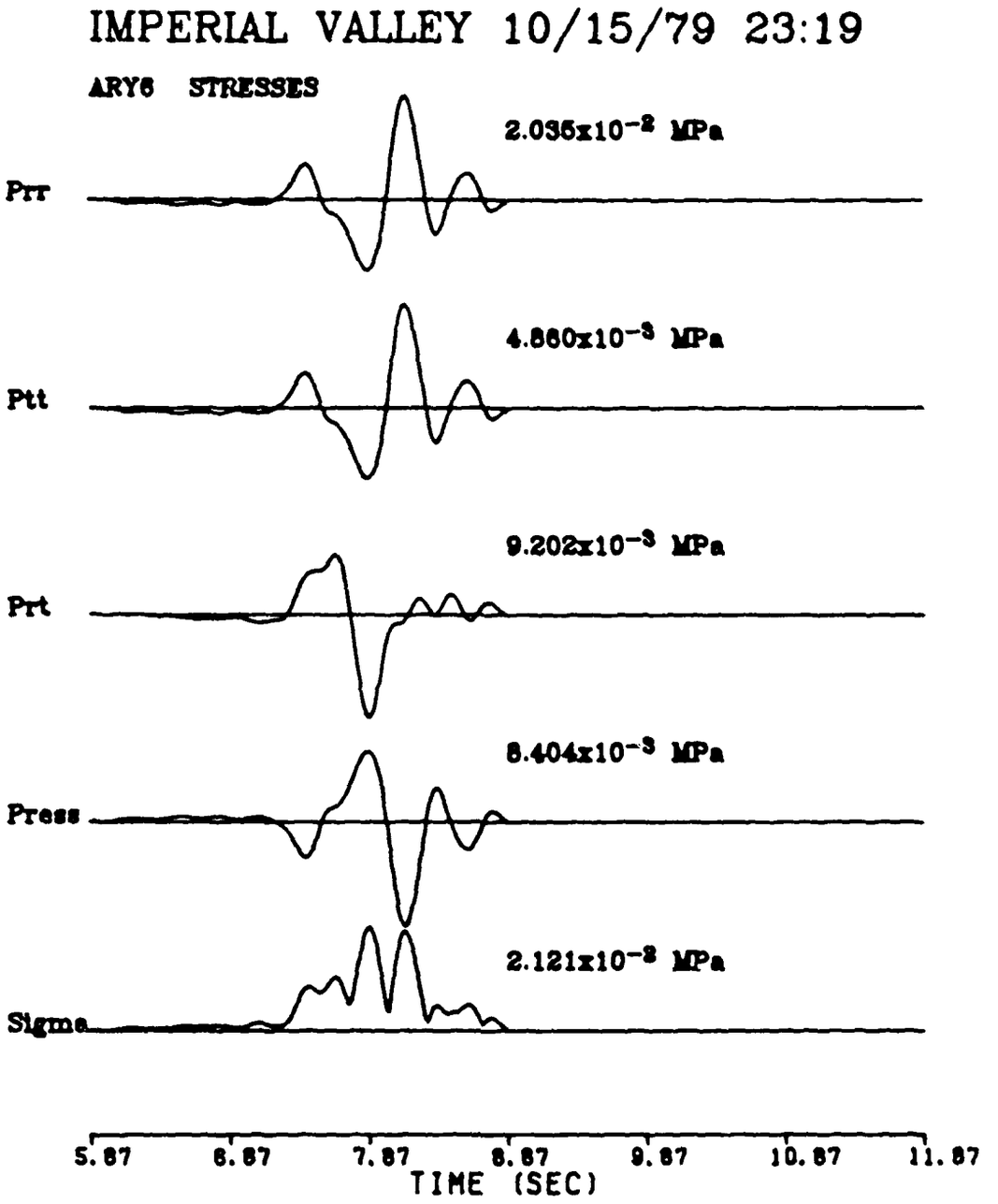
IMPERIAL VALLEY 10/15/79 23:19
ARY6 STRESSES
2.036x10-2 MPa
Prr
4.860x10-3 MPa
Ptt
9.202x10-3 MPa
Prt
8.404x10-3 MPa
Press
2.121x10-2 MPa
Sigma
5.87
6.87
7.87
8.87
9.87
10.87
11.87
TIME (SEC)

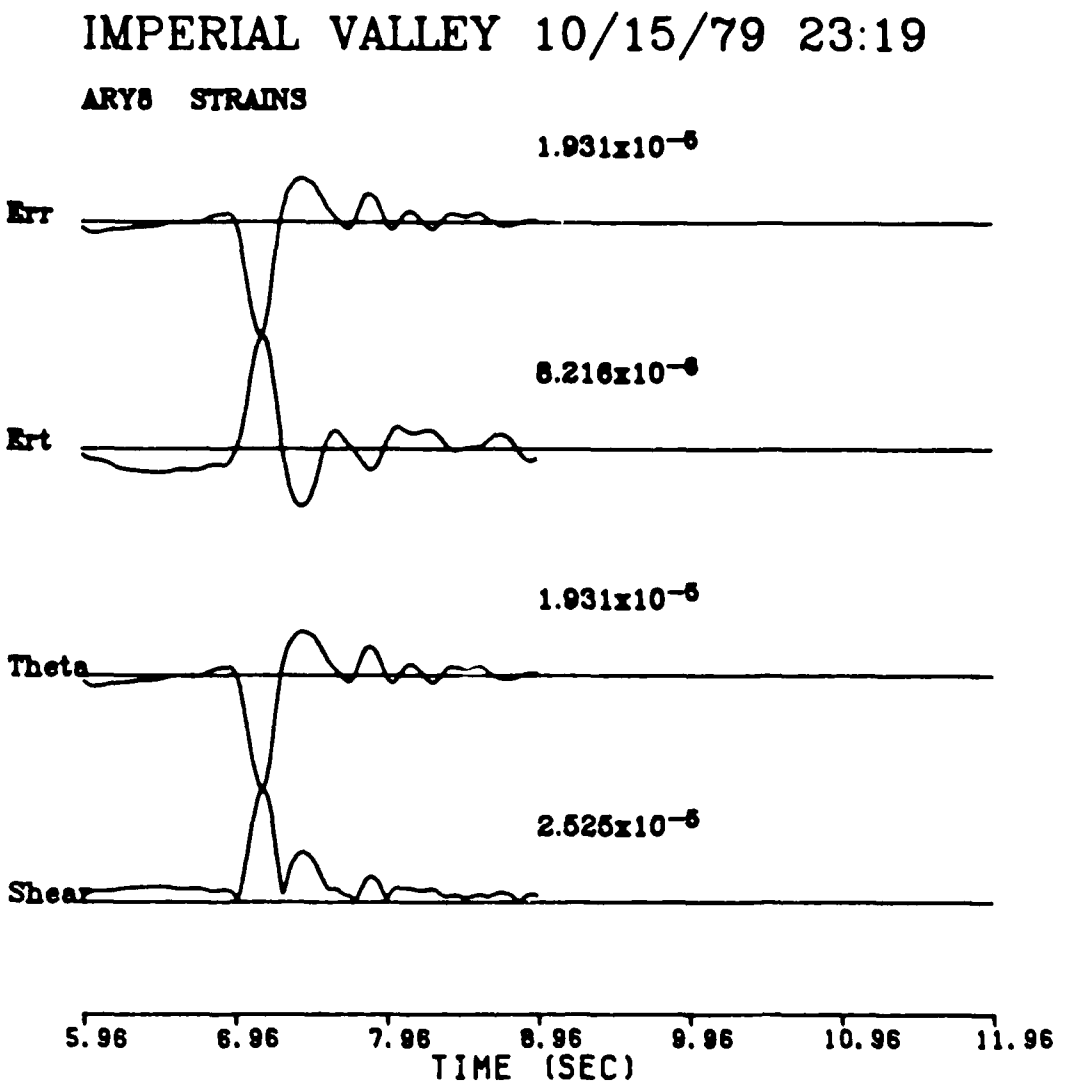
IMPERIAL VALLEY 10/15/79 23:19
ARY8 STRAINS
1.931x10⁻⁶
Err
8.216x10⁻⁸
Ert
1.931x10⁻⁶
Theta
2.525x10⁻⁶
Shear
5.96
6.96
7.96
8.96
9.96
10.96
11.96
TIME (SEC)

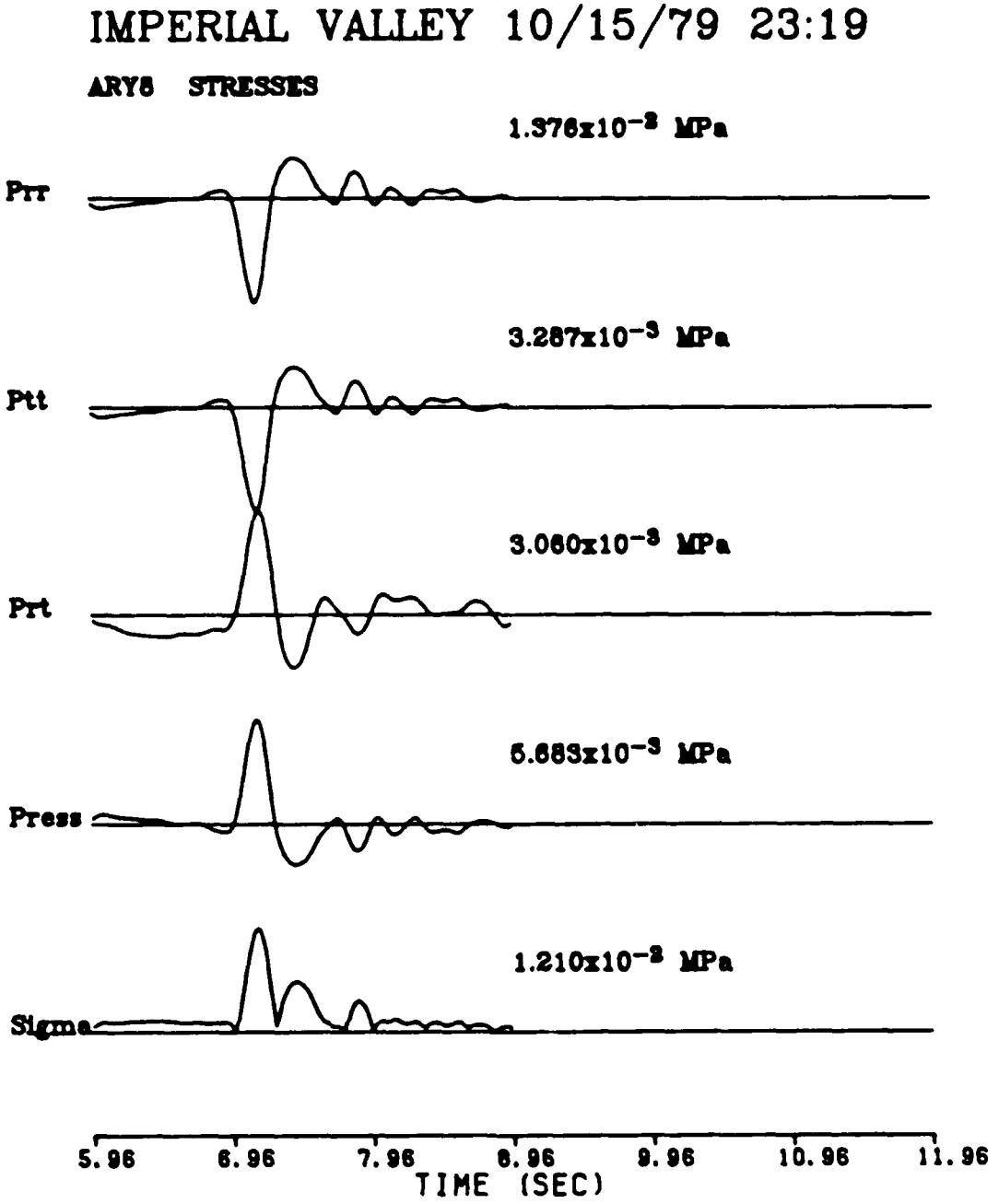
IMPERIAL VALLEY 10/15/79 23:19
ARY6 STRESSES
1.376x10-2 MPa
Prr
3.287x10-3 MPa
Ptt
3.060x10-3 MPa
Prt
5.683x10-3 MPa
Press
1.210x10-2 MPa
Sigma
5.96
6.96
7.96
8.96
9.96
10.96
11.96
TIME (SEC)

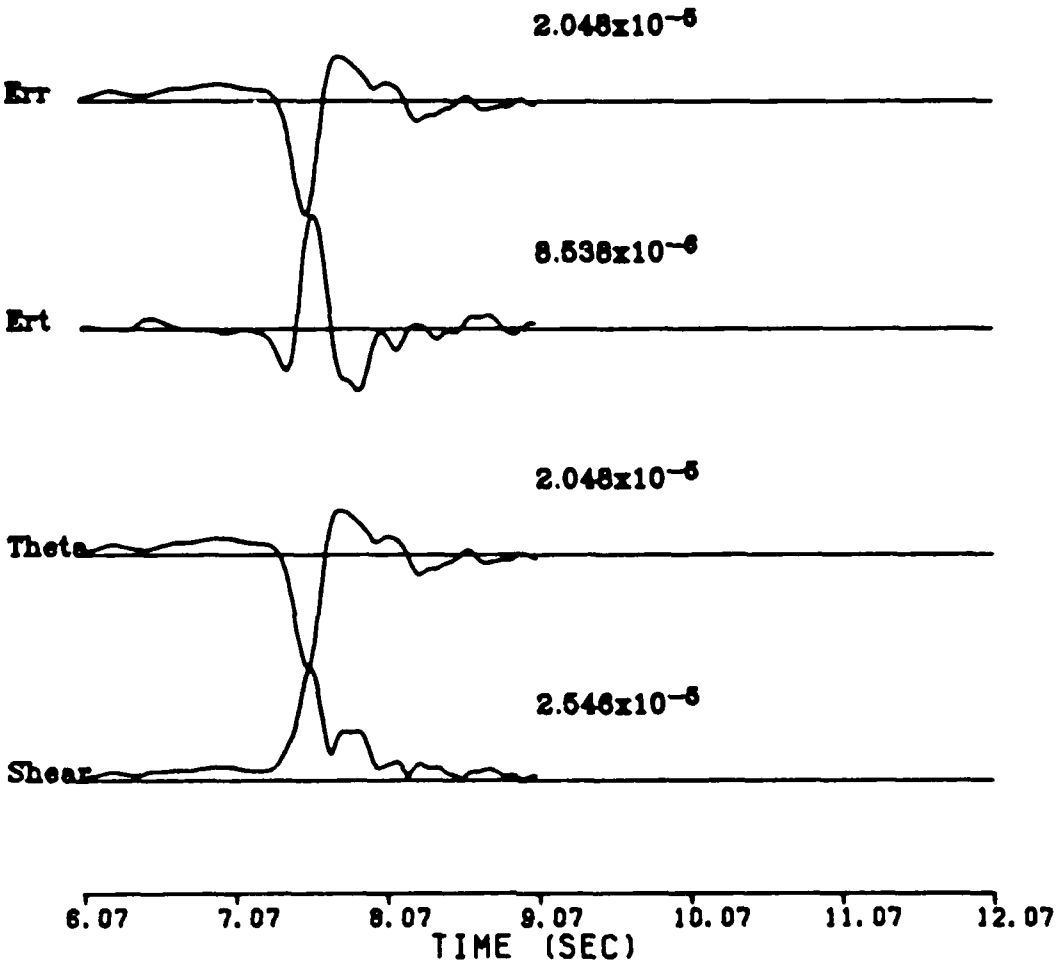
IMPERIAL VALLEY 10/15/79 23:19
ELCE STRAINS
2.048x10⁻⁵
Err
8.536x10⁻⁶
Ert
2.048x10⁻⁵
Theta
2.546x10⁻⁵
Shear
6.07
7.07
8.07
9.07
10.07
11.07
12.07
TIME (SEC)

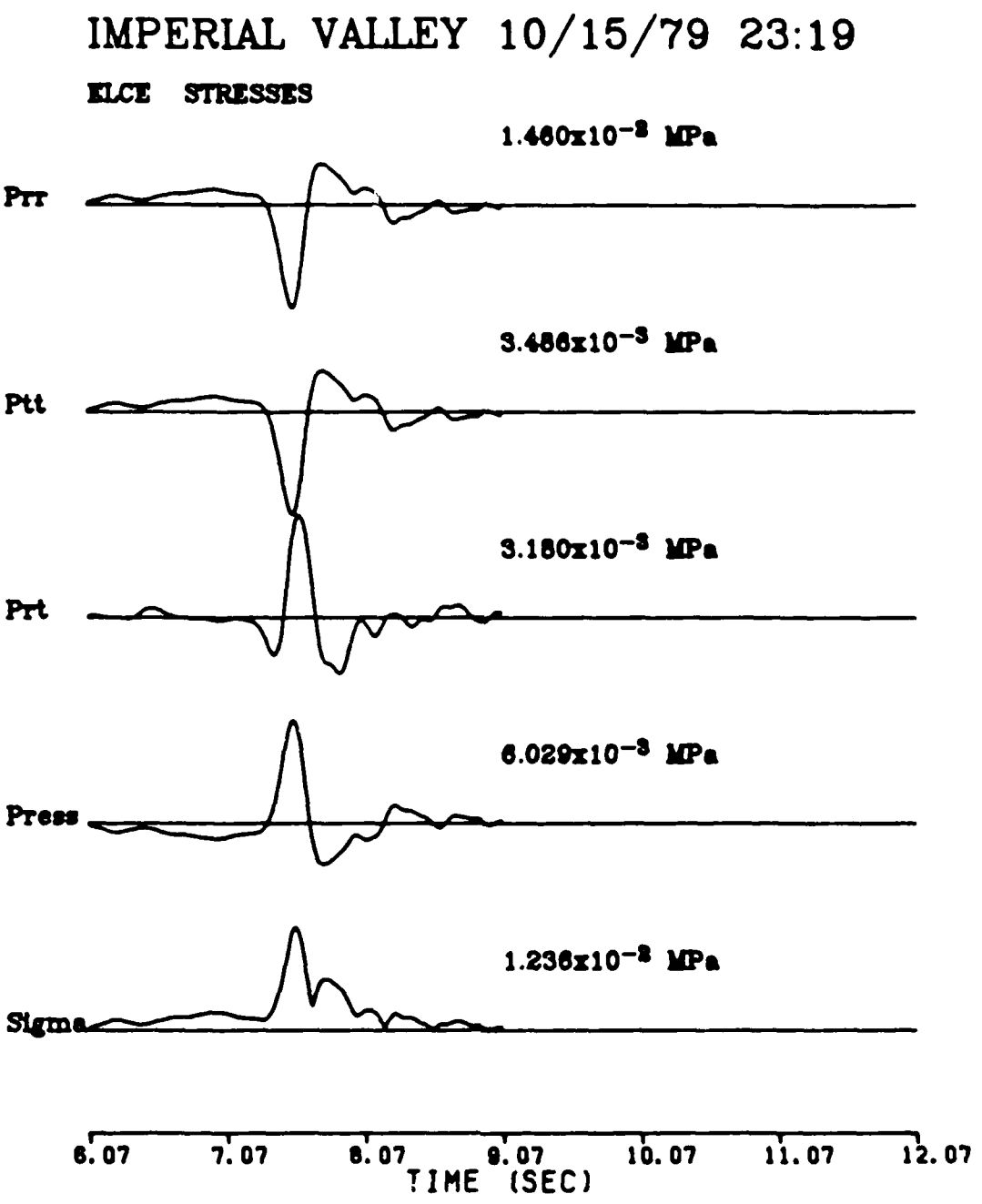
IMPERIAL VALLEY 10/15/79 23:19
ELCE STRESSES
1.460x10-2 MPa
Prr
3.486x10-3 MPa
Ptt
3.160x10-3 MPa
Prt
6.029x10-3 MPa
Press
1.236x10-2 MPa
Sigma
6.07
7.07
8.07
9.07
10.07
11.07
12.07
TIME (SEC)

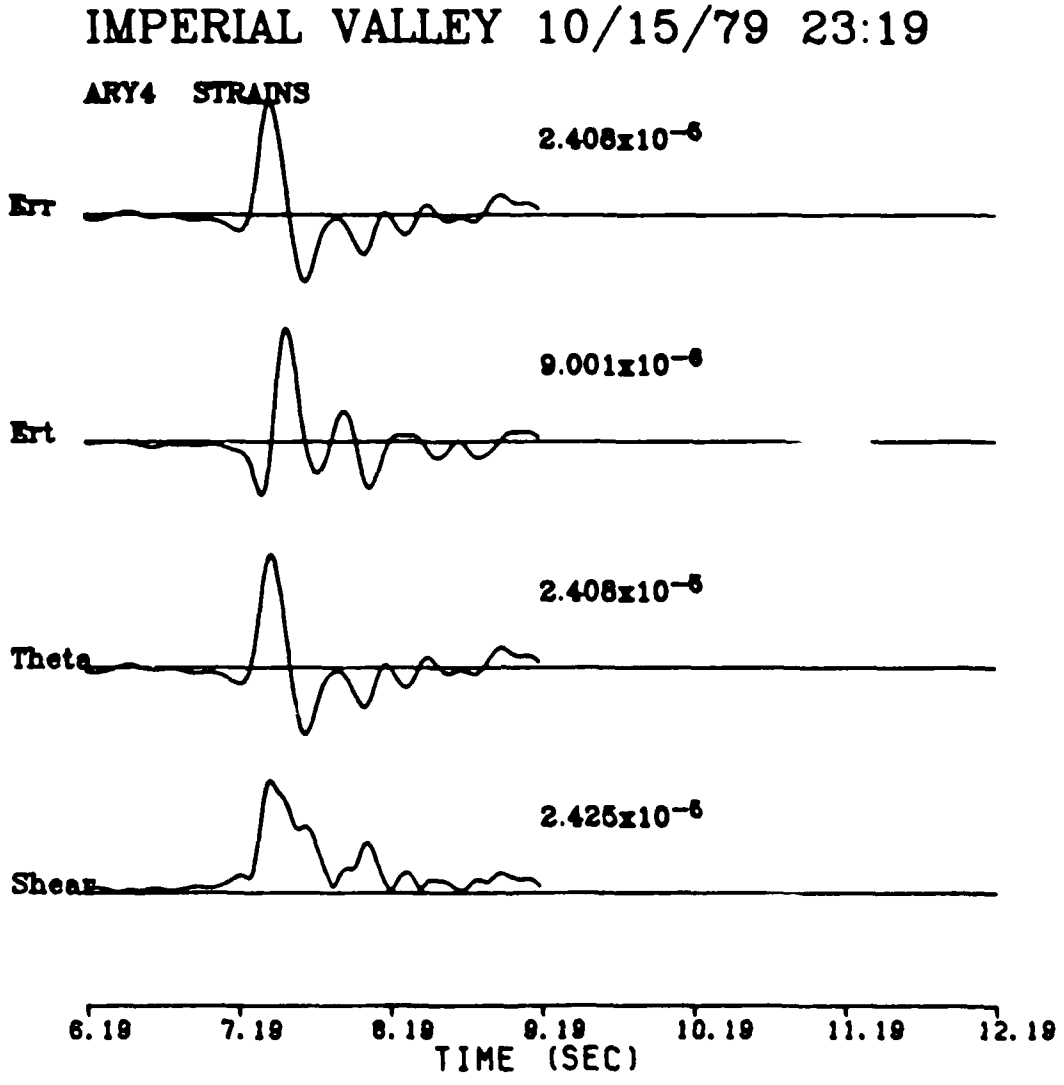
IMPERIAL VALLEY 10/15/79 23:19
ARY4 STRAINS
2.408x10⁻⁶
Err
9.001x10⁻⁶
Ert
2.408x10⁻⁶
Theta
2.425x10⁻⁶
Shear
6.19
7.19
8.19
9.19
10.19
11.19
12.19
TIME (SEC)

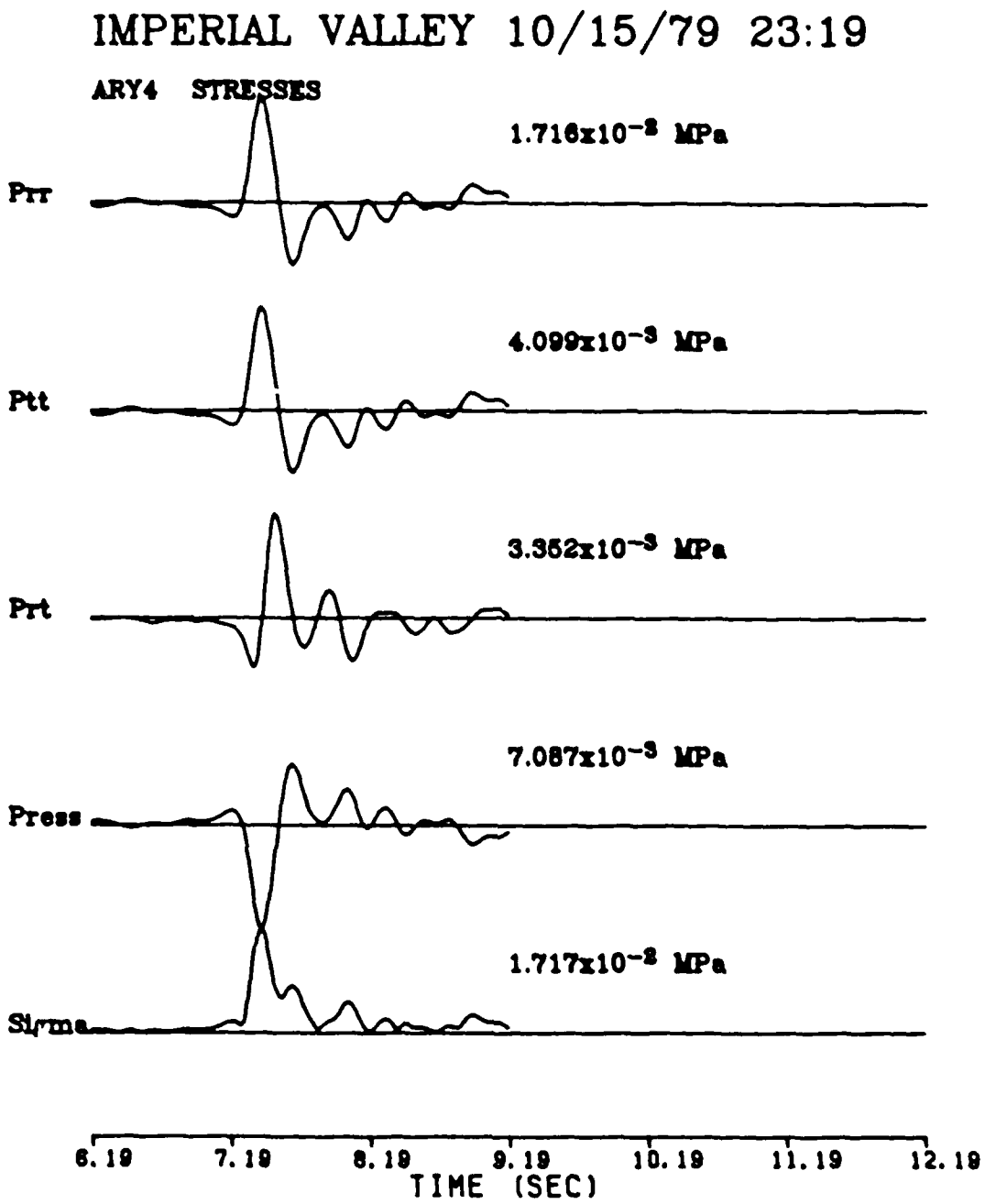
IMPERIAL VALLEY 10/15/79 23:19
ARY4 STRESSES
1.716x10⁻² MPa
Prr
4.099x10⁻³ MPa
Ptt
3.352x10⁻³ MPa
Prt
7.087x10⁻³ MPa
Press
1.717x10⁻² MPa
Sigma
6.19
7.19
8.19
9.19
10.19
11.19
12.19
TIME (SEC)

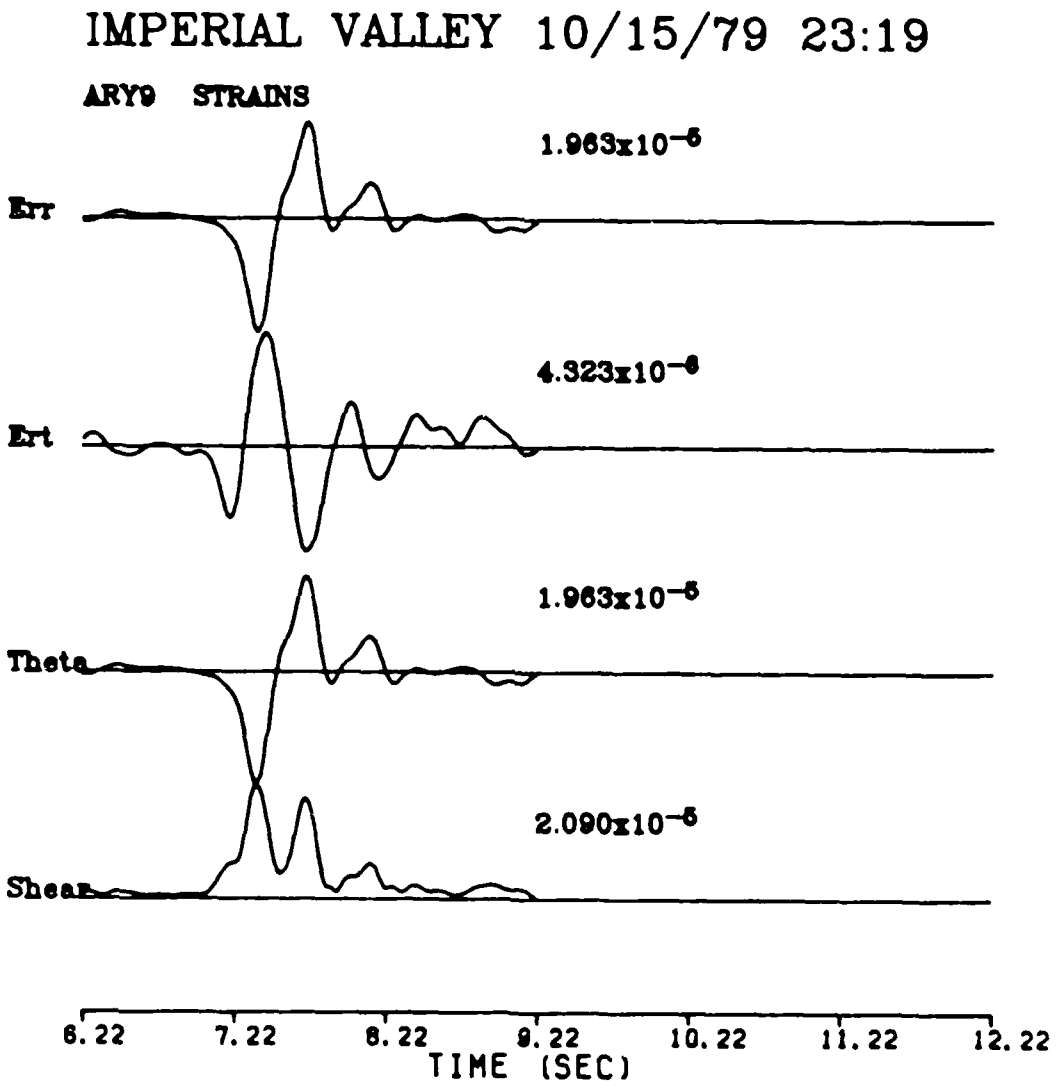
IMPERIAL VALLEY 10/15/79 23:19
ARY9 STRAINS
1.963x10⁻⁶
Err
4.323x10⁻⁶
Ert
1.963x10⁻⁶
Theta
2.090x10⁻⁶
Shear
6.22
7.22
8.22
9.22
10.22
11.22
12.22
TIME (SEC)

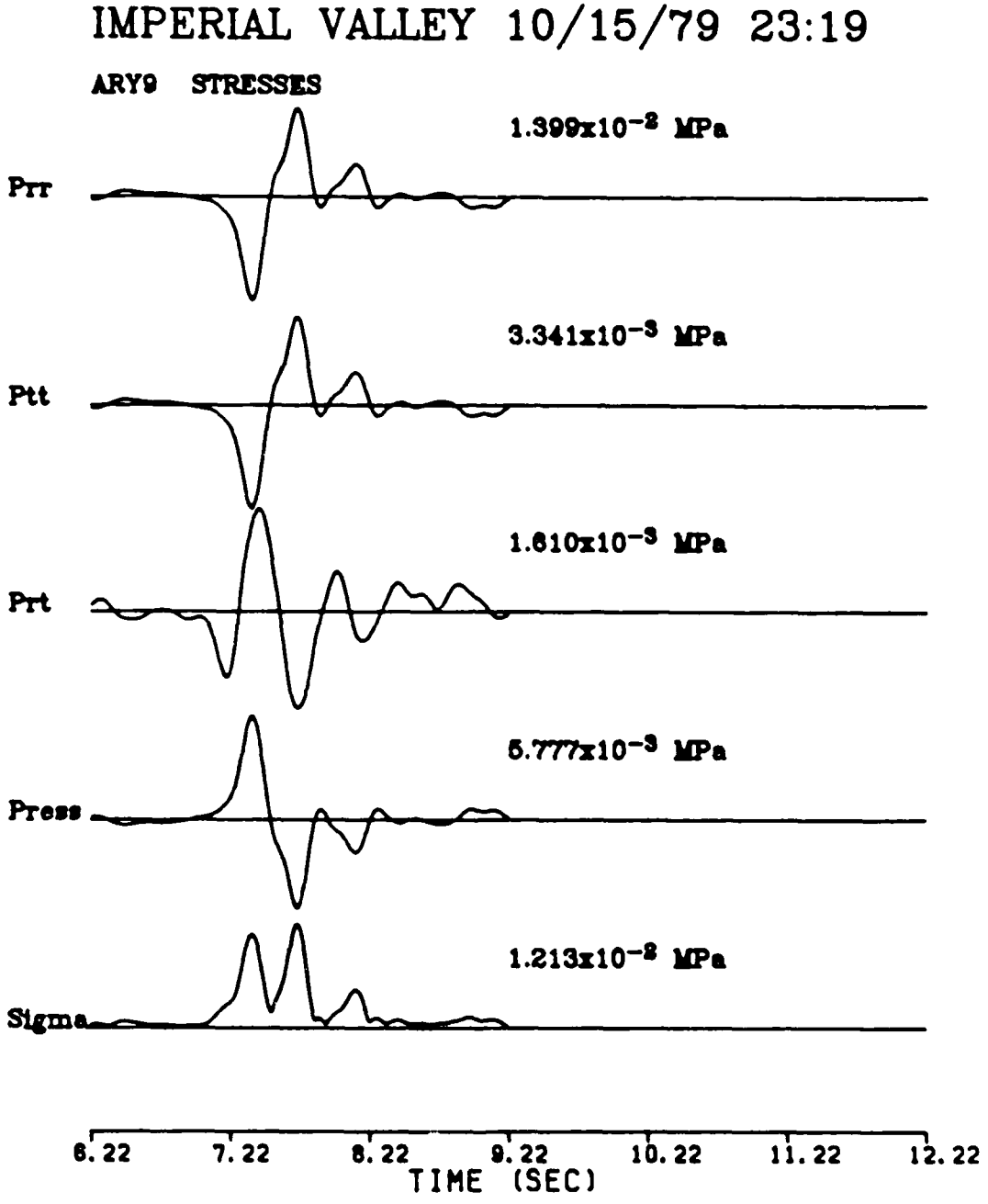
IMPERIAL VALLEY 10/15/79 23:19
ARY9 STRESSES
1.399x10-2 MPa
Prr
3.341x10-3 MPa
Ptt
1.610x10-3 MPa
Prt
5.777x10-3 MPa
Press
1.213x10-2 MPa
Sigma
6.22
7.22
8.22
9.22
10.22
11.22
12.22
TIME (SEC)

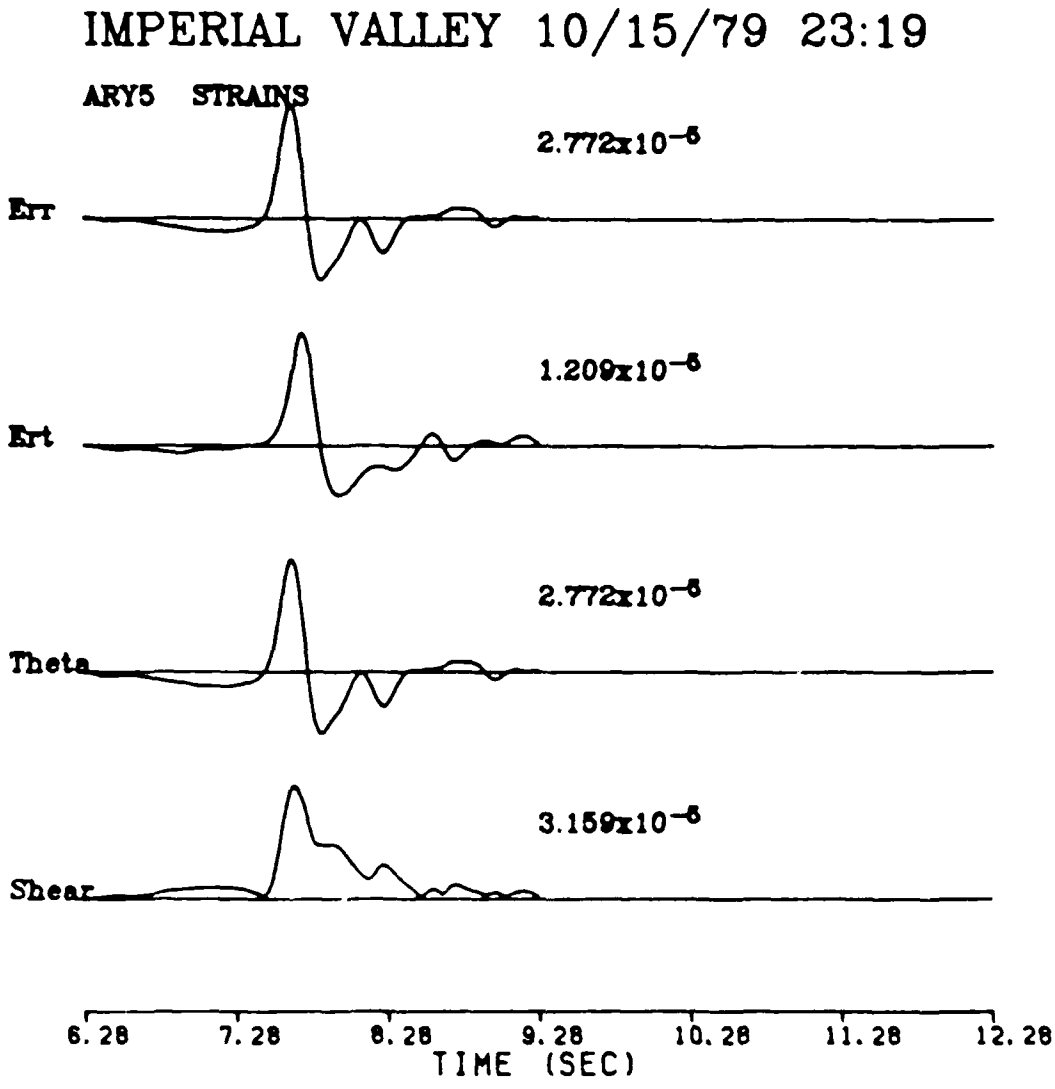
IMPERIAL VALLEY 10/15/79 23:19
ARY5 STRAINS
2.772x10⁻⁶
Err
1.209x10⁻⁶
Ert
2.772x10⁻⁶
Theta
3.159x10⁻⁶
Shear
6.28
7.28
8.28
9.28
10.28
11.28
12.28
TIME (SEC)

AD-A181 190 STRAINS AND STRESSES NEAR EXPLOSIONS AND EARTHQUAKES 2/2
(U) WOODWARD-CLYDE CONSULTANTS PASADENA CA
L J BURDICK ET AL. 15 OCT 86 WCCP-R-86-02
UNCLASSIFIED AFGL-TR-87-0089 F19628-85-C-0036 F/G 19/9 NL

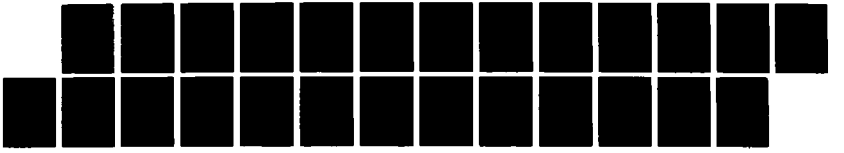

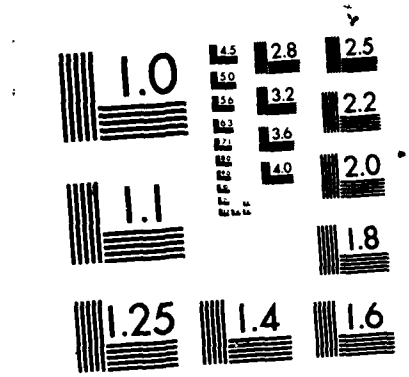

MICROCOPY RESOLUTION TEST CHART
NATIONAL BUREAU OF STANDARDS-1963-A

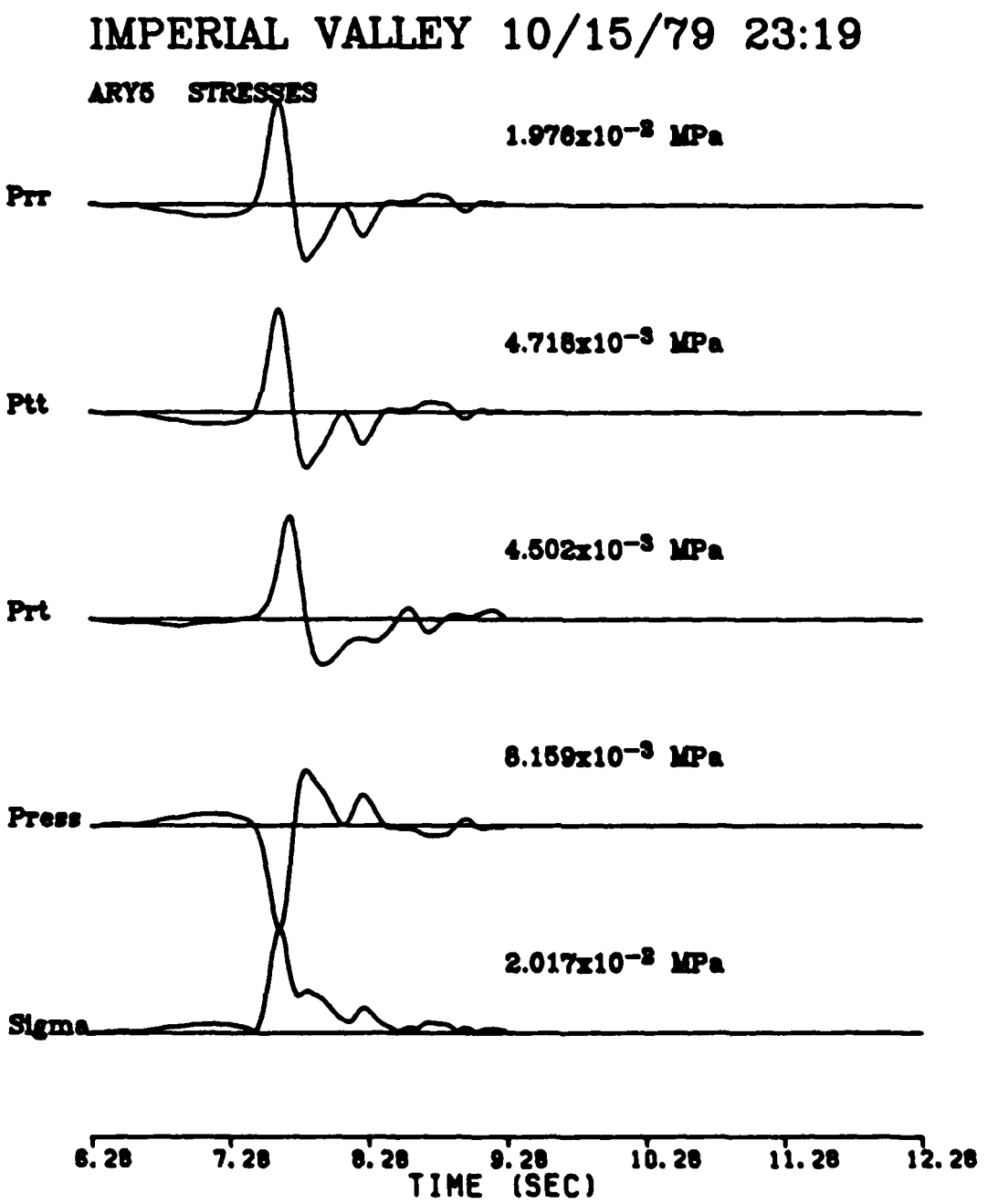
IMPERIAL VALLEY 10/15/79 23:19
ARY5 STRESSES
1.976x10-2 MPa
Prr
4.716x10-3 MPa
Ptt
4.502x10-3 MPa
Prt
8.159x10-3 MPa
Press
2.017x10-2 MPa
Sigma
6.28
7.28
8.28
9.28
10.28
11.28
12.28
TIME (SEC)

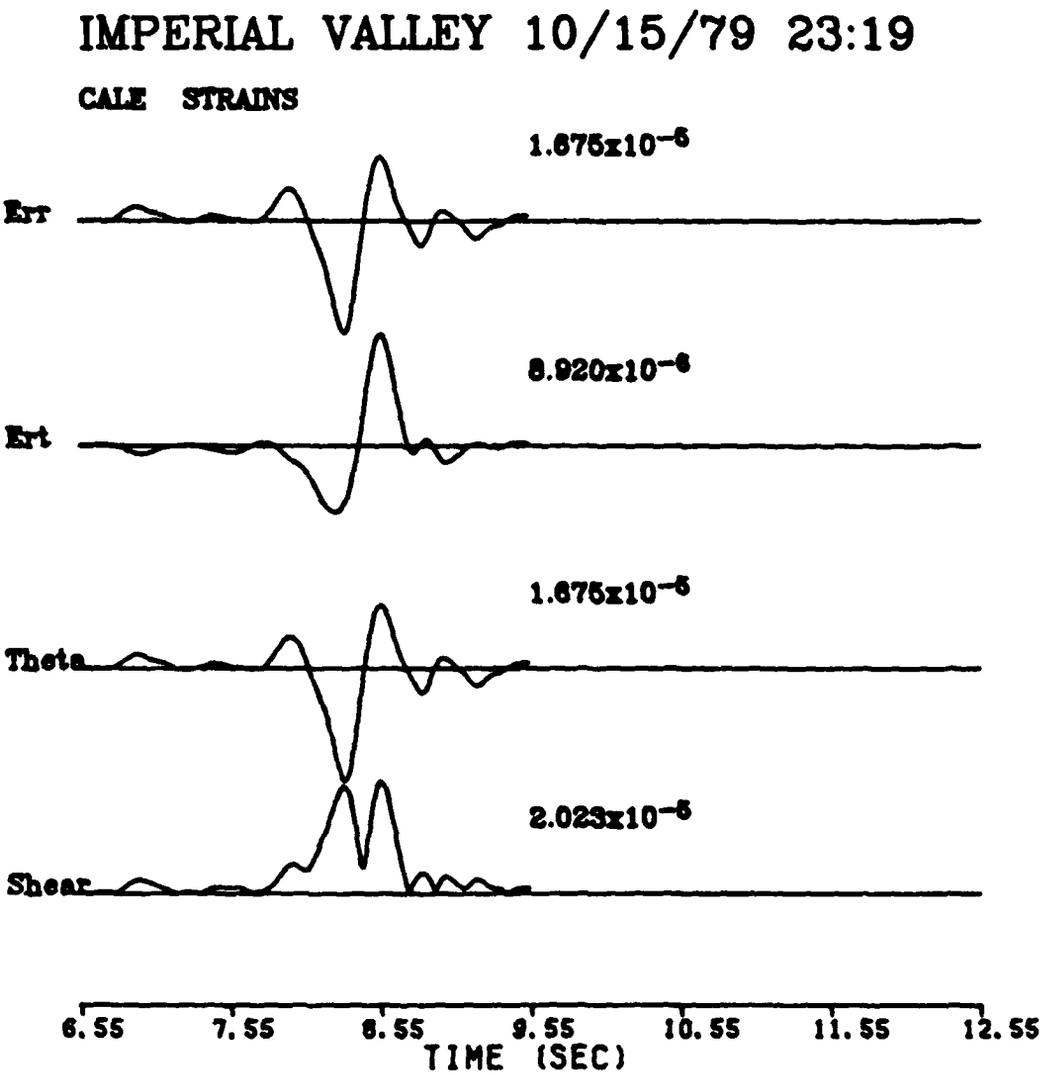
IMPERIAL VALLEY 10/15/79 23:19
CALE STRAINS
1.675x10⁻⁶
Err
8.920x10⁻⁶
Ert
1.675x10⁻⁶
Theta
2.023x10⁻⁶
Shear
6.55
7.55
8.55
9.55
10.55
11.55
12.55
TIME (SEC)

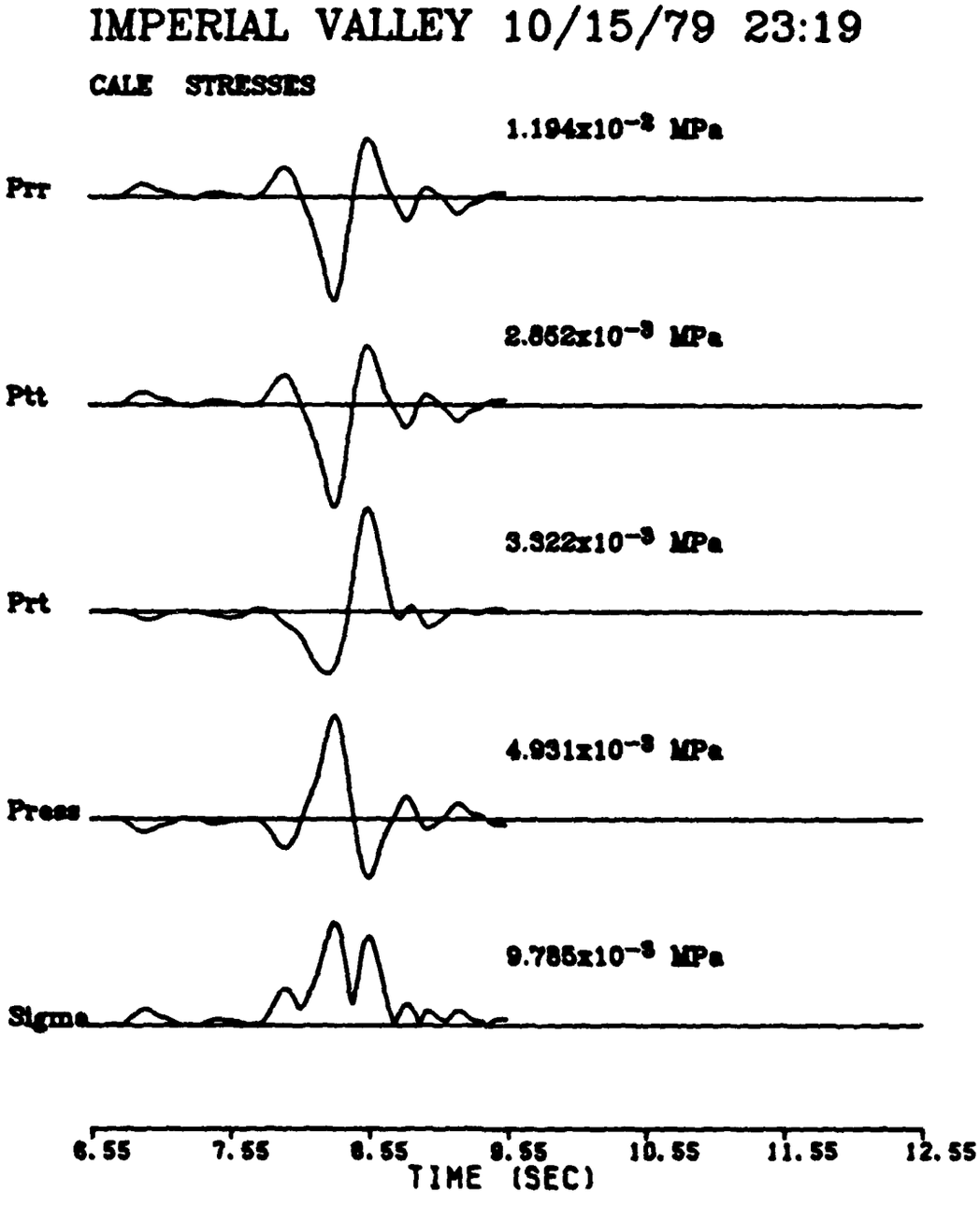
IMPERIAL VALLEY 10/15/79 23:19
CALE STRESSES
1.194x10⁻² MPa
Prr
2.852x10⁻³ MPa
Ptt
3.322x10⁻³ MPa
Prt
4.931x10⁻³ MPa
Press
9.785x10⁻³ MPa
Sigma
6.55
7.55
8.55
9.55
10.55
11.55
12.55
TIME (SEC)

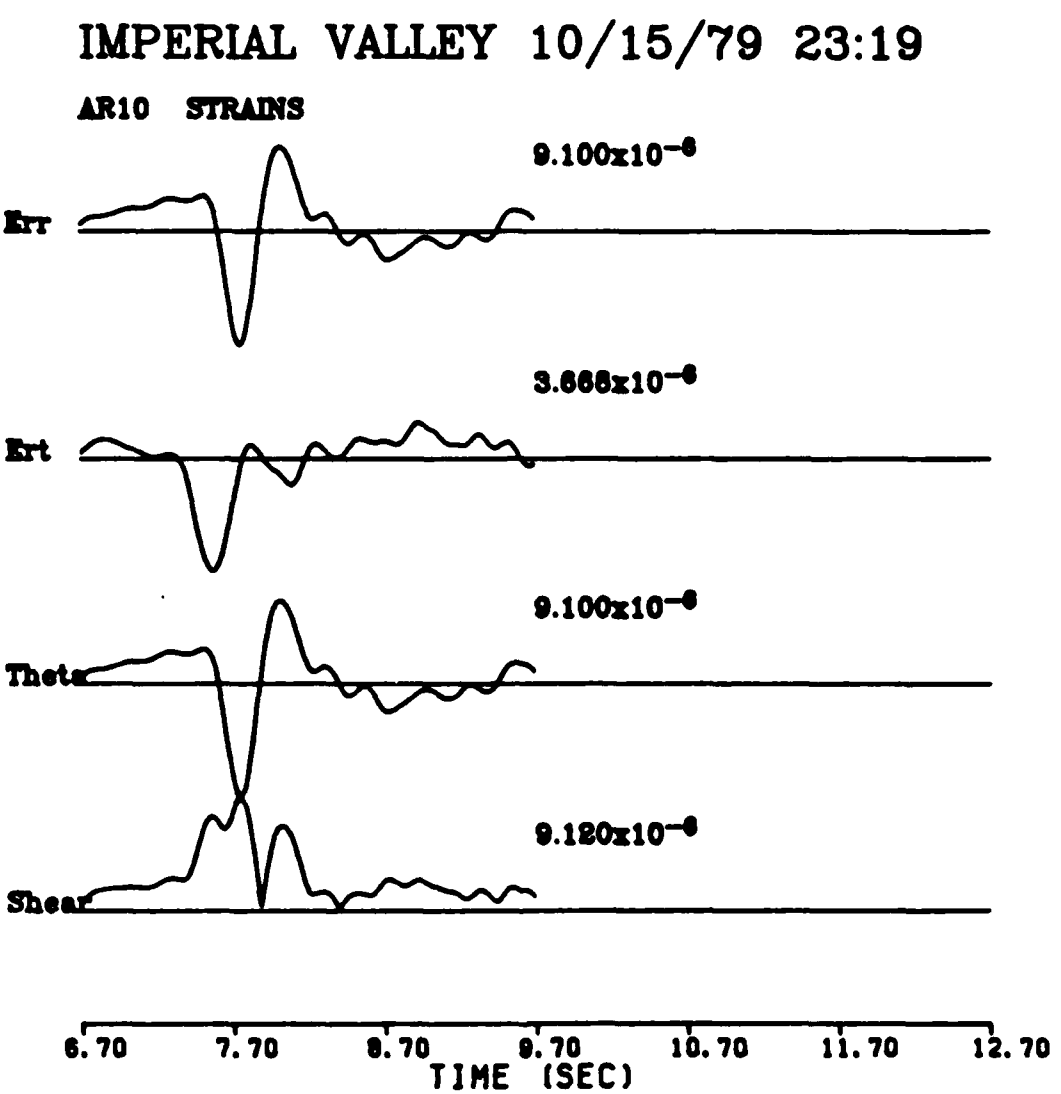
IMPERIAL VALLEY 10/15/79 23:19
AR10 STRAINS
9.100x10⁻⁶
Err
3.666x10⁻⁶
Ert
9.100x10⁻⁶
Theta
9.120x10⁻⁶
Shear
6.70
7.70
8.70
9.70
10.70
11.70
12.70
TIME (SEC)

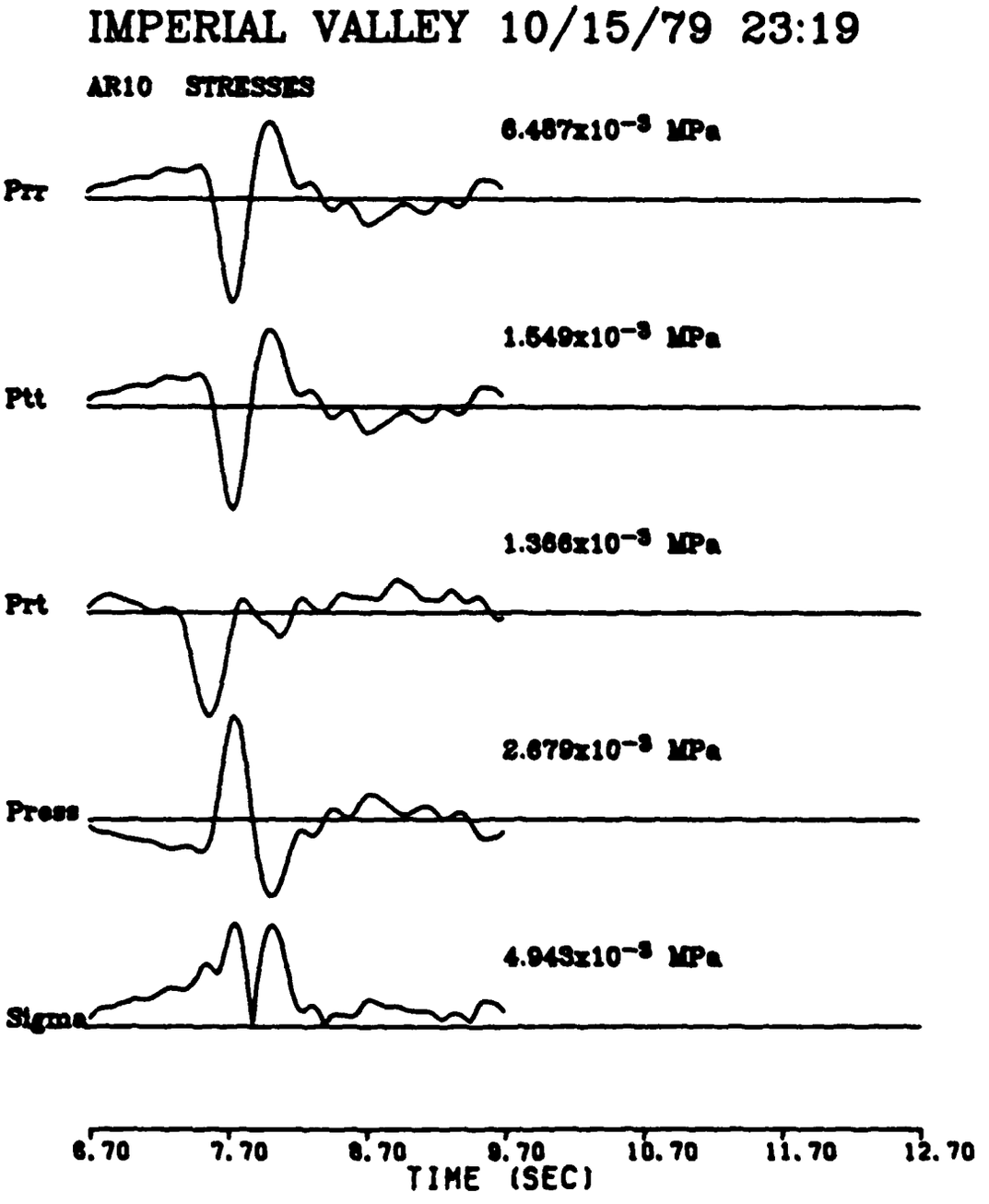
IMPERIAL VALLEY 10/15/79 23:19
AR10 STRESSES
6.487x10⁻³ MPa
Prr
1.549x10⁻³ MPa
Ptt
1.366x10⁻³ MPa
Prt
2.679x10⁻³ MPa
Press
4.943x10⁻³ MPa
Sigma
6.70
7.70
8.70
9.70
10.70
11.70
12.70
TIME (SEC)

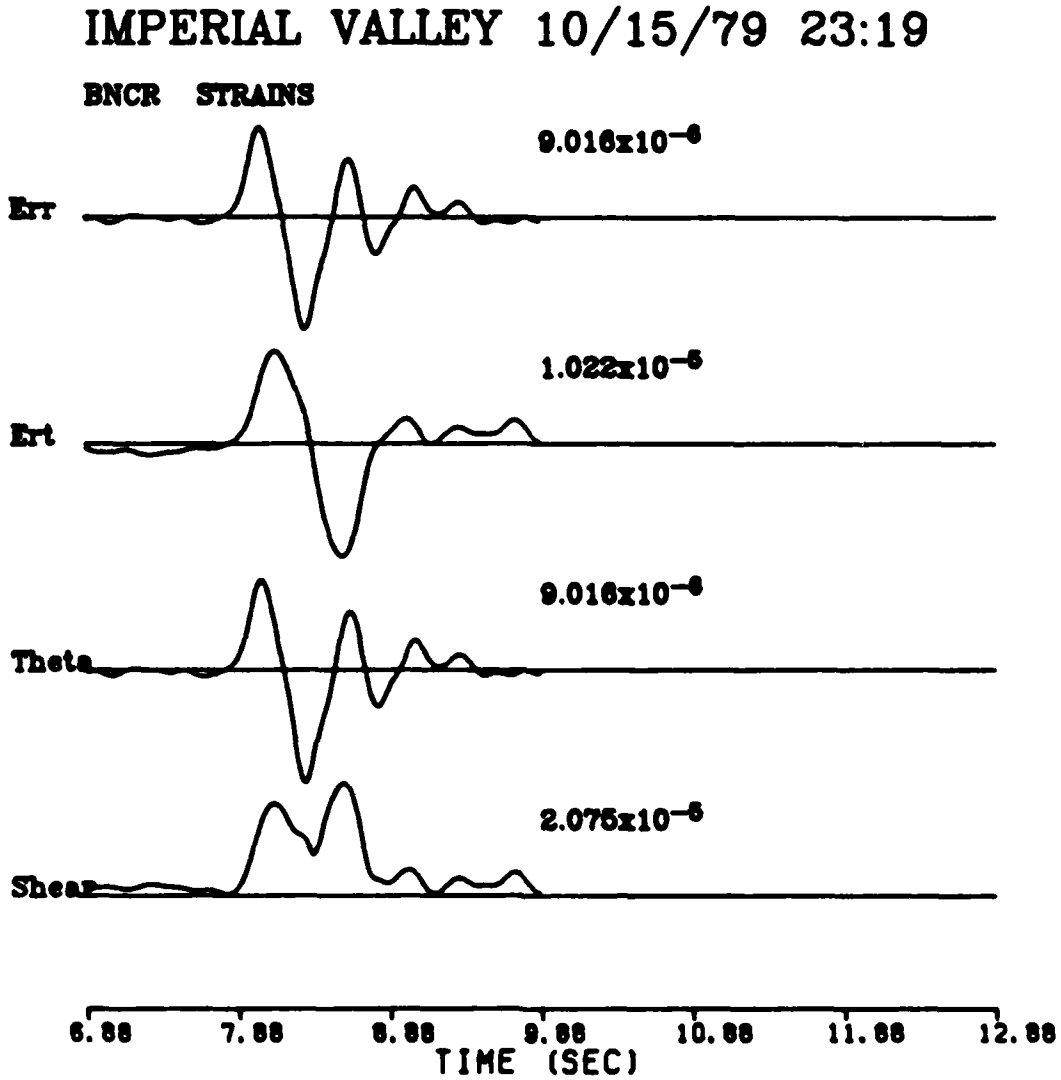
IMPERIAL VALLEY 10/15/79 23:19
BNCR STRAINS
9.016x10⁻⁶
Err
1.022x10⁻⁶
Ert
9.016x10⁻⁶
Theta
2.075x10⁻⁶
Shear
6.88
7.88
8.88
9.88
10.88
11.88
12.88
TIME (SEC)

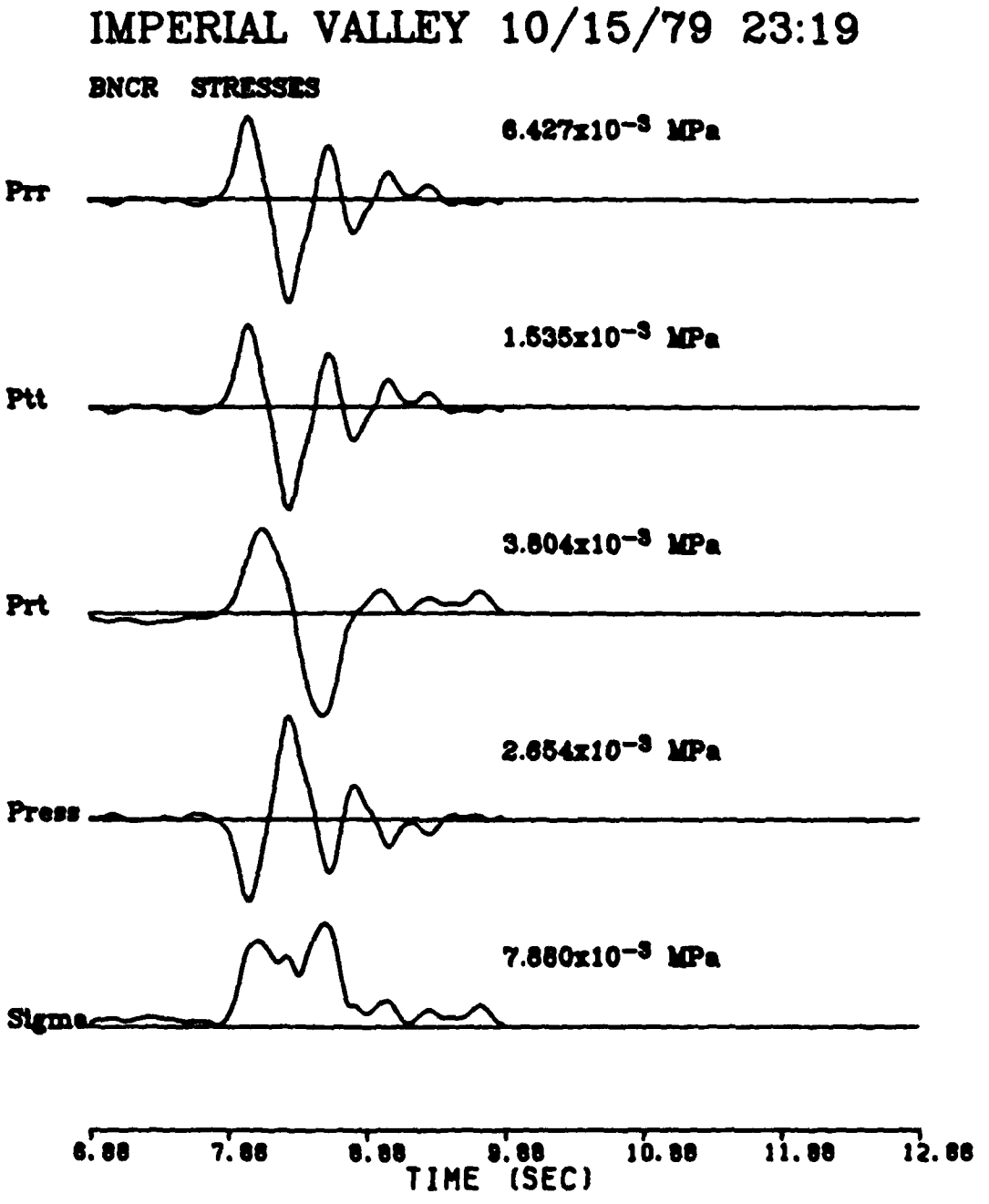
IMPERIAL VALLEY 10/15/79 23:19
BNCR STRESSES
6.427x10⁻³ MPa
Prr
1.535x10⁻³ MPa
Ptt
3.804x10⁻³ MPa
Prt
2.654x10⁻³ MPa
Press
7.680x10⁻³ MPa
Sigma
6.00
7.00
8.00
9.00
10.00
11.00
12.00
TIME (SEC)

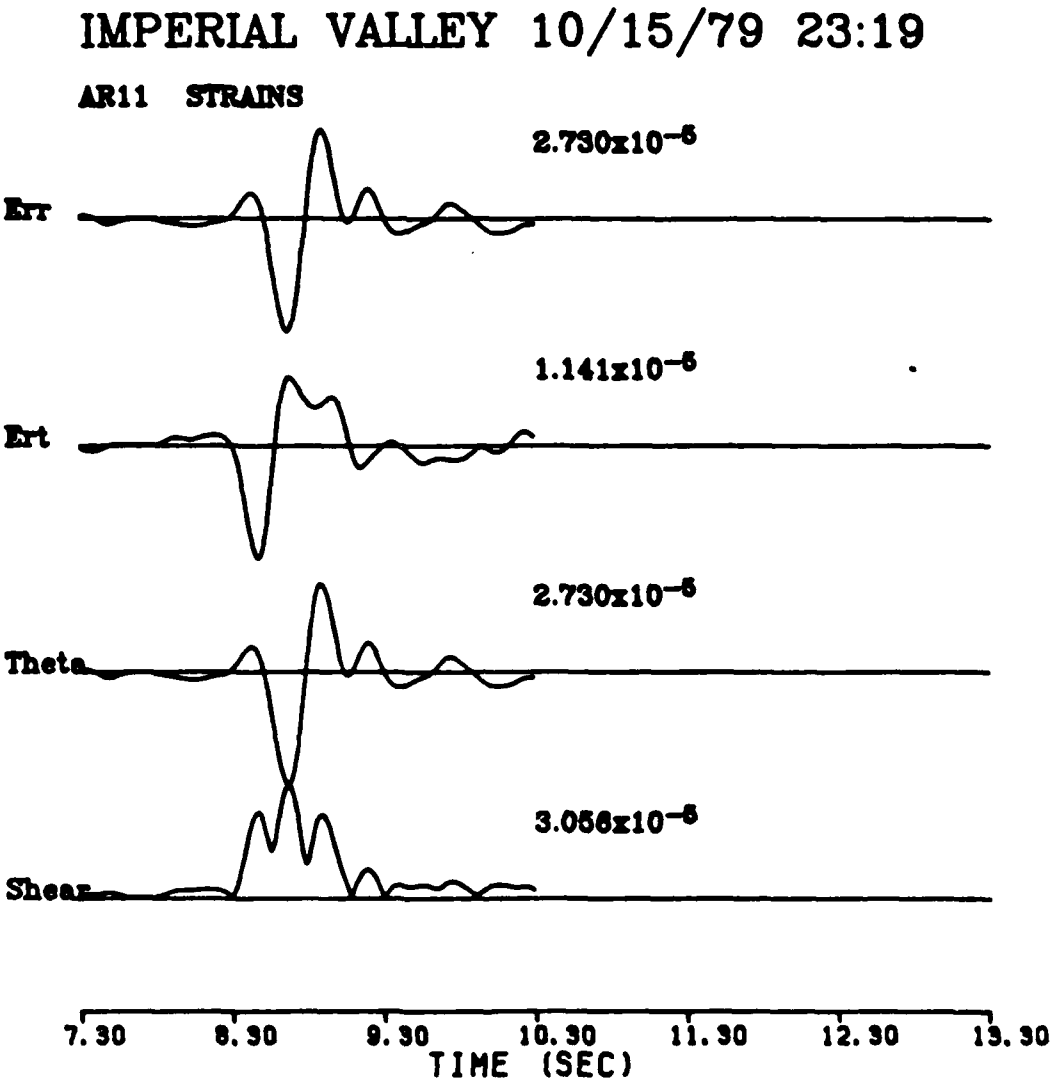
IMPERIAL VALLEY 10/15/79 23:19
AR11 STRAINS
2.730x10⁻⁶
Err
1.141x10⁻⁶
Ert
2.730x10⁻⁶
Theta
3.056x10⁻⁶
Shear
7.30
8.30
9.30
10.30
11.30
12.30
13.30
TIME (SEC)

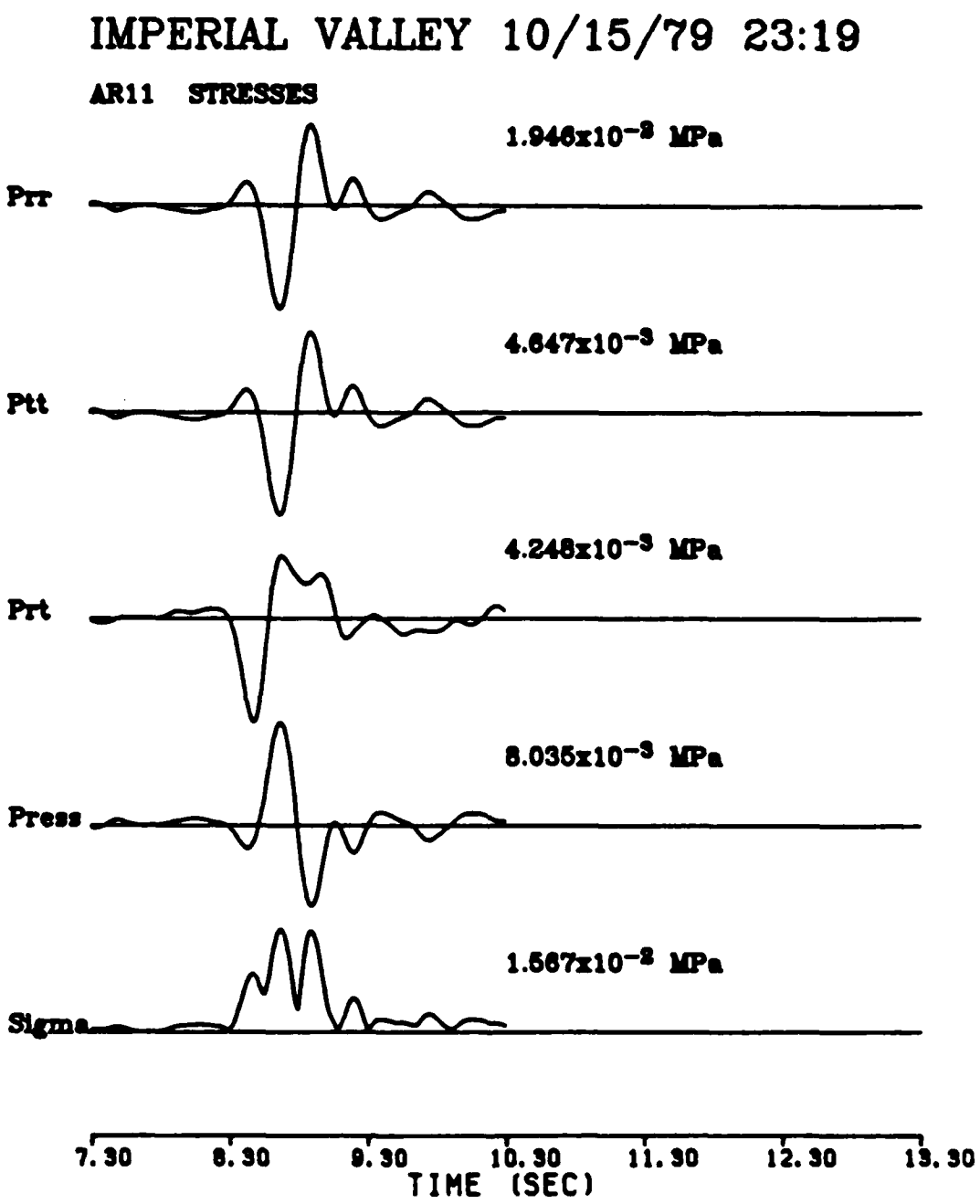
IMPERIAL VALLEY 10/15/79 23:19
AR11 STRESSES
1.946x10-2 MPa
Prr
4.647x10-3 MPa
Ptt
4.248x10-3 MPa
Prt
8.035x10-3 MPa
Press
1.567x10-2 MPa
Sigma
7.30
8.30
9.30
10.30
11.30
12.30
13.30
TIME (SEC)

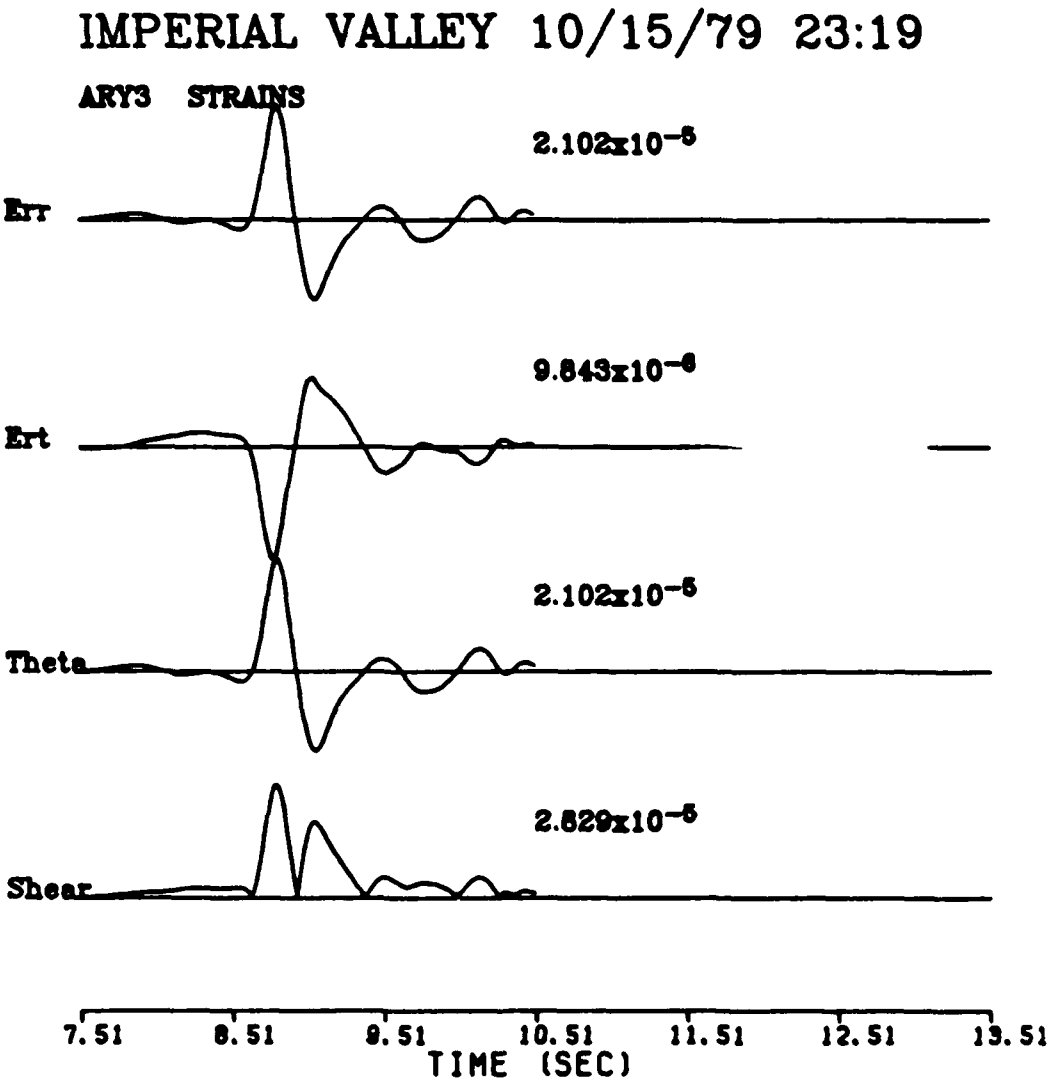
IMPERIAL VALLEY 10/15/79 23:19
ARY3 STRAINS
2.102x10⁻⁵
Err
9.843x10⁻⁶
Ert
2.102x10⁻⁵
Theta
2.629x10⁻⁵
Shear
7.51
8.51
9.51
10.51
11.51
12.51
13.51
TIME (SEC)

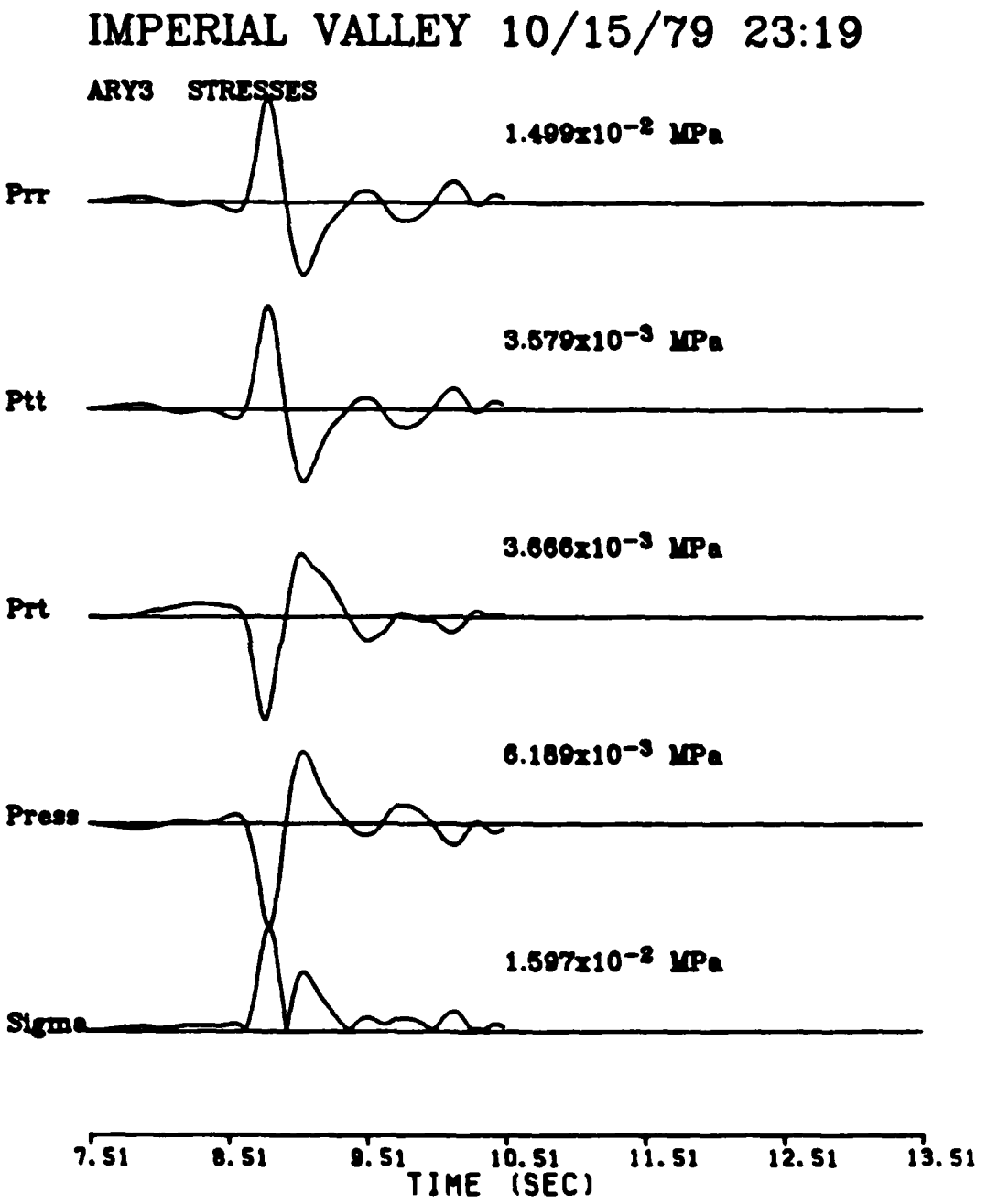
IMPERIAL VALLEY 10/15/79 23:19
ARY3 STRESSES
1.499x10-2 MPa
Prr
3.579x10-3 MPa
Ptt
3.666x10-3 MPa
Prt
6.189x10-3 MPa
Press
1.597x10-2 MPa
Sigma
7.51
8.51
9.51
10.51
11.51
12.51
13.51
TIME (SEC)

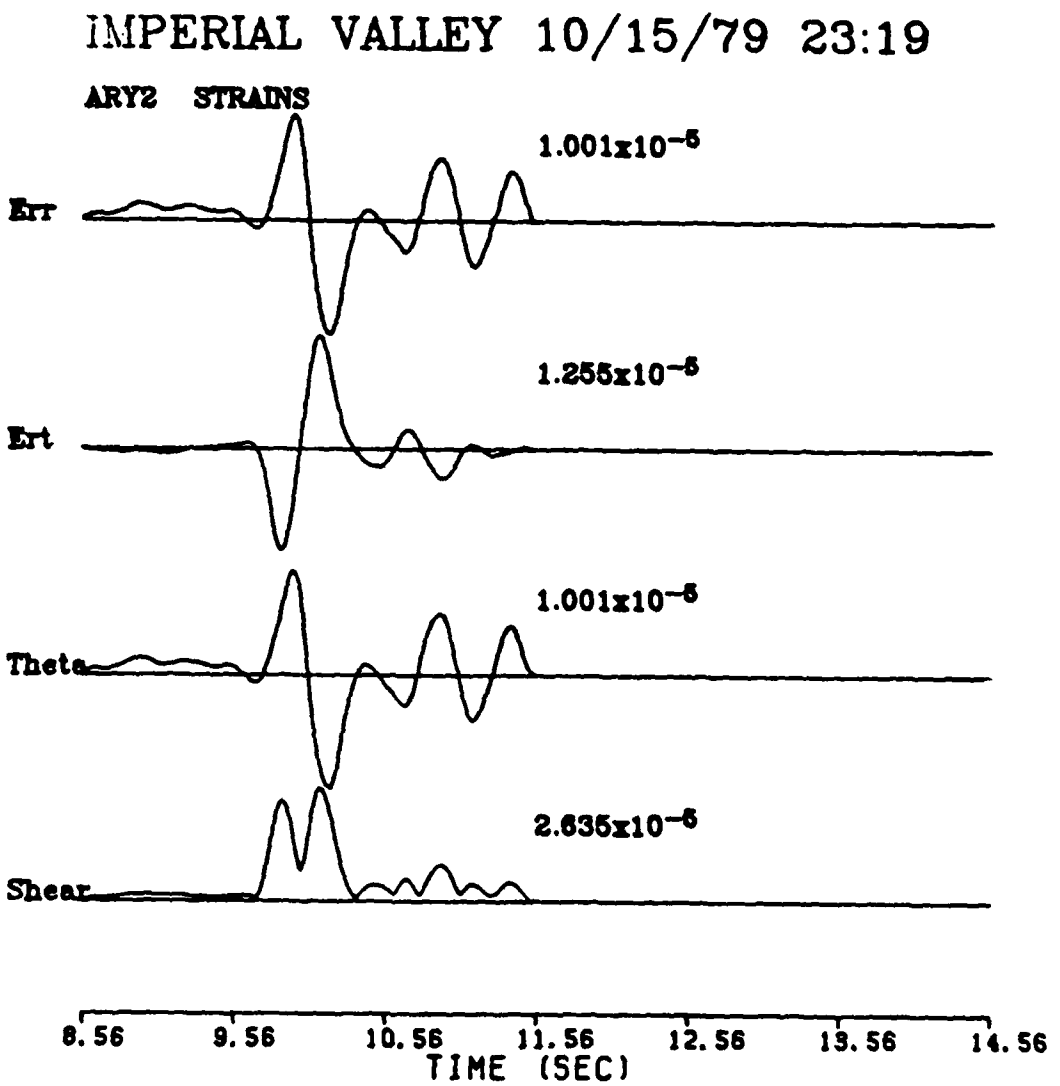
IMPERIAL VALLEY 10/15/79 23:19
ARY2 STRAINS
Err
1.001x10⁻⁵
Ert
1.255x10⁻⁵
Theta
1.001x10⁻⁵
Shear
2.635x10⁻⁵
8.56
9.56
10.56
11.56
12.56
13.56
14.56
TIME (SEC)

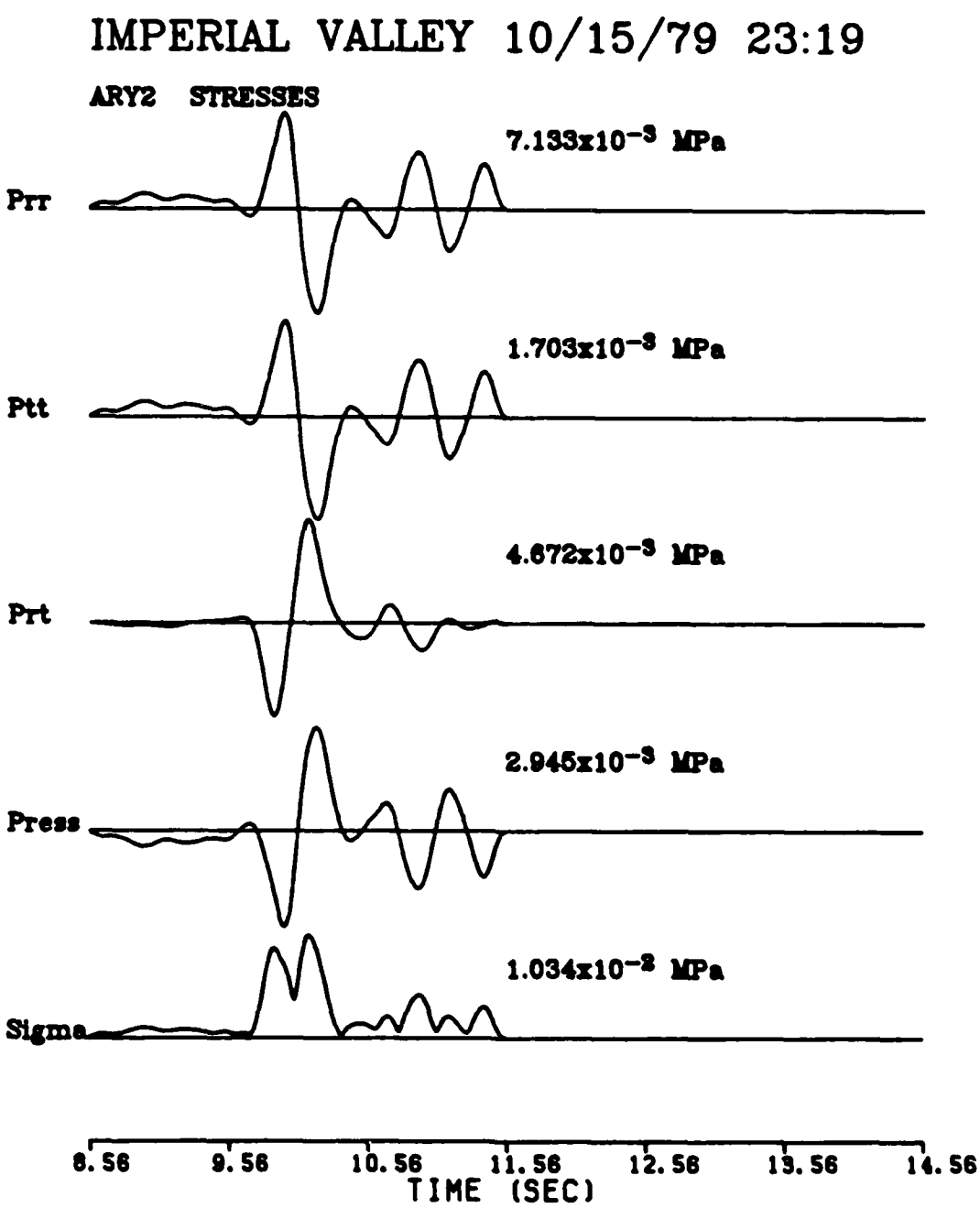
IMPERIAL VALLEY 10/15/79 23:19
ARY2 STRESSES
Prr
7.133x10-3 MPa
Ptt
1.703x10-3 MPa
Prt
4.672x10-3 MPa
Press
2.945x10-3 MPa
Sigma
1.034x10-2 MPa
8.56
9.56
10.56
11.56
12.56
13.56
14.56
TIME (SEC)

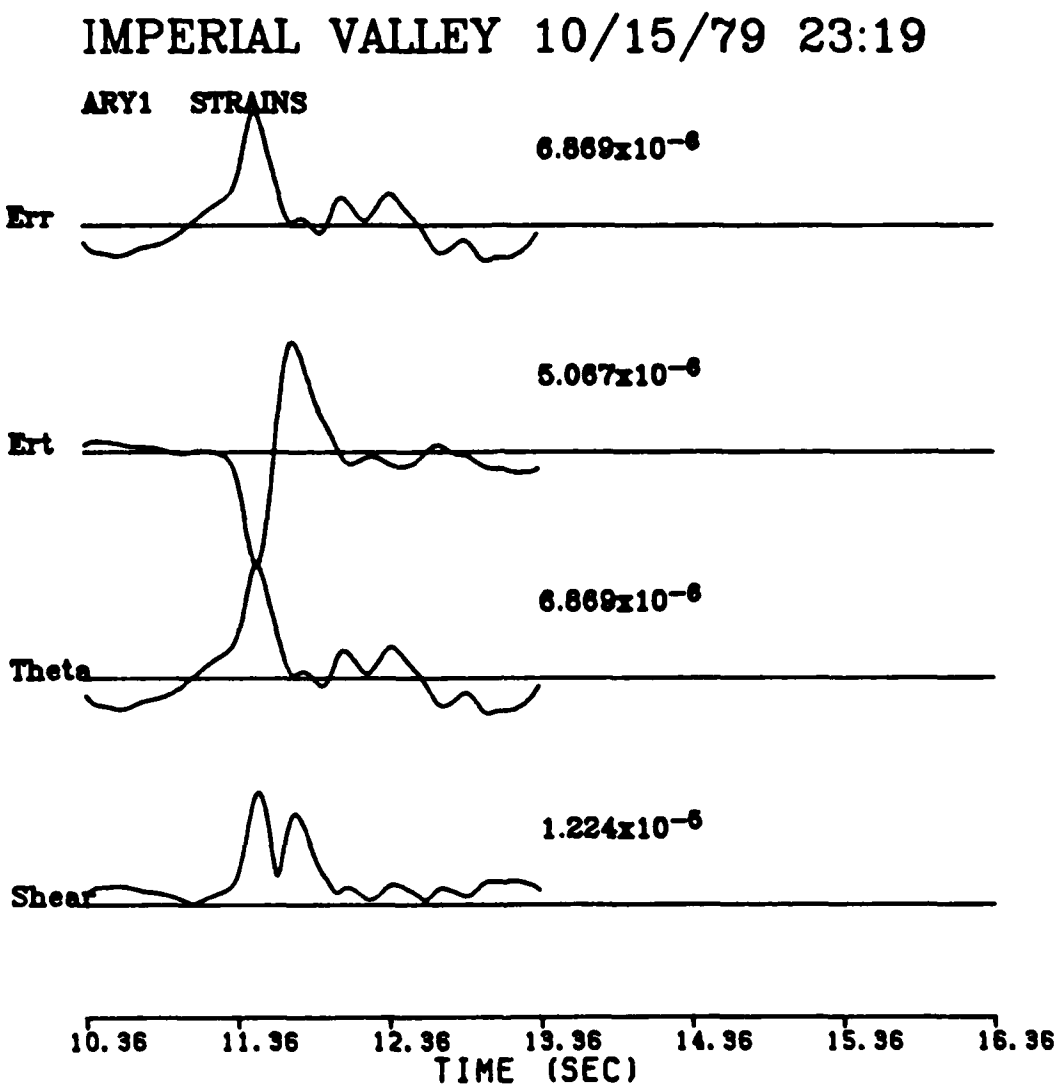
IMPERIAL VALLEY 10/15/79 23:19
ARY1 STRAINS
6.869x10⁻⁶
Err
5.067x10⁻⁶
Ert
6.869x10⁻⁶
Theta
1.224x10⁻⁶
Shear
10.36
11.36
12.36
13.36
14.36
15.36
16.36
TIME (SEC)

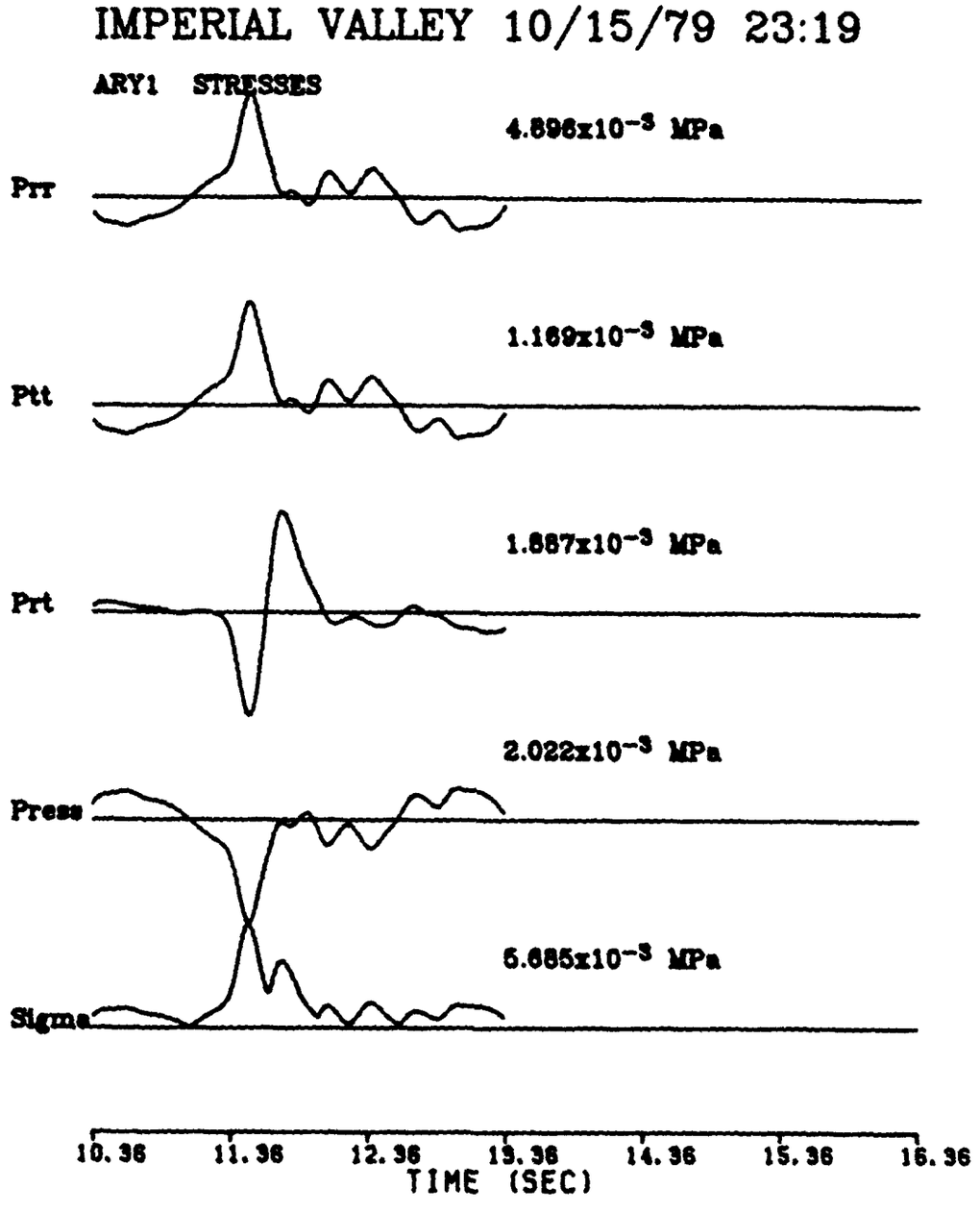
IMPERIAL VALLEY 10/15/79 23:19
ARY1 STRESSES
4.896x10-3 MPa
Prr
1.169x10-3 MPa
Ptt
1.887x10-3 MPa
Prt
2.022x10-3 MPa
Press
5.685x10-3 MPa
Sigma
10.36
11.36
12.36
13.36
14.36
15.36
16.36
TIME (SEC)

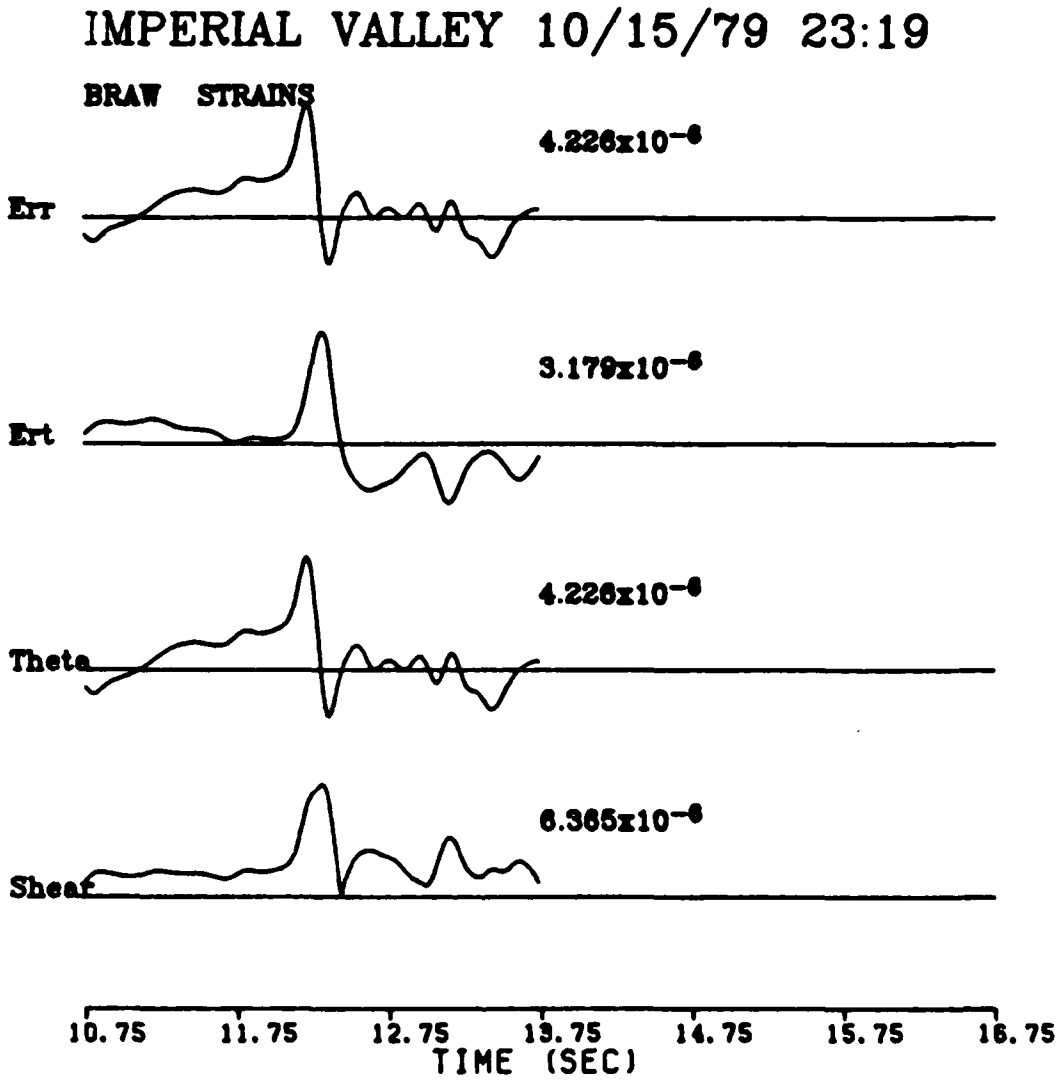
IMPERIAL VALLEY 10/15/79 23:19
BRAW STRAINS
4.226x10⁻⁶
Err
3.179x10⁻⁶
Ert
4.226x10⁻⁶
Theta
6.365x10⁻⁶
Shear
10.75
11.75
12.75
13.75
14.75
15.75
16.75
TIME (SEC)

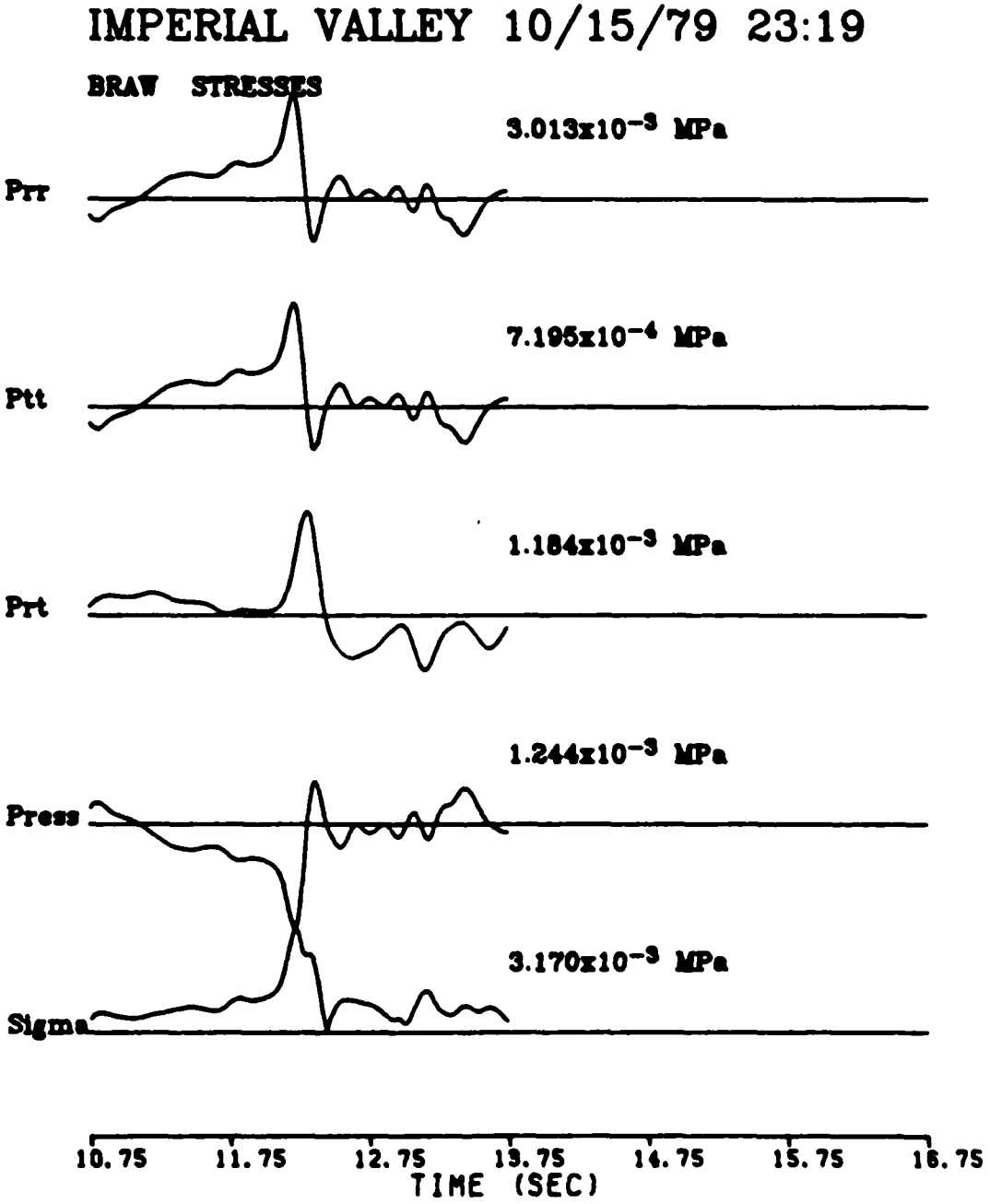
IMPERIAL VALLEY 10/15/79 23:19
BRAW STRESSES
3.013x10-3 MPa
Prr
7.195x10-4 MPa
Ptt
1.184x10-3 MPa
Prt
1.244x10-3 MPa
Press
3.170x10-3 MPa
Sigma
10.75
11.75
12.75
13.75
14.75
15.75
16.75
TIME (SEC)

DISTRIBUTION LIST

Dr. Monem Abdel-Gawad
Rockwell International Science Center
1049 Camino Dos Rios
Thousand Oaks, CA 91360

Professor Keiiti Aki
Center for Earth Sciences
University of Southern California
University Park
Los Angeles, CA 90089-0741

Professor Shelton S. Alexander
Geosciences Department
403 Deike Building
The Pennsylvania State University
University Park, PA 16802

Professor Charles B. Archambeau
Cooperative Institute for Research in Environmental Sciences
University of Colorado
Boulder, CO 80309

Dr. Thomas C. Bache Jr.
Science Applications Int'l Corp.
10210 Campus Point Drive
San Diego, CA 92121

Dr. James Bulau
Rockwell International Science Center
1049 Camino Dos Rios
P.O. Box 1085
Thousand Oaks, CA 91360

Dr. Douglas R. Baumgardt
Signal Analysis and Systems Division
ENSCO, Inc.
5400 Port Royal Road
Springfield, VA 22151-2388

Dr. S. Bratt
Science Applications Int'l Corp.
10210 Campus Point Drive
San Diego, CA 92121

Professor John Ebel
Department of Geology & Geophysics
Boston College
Chestnut Hill, MA 02167

Woodward-Clyde Consultants
Attn: Dr. Lawrence J. Burdick
Dr. Jeff Barker
P.O. Box 93245
Pasadena, CA 91109-3245 (2 copies)

Dr. Roy Burger
1221 Serry Rd.
Schenectady, NY 12309

Professor Robert W. Clayton
Seismological Laboratory
Division of Geological and Planetary Sciences
California Institute of Technology
Pasadena, CA 91125

Dr. Vernon F. Cormier
Earth Resources Laboratory
Department of Earth, Atmospheric and Planetary Sciences
Massachusetts Institute of Technology
42 Carleton Street
Cambridge, MA 02142

Professor Anton M. Dainty
Earth Resources Laboratory
Department of Earth, Atmospheric and Planetary Sciences
Massachusetts Institute of Technology
42 Carleton Street
Cambridge, MA 02142

Dr. Zoltan A. Der
Teledyne Geotech
314 Montgomery Street
Alexandria, VA 22314

Prof. Adam Dziewonski
Hoffman Laboratory
Harvard University
20 Oxford St.
Cambridge, MA 02138

Professor John Ferguson
Center for Lithospheric Studies
The University of Texas at Dallas
P.O. Box 830688
Richardson, TX 75083-0688

Dr. Jeffrey W. Given
Sierra Geophysics
11255 Kirkland Way
Kirkland, WA 98033

Prof. Roy Greenfield
Geosciences Department
403 Deike Building
The Pennsylvania State University
University Park, PA 16802

Professor David G. Harkrider
Seismological Laboratory
Division of Geological and Planetary Sciences
California Institute of Technology
Pasadena, CA 91125

Professor Donald V. Helmberger
Seismological Laboratory
Division of Geological and Planetary Sciences
California Institute of Technology
Pasadena, CA 91125

Professor Eugene Herrin
Institute for the Study of Earth & Man
Geophysical Laboratory
Southern Methodist University
Dallas, TX 75275

Professor Robert B. Herrmann
Department of Earth and Atmospheric Sciences
Saint Louis University
Saint Louis, MO 63156

Professor Lane R. Johnson
Seismographic Station
University of California
Berkeley, CA 94720

Professor Thomas H. Jordan
Department of Earth, Atmospheric and Planetary Sciences
Massachusetts Institute of Technology
Cambridge, MA 02139

Dr. Alan Kafka
Department of Geology & Geophysics
Boston College
Chestnut Hill, MA 02167

Professor Charles A. Langston
Geosciences Department
403 Deike Building
The Pennsylvania State University
University Park, PA 16802

Professor Thorne Lay
Department of Geological Sciences
1006 C.C. Little Building
University of Michigan
Ann Arbor, MI 48109-1063

Dr. George R. Mellman
Sierra Geophysics
11255 Kirkland Way
Kirkland, WA 98033

Professor Brian J. Mitchell
Department of Earth and Atmospheric Sciences
Saint Louis University
Saint Louis, MO 63156

Professor Thomas V. McEvilly
Seismographic Station
University of California
Berkeley, CA 94720

Dr. Keith L. McLaughlin
Teledyne Geotech
314 Montgomery Street
Alexandria, VA 22314

Professor Otto W. Nuttli
Department of Earth and Atmospheric Sciences
Saint Louis University
Saint Louis, MO 63156

Professor Paul G. Richards
Lamont-Doherty Geological Observatory
of Columbia University
Palisades, NY 10964

Dr. Norton Rimer
S-Cubed
A Division of Maxwell Laboratory
P.O. 1620
La Jolla, CA 92038-1620

Professor Larry J. Ruff
Department of Geological Sciences
1006 C.C. Little Building
University of Michigan
Ann Arbor, MI 48109-1063

Professor Charles G. Sammis
Center for Earth Sciences
University of Southern California
University Park
Los Angeles, CA 90089-0741

Dr. David G. Simpson
Lamont-Doherty Geological Observatory
of Columbia University
Palisades, NY 10964

Dr. Jeffrey L. Stevens
S-CUBED,
A Division of Maxwell Laboratory
P.O. Box 1620
La Jolla, CA 92038-1620

Professor Brian Stump
Institute for the Study of Earth
and Man
Geophysical Laboratory
Southern Methodist University
Dallas, TX 75275

Professor Ta-liang Teng
Center for Earth Sciences
University of Southern California
University Park
Los Angeles, CA 90089-0741

Dr. R. B. Tittmann
Rockwell International Science Center
1049 Camino Dos Rios
P.O. Box 1085
Thousand Oaks, CA 91360

Professor M. Nafi Toksoz
Earth Resources Laboratory
Department of Earth, Atmospheric and
Planetary Sciences
Massachusetts Institute of Technology
42 Carleton Street
Cambridge, MA 02142

Professor Terry C. Wallace
Department of Geosciences
Building #11
University of Arizona
Tucson, AZ 85721

Prof. John H. Woodhouse
Hoffman Laboratory
Harvard University
20 Oxford St.
Cambridge, MA 02138

Dr. G. Blake
US Dept of Energy/DP 331
Forrestal Building
1000 Independence Ave.
Washington, D.C. 20585

Dr. Michel Bouchon
Universite Scientifique et
Medicale de Grenoble
Laboratoire de Geophysique
Interne et Tectonophysique
I.R.I.G.M.-B.P. 68
38402 St. Martin D'Heres
Cedex FRANCE

Dr. Hilmar Bungum
NTNF/NORSAR
P O. Box 51
Norwegian Council of Science,
Industry and Research, NORSAR
N-2007 Kjeller, NORWAY

Dr. Alan Douglas
Ministry of Defense
Blacknest, Brimpton, Reading RG7-4RS
UNITED KINGDOM

Professor Peter Harjes
Institute for Geophysik
Rhur University
Bochum
P.O. Box 102148
4630 Bochum 1
FEDERAL REPUBLIC OF GERMANY

Dr. James Hannon
Lawrence Livermore National Laboratory
P.O. Box 808
Livermore, CA 94550

Dr. E. Husebye
NTNF/NORSAR
P.O. Box 51
N-2007 Kjeller, NORWAY

Dr. Arthur Lerner-Lam
Lamont-Doherty Geological Observatory
of Columbia University
Palisades, NY 10964

Mr. Peter Marshall
Procurement Executive
Ministry of Defense
Blacknest, Brimpton, Reading RG7-4RS
UNITED KINGDOM

Dr. B. Massinon
Societe Radiomana
27, Rue Claude Bernard
75005, Paris, FRANCE

Dr. Pierre Mechler
Societe Radiomana
27, Rue Claude Bernard
75005, Paris, FRANCE

Mr. Jack Murphy
S-CUBED
Reston Geophysics Office
11800 Sunrise Valley Drive
Suite 1212
Reston, VA 22091

Dr. Svein Mykkeltveit
NTNF/NORSAR
P.O. Box 51
N-2007 Kjeller, NORWAY

Dr. Carl Newton
Los Alamos National Laboratory
P.O. Box 1663
Mail Stop C 335, Group ESS3
Los Alamos, NM 87545

Dr. Peter Basham
Earth Physics Branch
Department of Energy and Mines
1 Observatory Crescent
Ottawa, Ontario
CANADA K1A 0Y3

Professor J. A. Orcutt
Geological Sciences Division
Univ. of California at San Diego
La Jolla, CA 92093

Dr. Frank F. Pilotte
Director of Geophysics
Headquarters Air Force Technical
Applications Center
Patrick AFB, Florida 32925-6001

Professor Keith Priestley
University of Nevada
Mackay School of Mines
Reno, Nevada 89557

Mr. Jack Raclin
USGS - Geology, Rm 3C136
Mail Stop 928 National Center
Reston, VA 22092

Dr. Frode Ringdal
NTNF/NORSAR
P.O. Box 51
N-2007 Kjeller, NORWAY

Dr. George H. Rothe
Chief, Research Division
Geophysics Directorate
Headquarters Air Force Technical
Applications Center
Patrick AFB, Florida 32925-6001

Dr. Alan S. Ryall, Jr.
Center for Seismic Studies
1300 North 17th Street
Suite 1450
Arlington, VA 22209-2308

Dr. Jeffrey L. Stevens
S-CUBED,
A Division of Maxwell Laboratory
P.O. Box 1620
La Jolla, CA 92038-1620

Dr. Lawrence Turnbull
OSWR/NED
Central Intelligence Agency
CIA, Room 5G48
Washington, DC 20505

Professor Steven Grand
Department of Geology
245 Natural History Bldg
1301 West Green Street
Urbana, IL 61801

DARPA/PM
1400 Wilson Boulevard
Arlington, VA 22209

Defense Technical Information Center
Cameron Station
Alexandria, VA 22314 (12 copies)

Defense Intelligence Agency
Directorate for Scientific and
Technical Intelligence
Washington, D.C. 20301

Defense Nuclear Agency
Shock Physics Directorate/SS
Washington, D.C. 20305

Defense Nuclear Agency/SPSS
ATTN: Dr. Michael Shore
6801 Telegraph Road
Alexandria, VA 22310

AFOSR/NPG
ATTN: Director
Bldg 410, Room C222
Bolling AFB, Washington, D.C. 20332

AFTAC/CA (STINFO)
Patrick AFB, FL 32925-6001

AFWL/NTESC
Kirtland AFB, NM 87171

U.S. Arms Control & Disarmament Agency
ATTN: Mrs. M. Hoinkes
Div. of Multilateral Affairs, Rm 5499
Washington, D.C. 20451

U.S. Geological Survey
ATTN: Dr. T. Hanks
National Earthquake Research Center
345 Middlefield Road
Menlo Park, CA 94025

SRI International
333 Ravensworth Avenue
Menlo Park, CA 94025

Center for Seismic Studies
ATTN: Dr. C. Romney
1300 North 17th Street
Suite 1450
Arlington, VA 22209 (3 copies)

Dr. Robert Blandford
DARPA/GSD
1400 Wilson Boulevard
Arlington, VA 22209-2308

Ms. Ann Kerr
DARPA/GSD
1400 Wilson Boulevard
Arlington, VA 22209-2308

Dr. Ralph Alewine III
DARPA/GSD
1400 Wilson Boulevard
Arlington, VA 22209-2308

Mr. Edward Giller
Pacific Sierra Research Corp.
1401 Wilson Boulevard
Arlington, VA 22209

Science Horizons, Inc.
Attn: Dr. Bernard Minster
Dr. Theodore Cherry
710 Encinitas Blvd., Suite 101
Encinitas, CA 92024 (2 copies)

Dr. Jack Evernden
USGS - Earthquake Studies
345 Middlefield Road
Menlo Park, CA 94025

Dr. Lawrence Braile
Department of Geosciences
Purdue University
West Lafayette, IN 47907

Dr. G.A. Bollinger
Department of Geological Sciences
Virginia Polytechnical Institute
21044 Derring Hall
Blacksburg, VA 24061

Dr. L. Sykes
Lamont Doherty Geological Observatory
Columbia University
Palisades, NY 10964

Dr. S.W. Smith
Geophysics Program
University of Washington
Seattle, WA 98195

Dr. L. Timothy Long
School of Geophysical Sciences
Georgia Institute of Technology
Atlanta, GA 30332

Dr. N. Biswas
Geophysical Institute
University of Alaska
Fairbanks, AK 99701

Dr. Freeman Gilbert
Institute of Geophysics &
Planetary Physics
Univ. of California at San Diego
P.O. Box 109
La Jolla, CA 92037

Dr. Pradeep Talwani
Department of Geological Sciences
University of South Carolina
Columbia, SC 29208

University of Hawaii
Institute of Geophysics
Attn: Dr. Daniel Walker
Honolulu, HI 96822

Dr. Donald Forsyth
Department of Geological Sciences
Brown University
Providence, RI 02912

Dr. Jack Oliver
Department of Geology
Cornell University
Ithaca, NY 14850

Dr. Muawia Barazangi
Geological Sciences
Cornell University
Ithaca, NY 14853

Rondout Associates
Attn: Dr. George Sutton
Dr. Jerry Carter
Dr. Paul Pomeroy
P.O. Box 224
Stone Ridge, NY 12484 (3 copies)

Dr. M. Sorrells
Geotech/Teledyne
P.O. Box 28277
Dallas, TX 75228

Dr. Bob Smith
Department of Geophysics
University of Utah
1400 East 2nd South
Salt Lake City, UT 84112

Dr. Anthony Gangi
Texas A&M University
Department of Geophysics
College Station, TX 77843

Dr. Gregory B. Young
ENSCO, Inc.
5400 Port Royal Road
Springfield, CA 22151

Dr. Ben Menaheim
Weizman Institute of Science
Rehovot, ISRAEL 951729

Weidlinger Associates
Attn: Dr. Gregory Wojcik
620 Hansen Way, Suite 100
Palo Alto, CA 94304

Dr. Leon Knopoff
University of California
Institute of Geophysics & Planetary
Physics
Los Angeles, CA 90024

Dr. Kenneth H. Olsen
Los Alamos Scientific Laboratory
Post Office Box 1663
Los Alamos, NM 87545

Prof. Jon F. Claerbout
Prof. Amos Nur
Dept. of Geophysics
Stanford University
Stanford, CA 94305 (2 copies)

Dr. Robert Burridge
Schlumberger-Doll Research Ctr.
Old Quarry Road
Ridgefield, CT 06877

Dr. Eduard Berg
Institute of Geophysics
University of Hawaii
Honolulu, HI 96822

Dr. Robert Phinney
Dr. F.A. Dahlen
Dept. of Geological & Geophysical Sci.
Princeton University
Princeton, NJ 08540 (2 copies)

Dr. Kin-Yip Chun
Geophysics Division
Physics Department
University of Toronto
Ontario, CANADA M5S 1A7

New England Research, Inc.
Attn: Dr. Randolph Martin III
P.O. Box 857
Norwich, VT 05055

Sandia National Laboratory
Attn: Dr. H.B. Durham
Albuquerque, NM 87185

Dr. Gary McCartor
Mission Research Corp.
735 State Street
P. O. Drawer 719
Santa Barbara, CA 93102

Dr. W. H. K. Lee
USGS
Office of Earthquakes, Volcanoes,
& Engineering
Branch of Seismology
345 Middlefield Rd
Menlo Park, CA 94025

AFGL/XO
Hanscom AFB, MA 01731-5000

AFGL/LW
Hanscom AFB, MA 01731-5000

AFGL/SULL
Research Library
Hanscom AFB, MA 01731-5000 (2 copies)

Secretary of the Air Force (SAFRD)
Washington, DC 20330

Office of the Secretary Defense
DDR & E
Washington, DC 20330

HQ DNA
Attn: Technical Library
Washington, DC 20305

Director, Technical Information
DARPA
1400 Wilson Blvd.
Arlington, VA 22209

Los Alamos Scientific Laboratory
Attn: Report Library
Post Office Box 1663
Los Alamos, NM 87544

Dr. Thomas Weaver
Los Alamos Scientific Laboratory
Los Alamos, NM 87544

Dr. Al Florence
SRI International
333 Ravenswood Avenue
Menlo Park, CA 94025-3493

END

7-87

DTIC